ACCEPTED MANUSCRIPT
APL Photonics
This is the author's peer reviewed, accepted manuscript. However, the online version of record will be different from this version once it has been copyedited and typeset.
PLEASE CITE THIS ARTICLE AS DOI:10.1063/5.0031230
AIP Publishing

Perspectives on Advances in High-Capacity, Free-Space Communications Using Multiplexing of Orbital-Angular-Momentum Beams

Alan E. Willner[1,a)], Zhe Zhao[1], Cong Liu[1], Runzhou Zhang[1], Haoqian Song[1], Kai Pang[1], Karapet Manukyan[1], Hao Song[1], Xinzhou Su[1], Guodong Xie[1], Yongxiong Ren[1], Yan Yan[1], Moshe Tur[2], Andreas F. Molisch[1], Robert W. Boyd[3,4], Huibin Zhou[1], Nanzhe Hu[1], Amir Minoofar[1], and Hao Huang[1]

[1] *Department of Electrical Engineering, University of Southern California, Los Angeles, CA 90089, USA*
[2] *School of Electrical Engineering, Tel Aviv University, Ramat Aviv 69978, Israel*
[3] *Department of Physics, University of Ottawa, Ottawa, ON, Canada*
[4] *The Institute of Optics, University of Rochester, Rochester, New York 14627, USA*
[a)] Author to whom correspondence should be addressed. Email: willner@usc.edu

Abstract

Beams carrying orbital-angular-momentum (OAM) have gained much interest due to their unique amplitude and phase structures. In terms of communication systems, each of the multiple independent data-carrying beams can have a different OAM value and be orthogonal to all other beams. This paper will describe the use of multiplexing and the simultaneous transmission of multiple OAM beams for enhancing the capacity of communication systems. We will highlight the key advances and technical challenges in the areas of: (a) free-space and fiber communication links, (b) mitigation of modal coupling and channel crosstalk effects, (c) classical and quantum systems, and (d) optical and RF beam multiplexing.

ACCEPTED MANUSCRIPT
APL Photonics
This is the author's peer reviewed, accepted manuscript. However, the online version of record will be different from this version once it has been copyedited and typeset.
PLEASE CITE THIS ARTICLE AS DOI:10.1063/5.0031230
AIP Publishing

I. Introduction and overview

In 1992, Allen et al.[1] reported that orbital angular momentum (OAM) can be carried by an optical vortex beam. This beam has a unique spatial structure, such that its amplitude has a ring-like doughnut profile and the phasefront "twists" in a helical fashion as it propagates. The number of 2π phase changes in the azimuthal direction represents the OAM mode order, and beams with different OAM values can be orthogonal to each other (Fig. 1). Such structured beams are a subset of the Laguerre–Gaussian (LG_{lp}) modal basis set in free space, which has two modal indices: (1) l represents the number of 2π phase shifts in the azimuthal direction and the size of the ring grows with l; and (2) p+1 represents the number of concentric amplitude rings[2,3]. This orthogonality enables multiple independent optical beams to be multiplexed, spatially co-propagate, and be demultiplexed – all with minimal inherent crosstalk[1,3,4].

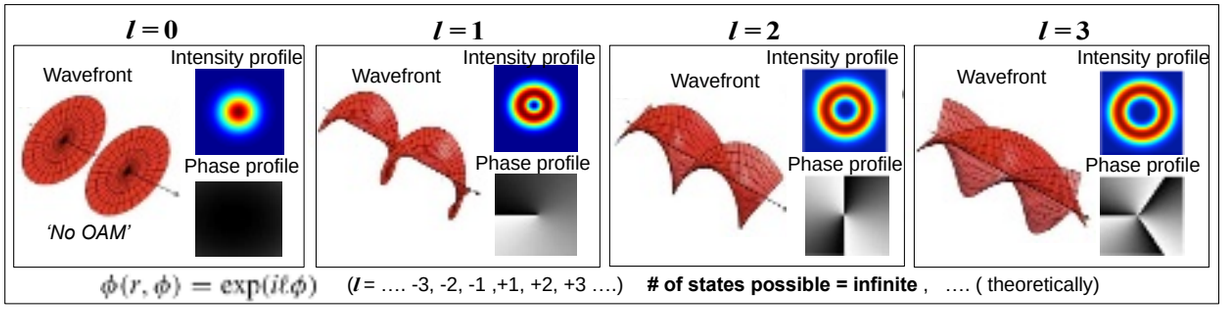

FIG. 1 The wavefronts, intensity profiles, and phase profiles of OAM modes l = 0, 1, 2, and 3. The OAM mode with a nonzero order has a donut-shaped intensity profile and helical phasefront. The size of the ring in the intensity profile grows with l. We note that p+1 represents the number of concentric amplitude rings and p=0 is shown in the figure. (© 2011 Optical Society of America).

This orthogonality is crucially beneficial for a communications system. It implies that multiple independent data-carrying optical beams can be multiplexed and simultaneously transmitted in either free-space or fiber, thereby multiplying the system's data capacity by the total number of beams (Fig. 2). Moreover, since all the beams are in the same frequency band, the system's spectral efficiency (i.e., bits/s/Hz) is also increased. These multiplexed orthogonal OAM beams are a form of mode-division multiplexing (MDM), which itself is a subset of space-division multiplexing (SDM)[5–7].

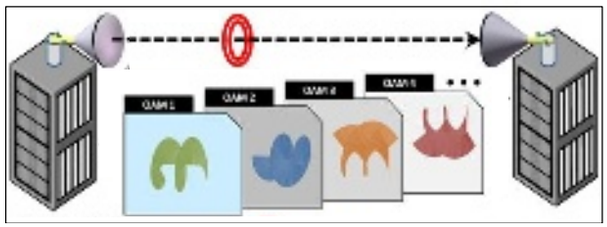

FIG. 2 Concept of OAM multiplexed FSO links, multiple OAM beams are co-axially transmitted through free space each carrying an independent data stream[8]. (© 2014 Macmillan Publishers)

MDM shares similarities with wavelength-division multiplexing (WDM), in which multiple independent data-carrying optical beams of different wavelengths can be multiplexed and simultaneously transmitted. WDM revolutionized optical communication systems and is ubiquitously deployed worldwide. Importantly, MDM is generally compatible with and can complement WDM, such that each of the many wavelengths can contain many orthogonal structured beams and thus dramatically increase data capacity[7,9,10].

The field of OAM-based optical communications: (i) is considered young and rich with scientific and technical challenges, (ii) holds promise for technological advances and applications, and (iii) has produced much research worldwide such that the number of publications per year has grown significantly[11]. Capacities, distances, and numbers of data channels have all increased, and approaches for mitigating degrading effects have produced encouraging results[4,11,12].

In this paper, we discuss the evolution of several sub-fields in OAM-based optical communications. We describe advances and perspectives on different aspects of this field, including: (a) free-space optical (FSO) communication links, (b) modal coupling effects and channel crosstalk mitigation techniques, (c) airborne and underwater systems, (d) quantum communications, (e) radio-frequency, millimeter-wave (mm-wave), and THz links, and (f) fiber-based systems. We note that this article will generally assume OAM multiplexed "free-space classical" optical communications as the basic default system, and separate subsections will be dedicated to the topics that deviate from this system (e.g., quantum, radio frequencies, or fiber). The intent of this article is to give

ACCEPTED MANUSCRIPT
APL Photonics
This is the author's peer reviewed, accepted manuscript. However, the online version of record will be different from this version once it has been copyedited and typeset.
PLEASE CITE THIS ARTICLE AS DOI:10.1063/5.0031230
AIP Publishing

a flavor of the advances as well as the growing interest in this field, and the reader is encouraged to explore more by consulting the references at the end.

II. OAM-based free-space MDM systems

A. High-capacity OAM-multiplexed communication links

OAM multiplexing has the potential to increase the total transmission rates in optical communication systems due to its ability to multiplex and simultaneously transmit multiple data-carrying channels on different OAM beams. As each OAM beam carrying an independent data stream co-propagates with other OAM beams, the spectral efficiency of the system (i.e., bits/sec/Hz) scales with the number of OAM beams utilized for multiplexing. As such, OAM beams can be carried on both orthogonal polarizations, and polarization-division multiplexing (PDM) can also be applied to further double the spectral efficiency of the system. The first use of OAM multiplexing for MDM communication links resulted in an FSO link that multiplexed four different OAM modes on two polarizations, with an aggregated data rate of 1.37 Tbit/s[7]. As shown in Fig. 3, on one polarization, four Gaussian beams carrying independent data channels (Data1, Data3, Data5, and Data7) were transformed into four OAM modes (OAM1, OAM2, OAM3, and OAM4) by adding different phase patterns. Conjugated phase patterns were used at the receiver to convert the OAM-carrying beams back into Gaussian beams. By utilizing PDM, four additional data channels (Data2, Data4, Data6, and Data8) were multiplexed and carried by the same OAM modes (OAM1, OAM2, OAM3, OAM4) on the other polarization, resulting in eight independent data channels on the same wavelength. This increased the spectral efficiency of the system eightfold.

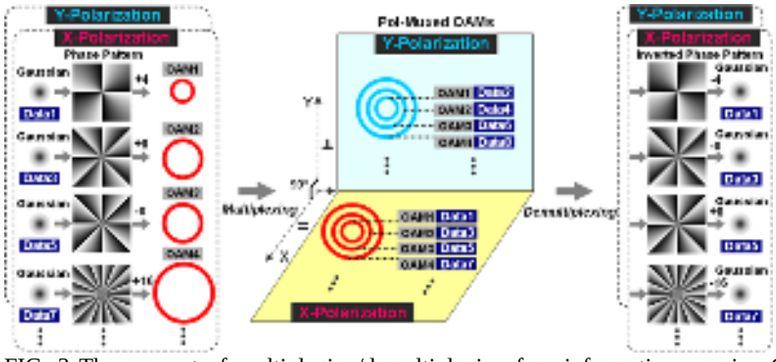

FIG. 3 The concept of multiplexing/demultiplexing four information-carrying OAM beams (left panel) combined with PDM (middle panel) to achieve a 1.37 Tbit/s aggregated rate. For demultiplexing, an OAM beam is converted back into a Gaussian beam that has high intensity at the center (right panel, second column), which can be separated from other 'doughnut shaped' OAM beams by a spatial filter. Pol-Muxed: polarization-multiplexed. (© 2012 Nature Research)

Moreover, WDM can be utilized to further increase the capacity of OAM multiplexed FSO links. The concept of combining OAM-multiplexing, PDM and WDM for capacity enhancement is presented in Fig. 4. OAM-multiplexing and PDM are combined and carried on the same frequency (Fig. 4(a, b)), and other independent data channels can be transmitted/received utilizing the other frequencies on the same OAM modes and both polarizations (Fig. 4(c)). As the OAM multiplexing and PDM are compatible with WDM, utilizing M different carrier frequencies allows to further increase the aggregated link capacity by M times. Thus, the combination of N-OAM based MDM, PDM, and M-frequency based WDM can increase the aggregated data rate of an FSO communication link by $2 \times N \times M$ times as compared to using a single Gaussian beam on a single frequency and polarization[9,10]. One demonstration of such a system combined 12 OAM modes, 2 polarizations, and 42 wavelengths, resulting in a total of 1008 data channels each carrying 100-Gbit/s data, to achieve an aggregated rate of 100.8 Tbit/s in the laboratory[9]. Fig. 4(d) shows the observed optical spectrum of a single OAM beam (l = +10) that carries the WDM signals[9]. Another work reported a demonstration of 26-OAM mode-multiplexing over 368 WDM and polarization-multiplexed with an aggregate data rate of 1.036 Pbit/s[10].

The experimental demonstrations of OAM-multiplexed communication links in the laboratory were generally conducted over short distances of ~ 1 meter. In recent years, there have been several experiments that investigated the potential of using OAM beams to achieve long-distance FSO links in the field environment, for example[13–15]:

(i) a 120-m FSO communication link with 400-Gbit/s data rate based on four-OAM multiplexing; each OAM beam carries 100-Gbit/s quadrature phase-shift keying (QPSK) modulated data channels[13];

(ii) a 260-m FSO data transmission link between two buildings using OAM multiplexing and 16-quadrature-amplitude-modulation (16-QAM) signals with an 80-Gbit/s aggregated bit rate[14].

The expansion of an OAM-based link over much longer distances might give rise to several challenges, including the divergence of the OAM beams, system pointing and misalignment, and atmospheric turbulence effects. Significant efforts have been made to achieve such links over longer distances. An FSO link based on the OAM encoding scheme was demonstrated over a distance of ~143 km between two islands[15]. An OAM-based encoding scheme can be achieved by sequentially transmitting different OAM beams, each representing a data symbol, within each time slot. Compared to a binary signal, which has two possible data bit values

ACCEPTED MANUSCRIPT
APL Photonics
This is the author's peer reviewed, accepted manuscript. However, the online version of record will be different from this version once it has been copyedited and typeset.
PLEASE CITE THIS ARTICLE AS DOI:10.1063/5.0031230
AIP Publishing

of "0" and "1", an *M*-ary OAM encoding signal may have many values, ranging from "0" to "*M*-1". The number of data bits per unit time can reach $\log_2 M$, and thus, the data capacity in each channel can be increased.

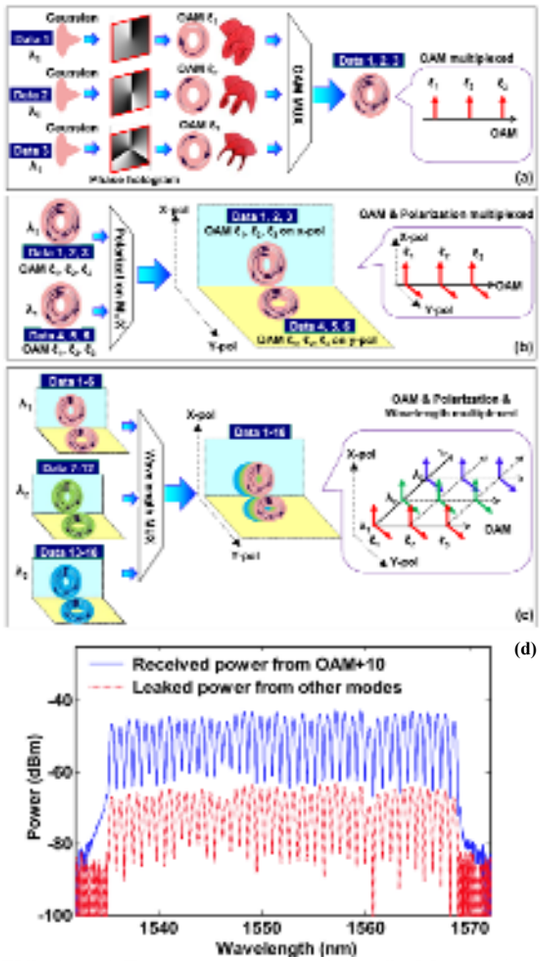

FIG. 4 (a-c) The concept of combining OAM multiplexing with PDM and WDM to increase the link capacity. (a) Multiplexing multiple data channels on OAM-carrying beams. (b) Combining OAM multiplexing with PDM. (c) Combining OAM and PDM multiplexing with WDM, 12 OAM modes, 2 polarizations, and 42 wavelengths were multiplexed in total to achieve a 100.8 Tbit/s aggregated data rate. (d) Measured optical spectrum of the WDM signal carried on the OAM beam with l = +10. (© 2014 Optical Society of America)

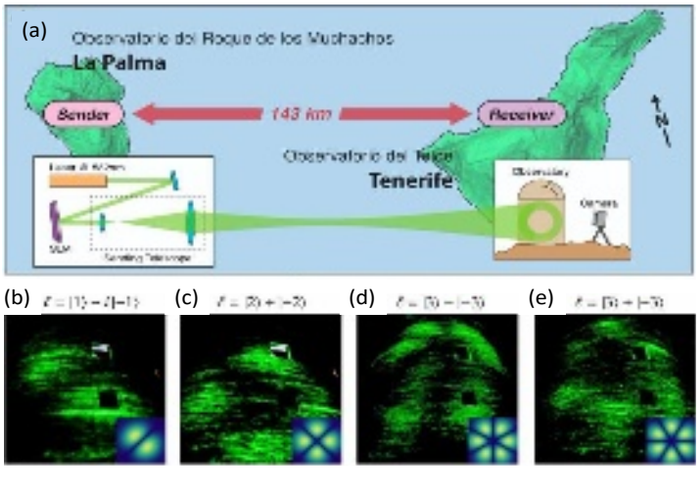

ACCEPTED MANUSCRIPT
APL Photonics
This is the author's peer reviewed, accepted manuscript. However, the online version of record will be different from this version once it has been copyedited and typeset.
PLEASE CITE THIS ARTICLE AS DOI:10.1063/5.0031230
AIP Publishing

FIG. 5 (a) The layout sketch of an OAM-encoded link over a distance of ~ 143 km. At the transmitter, OAM beams were generated by shining Gaussian beams on to a spatial light modulator (SLM). A telescope was used to collimate OAM beams for decreasing the divergence effects. (b-d) Examples of superposed OAM (vortex) modes observed at the receiver. The intensity profiles were distorted mainly due to the atmospheric turbulence effects. (© 2016 United States National Academy of Sciences)

Figure 5(a) shows the link layout for sending and receiving the OAM modes in the above-mentioned 143-km link[15]. The observed patterns of four different OAM mode superpositions are shown in Fig. 5(b-e). Under the relatively weak turbulence, the lobed modal structure was visible for mode superpositions with l = {-1, +1}, {-2, +2}, or {-3, +3}. In order to recover the encoded data, an artificial neural network-based pattern recognition algorithm was used to distinguish images of different OAM mode superpositions. The received mode superpositions could be identified with an accuracy of >80% up to OAM mode order l=3, and the decoded message had an error rate of 8.33%. The results indicate that the free-space transmission of OAM modes over a 100-km-scale distance is feasible.

B. Two-dimensional modal basis sets

Although there has been significant interest in OAM as a modal basis set for MDM communications, what is the rationale for choosing OAM over other types of modes? On a fundamental level, MDM requires that you can efficiently combine and separate different modes, so almost any complete orthogonal basis set could work. Indeed, many different types of modes were demonstrated in free-space and fiber, including Hermite–Gaussian (HG), LG, and linearly polarized (LP) modes[5, 7, 16-20]. In discussions with Robert Boyd and Miles Padgett[21], two practical issues seemed to emerge as to reasons that one "might" prefer OAM modes (as a subset of LG modes) to other modal basis sets:

(i) OAM modes are round, and free-space optical components are readily available in round form.

(ii) It is important to maintain interchannel orthogonality and minimize crosstalk. This can be accomplished by fully capturing the specific parameter that defines the modal orthogonality. For a case in which different channels can be defined by different OAM l values, the channel and mode can be fully determined by azimuthally capturing a full 360° circle no matter the size of the round aperture[22, 23].

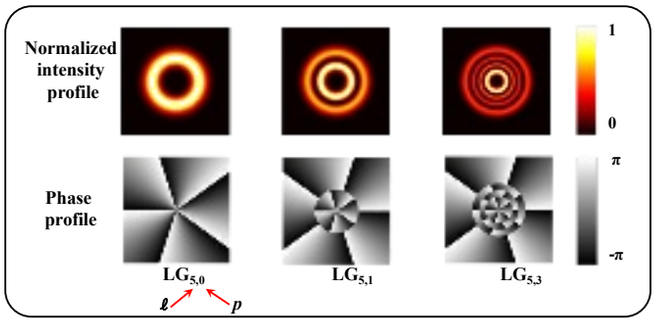

FIG. 6 Intensity and phase profiles of LG beams with non-zero radial index p, and azimuthal index l. The values of p+1 and l represent the number of rings in the intensity profile for the non-zero l value and the number of 2π phase changes along the azimuthal direction in the phase profile. LG beams with different pairs of indices (l, p) are orthogonal to each other[24]. (© 2017 Optical Society of America)

Structured beams from a modal basis set can generally be described by two modal indices, such that the beam can be fully described by these coordinates. For example, LG modes have l (azimuthal) and p (radial) components, whereas HG beams have n (horizontal) and m (vertical) components. OAM modes are a subset of a full LG modal basis set, which can be characterized by two indices: the radial index p and the azimuthal index l, as shown in Fig. 6. The electrical field of an LG beam can be represented by[2, 18]:

$$LG_{\ell,p}(r,\phi,l,p,\omega_0) = \frac{\sqrt{2}r^{|l|}}{\omega_0{}^{|l|+1}} exp\left(-\frac{r^2}{\omega_0{}^2} + il\phi\right) LP_p^{|l|}\left(\frac{2r^2}{\omega_0{}^2}\right) \quad (1)$$

where ω_0 is the beam waist, $LP_p^{|l|}$ is the generated Laguerre polynomials, and (r, ϕ) is the cylindrical coordinate. However, the vast majority of publications on MDM-based FSO communications utilized only a change in a single modal index. Specifically, each beam commonly had a different l value but the same p=0 value[7,8,10,13,15, 25]. LG beams with different p values can also be utilized in MDM FSO links. For example, there has been an experimental demonstration of a 200-Gbit/s MDM link based on the multiplexing of LG modes with the same l value but different p values[18]. It should be noted that these works utilized one-dimensional modal basis sets, which means that they only varied one of the two modal indices (l, p). While this one-dimensional system can accommodate many orthogonal beams, a system designer could also use the other beam modal index in order to possibly achieve a larger two-dimensional set of data channels. This two-dimensional approach was shown experimentally for LG and HG beams[17,18]. It is important to note that a significant challenge is the sufficient capture of the beam at the receiver aperture to ensure accurate phase recovery and orthogonality along both indices[18].

ACCEPTED MANUSCRIPT
APL Photonics
This is the author's peer reviewed, accepted manuscript. However, the online version of record will be different from this version once it has been copyedited and typeset.
PLEASE CITE THIS ARTICLE AS DOI:10.1063/5.0031230
AIP Publishing

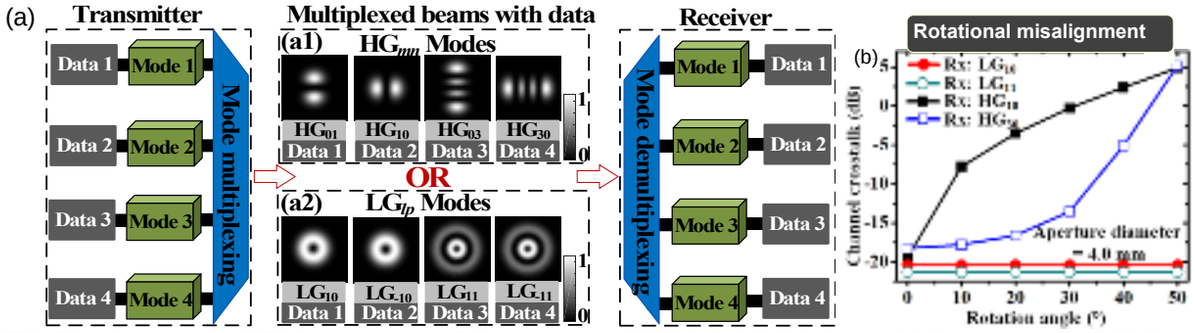

FIG. 7 (a) Concept of an MDM link using four LG modes or four HG modes, each carrying 100 Gbit/s signal (i.e., 400 Gbit/s in total). (b) Measured crosstalk for each mode when all four HG or LG modes are transmitted with various receiver rotation angles (© 2018 Optical Society of America).

Theoretically, LG beams with different pairs of indices (l, p) are orthogonal to each other. Therefore, extending the 1-dimensional modal basis sets (e.g., LG beams with only l or p index changing) to 2-dimensional ones (e.g., LG beams with both l and p indices changing) could provide a larger two-dimensional modal space for orthogonal data-carrying channels and increase the transmission capacity of a communication link. A four-fold multiplexing of LG modes was experimentally demonstrated to achieve a 400-Gbit/s communication link[17]. In this experiment, a two-dimensional LG modal set was used and both two modal indices (l, p) were varied. In addition, four HG modes were utilized to achieve such a four-channel MDM link (Fig. 7(a)), and the effects of aperture size as well as lateral and rotational misalignments on the crosstalk performance were also investigated[17]. Due to different symmetric properties of LG modes and HG modes, they might present different crosstalk performance under different misalignments in the MDM link. It was found that: (1) a limited-size aperture at the receiver causes power loss for both LG and HG beams; (2) a lateral misalignment between the transmitter and receiver causes crosstalk for LG beams, while HG beams with a zero m or n index are more tolerant to lateral misalignment due to the axial symmetry; and (3) a rotational misalignment causes crosstalk for HG beams, but does not tend to influence LG modes due to their circular symmetry, as shown in Fig. 7 (b).

III. Basic challenges and effects for OAM-based MDM communication system

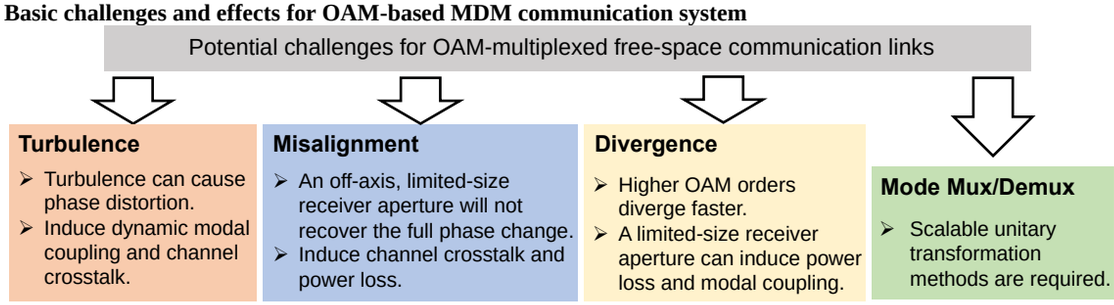

FIG. 8 Potential challenges for an OAM-multiplexed FSO communication link. Turbulence effects distort the beam phasefront thus inducing dynamic modal coupling and channel crosstalk. A misaligned, off-axis, limited-size receiver aperture would not recover the full phase change and will induce channel crosstalk and power loss. Beam divergence effects could be important for a long-distance transmission: higher-order OAM-carrying beams diverge faster, which could lead to power loss and modal coupling due to the limited receiver size. The mode multiplexing and demultiplexing requires methods to achieve scalable unitary transformation. Mux: multiplexing; Demux: demultiplexing.

A key issue in almost any MDM communication system is dealing with intermodal power coupling and deleterious inter-data-channel crosstalk. There are many causes of modal coupling and crosstalk, including the following for OAM-multiplexed FSO communication links, as shown in Fig. 8:

(a) ***Turbulence***: Atmospheric turbulence can cause a phase distortion at different cross-sectional locations of a propagating beam. Given this phase change distribution in a changing environment, power can couple from the intended mode into others dynamically (e.g., perhaps changes on the order of milliseconds)[26–29].

(b) ***Misalignment***: Misalignment between the transmitter and receiver means that the receiver aperture is not coaxial with the incoming OAM beams. In order to operate an OAM-multiplexed link, one needs to know which modes that are being transmitted. A receiver aperture that captures power around the center of the beam will recover the full azimuthal phase change and know which l mode was transmitted. However, a limited-size receiver aperture that is off-axis will not recover the full phase change and inadvertently "think" that some power resides in other l and/or p modes[30].

(c) ***Divergence***: FSO beams of higher OAM orders diverge faster than lower-order OAM beams, thus making it difficult to fully capture the higher-order OAM beams with a limited-sized receiver aperture. Power loss occurs if the beam power is not fully

ACCEPTED MANUSCRIPT
APL Photonics
This is the author's peer reviewed, accepted manuscript. However, the online version of record will be different from this version once it has been copyedited and typeset.
PLEASE CITE THIS ARTICLE AS DOI:10.1063/5.0031230
AIP Publishing

captured, but even modal coupling can occur due to the truncation of the beam's radial profile. This truncation can result in power being coupled to some other LG beams with different p values (p modes)[30-32].

(d) ***Mode multiplexing/demultiplexing***: Mode multiplexing and demultiplexing is another challenge in OAM-multiplexing based systems, which requires a scalable unitary transformation. Various studies have addressed this challenge, including: a) multi-plane light conversion (MPLC) achieved by shaping the wavefront of the light at multiple propagating distances to accomplish mode conversion between Gaussian beams at different locations and different HG/LG beams[33,34], b) log-polar-based mode sorter that geometrically transforms the spiral spatial phase of OAM beams into a tilted spatial phase[35,36], and c) designing refractive index distribution of the fiber designed to achieve in-fiber mode conversion from the fundamental mode to the vector mode[37].

It should also be mentioned that: (i) modal coupling "tends" to be higher to the adjacent modes, and (ii) separating data channels with a larger modal differential can help in alleviating the problem[28, 38, 39]. Of course, larger modal separation leads to larger beam divergence, so a trade-off analysis is usually recommended.

A. Atmospheric turbulence

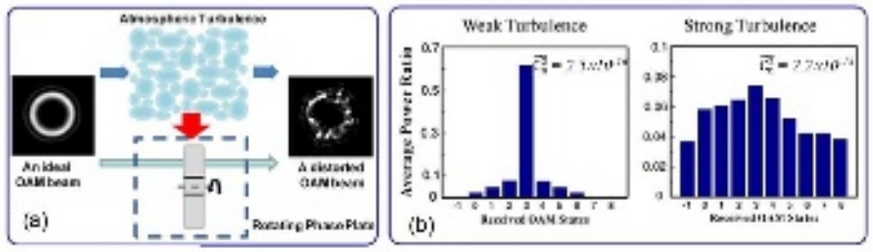

FIG. 9 (a) A rotating phase plate is used as an atmospheric turbulence emulator. The OAM beam intensity profile is distorted after passing through the phase plate. (b) Measured power distribution of an OAM beam after passing through the turbulence emulator with weak and strong atmospheric turbulence, respectively. $\widetilde{C_n^2}$: the effective atmospheric structure constant, larger $\widetilde{C_n^2}$ indicates stronger turbulence effects (© 2013 Optical Society of America)

Atmospheric turbulence is one important challenge that needs to be considered for an OAM-multiplexed FSO communication system. Inhomogeneities in the temperature and pressure of the atmosphere can lead to variations in the refractive index along the transmission path[27,40]. As in an OAM-multiplexed link, the orthogonality among multiple co-propagating OAM beams depends on their helical phasefront, turbulence-induced refractive index inhomogeneities can cause intermodal crosstalk between different data channels with different OAM orders, as they can easily distort the phasefront of OAM beams (Fig. 9(a)) [28,41,42].

The effects of atmospheric turbulence on the OAM-multiplexed systems performance have been experimentally evaluated in the laboratory in several ways[27-29]. One example of the atmospheric effects emulation in the laboratory is shown in Fig. 9(a), which presents the concept of using a rotating phase plate to emulate the turbulence effects. The phase screen plate is mounted on a rotating stage and placed in the optical path of the beams. On the rotating plate, the pseudorandom phase distribution obeys Kolmogorov spectrum statistics[28]. The strength of the emulated turbulence effect generally depends on the Fried parameter r_0, and the beam size that is incident on the plate. In order to evaluate the turbulence effects, the modal crosstalk is characterized by measuring the power of the distorted beam in each OAM mode. Figure 9(b) presents the normalized power distribution among the neighboring OAM modes under weak and strong turbulences for an OAM +3 transmitted beam. It is shown that under the weak turbulence, the majority of the power is still in the transmitted OAM mode (i.e. OAM +3), and only a small part of the power is coupled into other neighboring OAM modes. However, as the turbulence strength increases, the power coupling into other OAM modes becomes higher, which could induce severe signal fading and crosstalk.

B. Misalignment

The efficient multiplexing and de-multiplexing of OAM beams requires coaxial propagation and reception of the transmitted modes. Unlike the case of using Gaussian beams, any misalignment between the transmitter and receiver apertures or only partial collection of the OAM beams at the receiver would result not only in power loss but, more severely, in interchannel crosstalk (i.e., power coupled into other modes). In an ideal OAM multiplexed communication link, the transmitter and receiver would be perfectly aligned (i.e., the center of the receiver would overlap with the center of the transmitted beam, and the receiver plane would be perpendicular to the line connecting their centers, as shown in Fig. 10(a)). However, due to jitter and vibration of the transmitter/receiver platform, the transmitter and receiver may have relative lateral shift (i.e., lateral displacement) or angular shift (i.e., receiver angular error), as depicted in Figs. 10(b) and (c), respectively. Both types of misalignment may lead to degradation of system performance.

Figure 10 (d) and (e) illustrates the effect of the lateral displacement and receiver angular error when only OAM +3 is transmitted with a beam diameter of 3 cm[30]. Given a fixed link distance of 100 m, the power coupling into other modes increases with an increase in the lateral displacement or receiver angular error, whereas the power on OAM +3 (i.e., the transmitted mode) decreases.

ACCEPTED MANUSCRIPT
APL Photonics
This is the author's peer reviewed, accepted manuscript. However, the online version of record will be different from this version once it has been copyedited and typeset.
PLEASE CITE THIS ARTICLE AS DOI:10.1063/5.0031230
AIP Publishing

This is because a larger lateral/angular displacement causes a larger mismatch between the received OAM beams and the receiver. The power coupled into OAM +2 and OAM +4 is greater than that of OAM +1 and OAM +5 due to their smaller mode spacing from OAM +3. This indicates that a system with larger mode spacing is more tolerant to the lateral displacement.

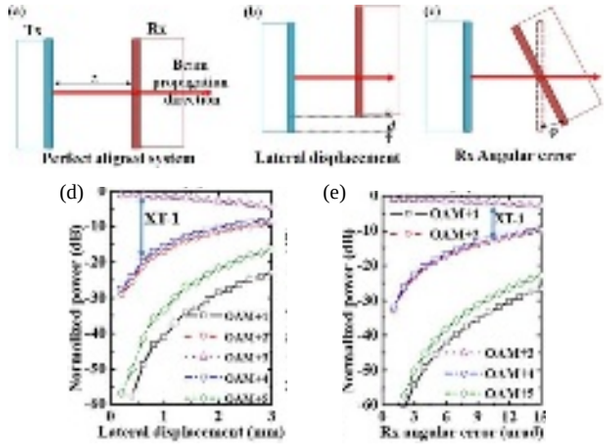

FIG. 10 (a-c) Three different cases of alignment between the transmitter and receiver: (a) a perfectly aligned system, (b) a system with lateral displacement, and (c) a system with receiver angular error. (d-e) Simulated power distribution among different OAM modes as a function of (c) lateral displacement and (d) receiver angular error over a 100-m link for which only the OAM 3 is transmitted. The transmitted beam size is 3 cm and the receiver aperture size is 4.5 cm. Tx: transmitter; Rx: receiver; z: transmission distance; d: displacement; φ: angular error. XT-1: crosstalk between neighboring OAM modes. (© 2015 Optical Society of America)

C. Beam divergence

For a communication link, it is preferable to collect as much signal power as possible at the receiver to ensure a sufficient signal-to-noise ratio (SNR). Based on diffraction theory, a light beam diverges while propagating in free space. Since optical elements usually have limited-size apertures, the diverged beam might be too large to be fully collected, resulting in signal power loss. For an OAM-multiplexed link, the transmitted beams with higher OAM orders diverge faster than lower-order OAM beams. This makes it difficult to fully capture them with a limited-size receiver aperture, which leads to signal power loss. Moreover, a limited-size receiver aperture can also degrade the orthogonality between p modes[30-32, 43], as shown in Fig.11. Truncation might occur in the beam's radial profile, and this could potentially induce a modal coupling from the desired mode to some other LG beams with different p values (p modes)[31,43]. For an MDM link using LG modes with different p values, this modal coupling might cause channel crosstalk. The divergence effect of an LG beam mainly depends on the frequency, transmission distance, beam waist at the transmitter, and mode indices. Therefore, in order to reduce the signal power loss and channel crosstalk, the key parameters related to the beam divergence needs to be carefully considered when designing an OAM-based link.

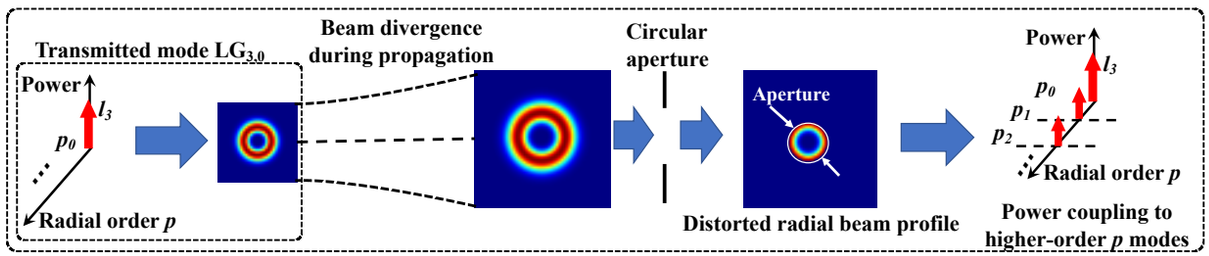

FIG. 11 The concept of circular aperture truncation effects to OAM-carrying beams due to OAM beam divergence and limited-size receiver aperture. OAM l=3 mode (i.e., LG l=3, p=0 mode) is shown as an example: the beam diverges during propagation, and the radial beam profile is distorted at the receiver side due to the circular truncation, which induce a modal coupling from the transmitted mode to some other LG modes with different higher order p values.

IV. Advances in crosstalk mitigation for OAM-multiplexed communication links

Crosstalk mitigation is one of the key challenges for OAM multiplexed communications. Various optical and digital techniques have been proposed for crosstalk mitigation in OAM-multiplexed links, as shown in Fig. 12. Conventional approaches for crosstalk mitigation include:

(i) ***Adaptive optics (AO)***:AO, such as by using digital micromirrors, spatial light modulators (SLMs) or multi-plane-light-converters (MPLCs), can mitigate modal crosstalk[44-47]. For example, if atmospheric turbulence causes a certain phase distortion on an optical beam, an SLM at the receiver can induce an inverse phase function to partially undo the effects of turbulence[45]. Typically, there could be a feedback loop, such that a data or probe beam is being monitored for dynamic changes and the new

ACCEPTED MANUSCRIPT

APL Photonics

This is the author's peer reviewed, accepted manuscript. However, the online version of record will be different from this version once it has been copyedited and typeset.
PLEASE CITE THIS ARTICLE AS DOI:10.1063/5.0031230

phase function is fed to an SLM, as shown in Fig. 13 (a1). With the usage of the AO system, the distorted OAM beams can be efficiently compensated, as shown in Fig. 13 (a2, a3);

(ii) ***Electrical digital signal processing (DSP)***: Crosstalk due to modal coupling has many similarities to crosstalk that occurs in multiple-transmitter-multiple-receiver (i.e., multiple-input multiple-output, MIMO) radio systems[48,49], as shown in Fig. 13 (b1). Multiple optical modes are similar to parallel radio frequency (RF) beams that experience crosstalk. Similar to electronic DSP that can undo much of the crosstalk in MIMO RF systems, these DSP approaches could also be used for mitigating OAM modal crosstalk[50]. With MIMO equalization, the error vector magnitude (EVM) of the four channels can be improved, as shown in Fig. 13 (b2, b3). The EVM is a parameter that could quantify the performance of a communication system, and a lower EVM value indicates a better signal quality.

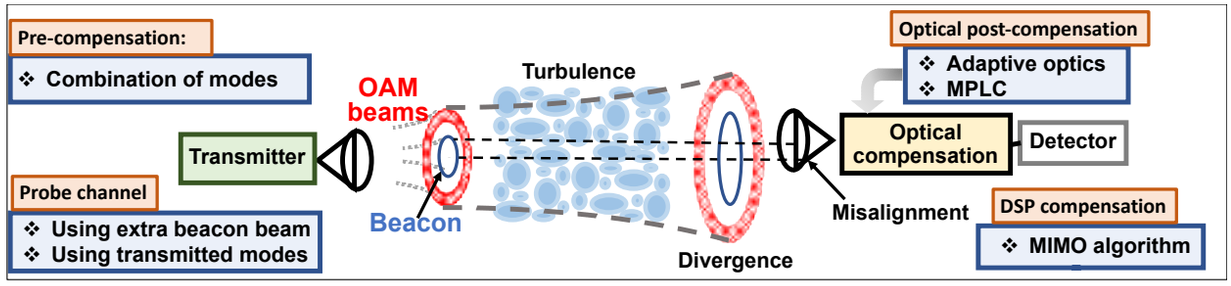

FIG. 12 Different crosstalk mitigation approaches for an OAM-multiplexed FSO link. An extra beacon beam or the transmitted data-carrying modes can be used as a probing channel to characterize the distortion from the turbulent media. Reports have shown various approaches for crosstalk mitigation: Optical approaches (e.g, AO, combinations of modes, MPLC-based method) have been utilized to mitigate crosstalk at the transmitter and/or receiver, while MIMO method have been utilized to mitigate crosstalk at the receiver in the electrical domain.

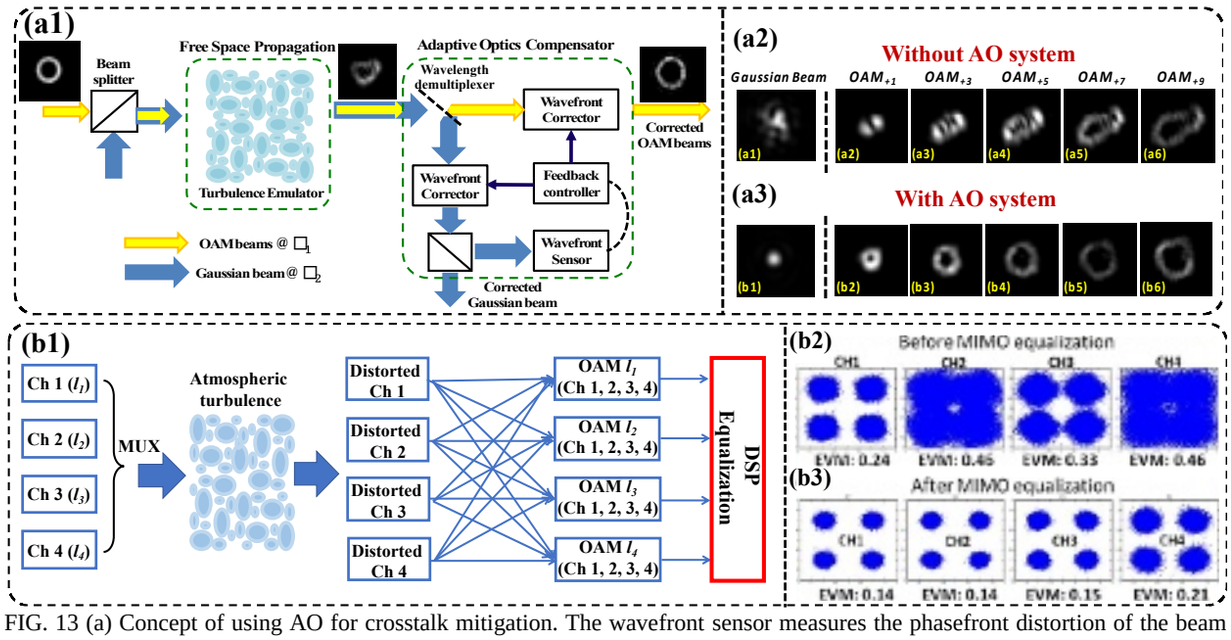

FIG. 13 (a) Concept of using AO for crosstalk mitigation. The wavefront sensor measures the phasefront distortion of the beam and the corresponding correction pattern is loaded on the wavefront corrector to undo the distortion. (a2-a3) The measured OAM beam profiles after being transmitted through the turbulent medium without and with the AO compensation. With the AO system, the distorted OAM beams can be efficiently compensated. (b1) Concept of using MIMO DSP to mitigate the modal crosstalk in the electrical domain. (b2, b3) Measured EVMs of the OAM-multiplexed channels. With MIMO equalization, the EVMs of the four channels can be improved. (©2014 Optical Society of America).

In the conventional receiving system for an OAM multiplexed link, mitigating OAM crosstalk and channel demultiplexing are typically achieved separately[33,45]. As mentioned above, AO and DSP can be applied to mitigate crosstalk. Additionally, MPLC has been demonstrated as a scalable and reconfigurable mode demultiplexer[33,34]. It might be desirable to mitigate crosstalk and demultiplex channels simultaneously. Recently, it was shown that the wavefront-shaping-and-diffusing method could simultaneously mitigate turbulence and demultiplex channels, but this approach involves some power loss involved in this approach[51-53]. Another approach is to use an MPLC to mitigate crosstalk and demultiplex channels, and this method theoretically

ACCEPTED MANUSCRIPT

APL Photonics

This is the author's peer reviewed, accepted manuscript. However, the online version of record will be different from this version once it has been copyedited and typeset.
PLEASE CITE THIS ARTICLE AS DOI:10.1063/5.0031230

has no inherent power loss[54,55]. Such an approach was demonstrated experimentally using a single MPLC to simultaneously mitigate the turbulence-induced crosstalk and demultiplex two channels carried by OAM modes[55]. As Fig. 14 (a) shows, input coaxial OAM beams having different mode orders are converted to Gaussian beams at different output positions using the cascaded phase patterns calculated by the wavefront-matching method[33,34]. To mitigate turbulence-induced crosstalk, the patterns are updated by combining the genetic algorithm with the wavefront matching method. Figure 14 (b) shows the measured crosstalk matrix without turbulence, without and with crosstalk mitigation under the turbulence for various OAM multiplexing cases of $\ell = \{-1, +1\}$ and $\ell = \{-1, +2\}$. Without crosstalk mitigation, the crosstalk performance for $\ell = \{-1, +1\}$ and $\ell = \{-1, +2\}$ is increased by >13.1 dB and >9.2 dB, respectively, compared with cases without turbulence, respectively. Applying crosstalk mitigation results in mitigation of >11.4 dB and >7.2 dB for $\ell = \{-1, +1\}$ and $\ell = \{-1, +2\}$, respectively. These results show that a single MPLC could be reconfigured to achieve simultaneous crosstalk mitigation and channel demultiplexing for different OAM multiplexing cases.

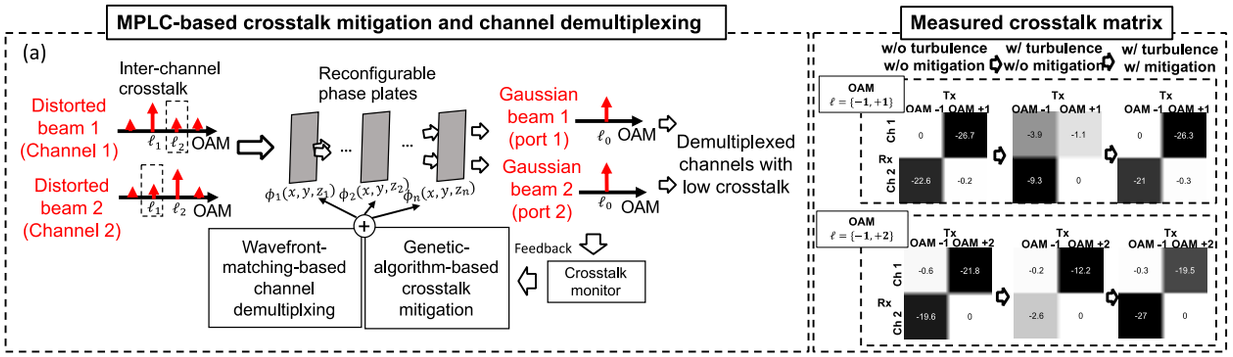

FIG. 14 (a) The concept of the MPLC-based crosstalk mitigation and channel demultiplexing. (b) Measured crosstalk matrix for channel demultiplexing without turbulence, without and with MPLC-based crosstalk mitigation under the turbulence.

Besides, there is an increasing array of potential methods for crosstalk mitigation in OAM-based links, advanced technologies including artificial neural network-based pattern recognition algorithm[15] are also considered. As with most issues, cost and complexity will play a key role in determining which, if any, mitigating approach should be used. In this section, we will discuss the recent advances of crosstalk mitigation approaches for OAM-multiplexed FSO communications as shown in Fig. 15. Specifically, we will mainly discuss approaches based on transmitting the coherent combination of multiple OAM modes at the transmitter for turbulence mitigation.

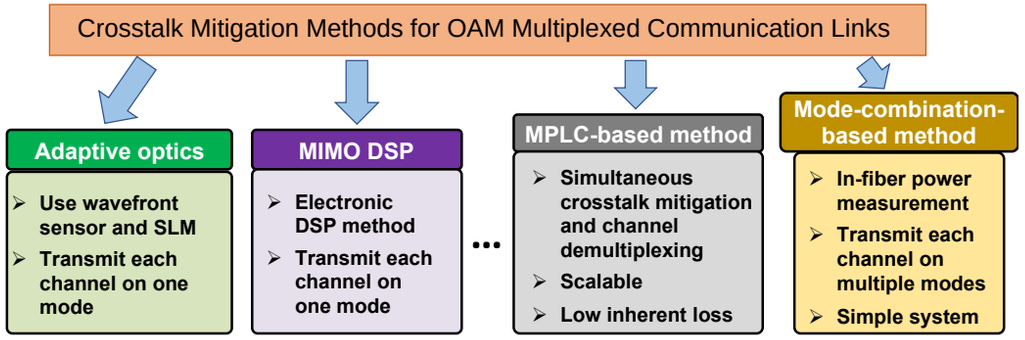

FIG. 15 Crosstalk mitigation methods for OAM-multiplexed communication links.

Mode-combination-based mitigation

Aside from the conventional crosstalk mitigation approaches, it would be beneficial to develop an alternative approach that: (a) only needs in-fiber power measurement instead of using wavefront sensors to measure the spatial amplitude and phase profile of the optical beams, and (b) can mitigate the crosstalk from other data channels without recovering all the data channels at the receiver. Recently, multiple optical approaches have been developed to address these issues[43, 56-59]. These approaches are based on the transmission or detection of a combination of multiple spatial modes. The steps to achieve this includes: (i) measuring the complex transmission matrix of the imperfect MDM links using the modal power distribution; (ii) calculating the phase patterns to generate/detect different combinations of multiple modes based on the measured transmission matrix; and (iii) applying the phase patterns to mitigate the crosstalk[43,56]. This method is feasible because a structured beam can be decomposed into a set of LG modes that carry OAM, as shown in Fig. 16. The coefficient of each LG mode in the decomposition can be complex, containing both amplitude and phase information. Therefore, one can control the amplitude and phase shift for each LG mode, and coherently combine all modes to generate a structured beam that performs the desired function.

ACCEPTED MANUSCRIPT
APL Photonics
This is the author's peer reviewed, accepted manuscript. However, the online version of record will be different from this version once it has been copyedited and typeset.
PLEASE CITE THIS ARTICLE AS DOI:10.1063/5.0031230
AIP Publishing

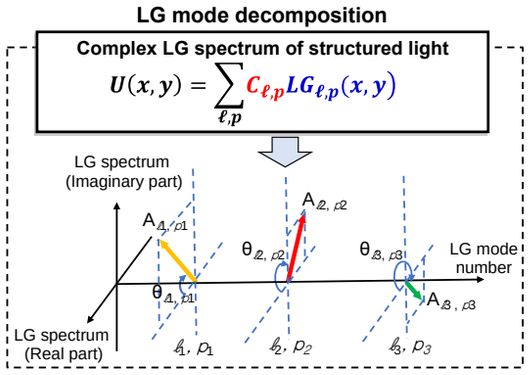

FIG. 16 The concept of the LG mode decomposition and the complex LG spectrum. A structured beam can be decomposed into a set of LG modes that carry OAM. The complex coefficient, i.e., each element of the complex LG spectrum, can be calculated using the overlapped integral between the electric fields of the structured beam and each LG mode. We can control the amplitude (A) and phase shift ($\boldsymbol{\theta}$) for each LG mode, and coherently combine all modes to generate a structured beam.

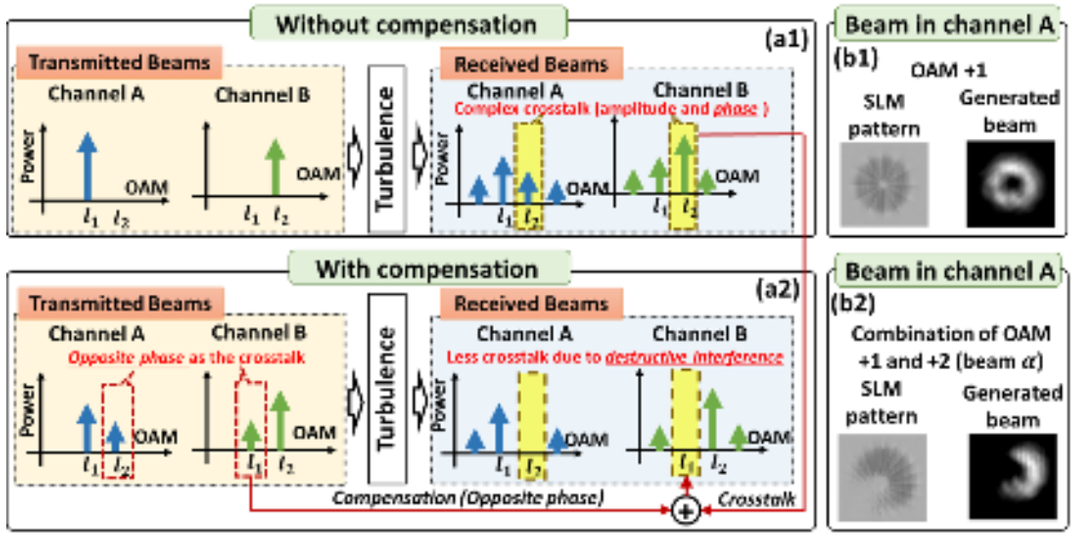

FIG. 17 (a) The concept of the turbulence compensation utilizing the inverse transmission matrix method: (a1) transmitting pure OAM modes without applying the compensation approach; and (a2) transmitting the combination of OAM modes while compensating for the turbulence effects. (b) An example of the SLM patterns and the generated beams intensity profiles in the cases of transmission (b1) without compensation and (b2) with compensation. (© 2020 Optical Society of America)

An optical turbulence mitigation approach based on mode combination has been recently demonstrated[56]. The experimental results for a 200-Gbit/s two-OAM-multiplexed links showed that the inter-channel crosstalk could be reduced by > 10 dB. The concept of turbulence compensation using mode combination is illustrated in Fig. 17 (a). At the transmitter side, the inverse transmission matrix is applied using a compensation phase pattern at the transmitter for each channel, which results in the signal from each transmitted channel being carried by the combination of multiple (e.g., 2) OAM modes with designed complex weights. The weights are calculated based on the inverse of the complex transmission matrix under the corresponding turbulence realization, and such combinations of OAM modes could perform the inverse function of turbulence-induced crosstalk. When the beams from the two channels are transmitted through the turbulence, the signals on the two transmitted modes will couple to their neighboring modes and experience coherent interference on those modes. Therefore, the channels could have little power on the designated modes due to their destructive interference and relatively high power on the others. By receiving the mode on which the undesired channel has little power, the desired channel can be recovered with little inter-channel crosstalk. The same concept can be applied to recover the second channel when receiving another mode. As an example, the compensation phase patterns used for beam generation in channel A and the intensity profiles of the generated beams are shown in Fig. 17 (b).

This approach was demonstrated for two-OAM (l = +1 and l = +2) multiplexed channels each carrying a 100-Gbit/s QPSK signal[56]. When the compensation approach was applied, the transmitted channels A and B carried beams α and β, respectively, which were combinations of OAM l = +1 and l = +2. The receivers for channels A and B recovered the signals on OAM modes l = +1 and l = +2, respectively. The results of this demonstration are shown in Fig. 18. The back-to-back case is illustrated in Fig. 18 (a1). As

ACCEPTED MANUSCRIPT
APL Photonics
This is the author's peer reviewed, accepted manuscript. However, the online version of record will be different from this version once it has been copyedited and typeset.
PLEASE CITE THIS ARTICLE AS DOI:10.1063/5.0031230
AIP Publishing

shown in Fig. 18(a2), with the turbulence effect, the inter-channel crosstalk increases to −8.7 dB and −5.5 dB for channels A and B, respectively, in the absence of the compensation, and this crosstalk decreases to −22.1 dB and −17.8 dB for the two channels with the compensation. The bit error rate (BER) performance for the channels is shown in Fig. 18(b). By applying pre-compensation phase patterns in the link, the BER performance can be improved. These results indicate that transmitting a combination of multiple OAM modes with designed mode weights instead of a single OAM mode could improve the performance of an OAM-multiplexed link by reducing the crosstalk.

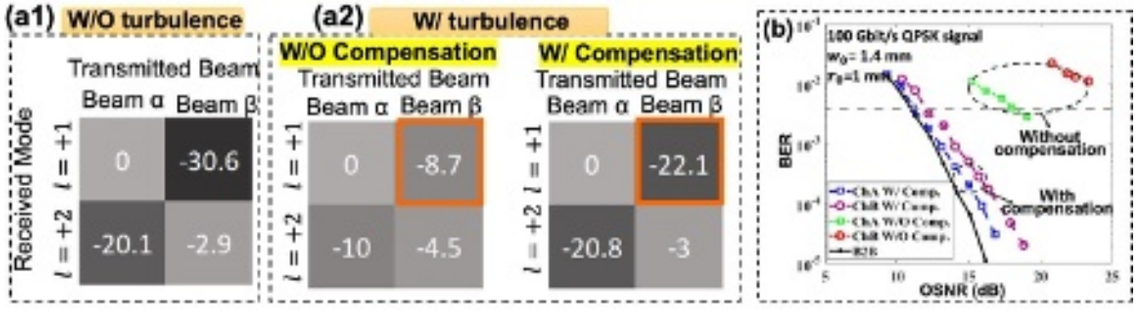

FIG. 18 (a1, a2) The measured, normalized transmission intensity matrices and (b) BER measurements for the channels without and with compensation. In the demonstration, channel A receives OAM l = +1, while channel B receives OAM l = +2. In the link without compensation, channels A and B transmit OAM l = +1 and l = +2, respectively. Beam α and β are the combinations of OAM +1 and +2 transmitted by channels A and B, respectively, when the compensation is applied. (© 2020 Optical Society of America)

In addition, the mode-combination-based approach was also utilized to mitigate the effect of the limited-size aperture or a misalignment in an MDM link[43]. This can be achieved by transmitting each data channel on a combination of multiple LG modes, as shown in Fig. 19(a). The complex transmission matrix **H** of the link can be factorized by singular value decomposition (SVD) and written as $\mathbf{H} = \mathbf{U} \cdot \sum \cdot \mathbf{V}^*$. At the transmitter side, the orthogonal beams are generated by using complex combinations of multiple LG modes, of which the complex weights (amplitude and phase) are given by the orthogonal column vectors of **V**. After passing through a given link (**H**) with a limited-size aperture or misalignments, the resulting beams on different channels would still be mutually orthogonal. Such beams are composed of multiple LG modes, the complex weights of which are the orthogonal row vectors multiplied by singular values in the matrix $\sum$. These resulting beams are still orthogonal to each other, and thus can be demultiplexed with little crosstalk based on the orthogonal row vectors of the inversed **U** matrix (Fig. 19(b)). Besides the orthogonalization, intensity profiles of the transmitted beams would also be spatially shaped, which might simultaneously reduce the power loss caused by the limited-size aperture or the misalignment.

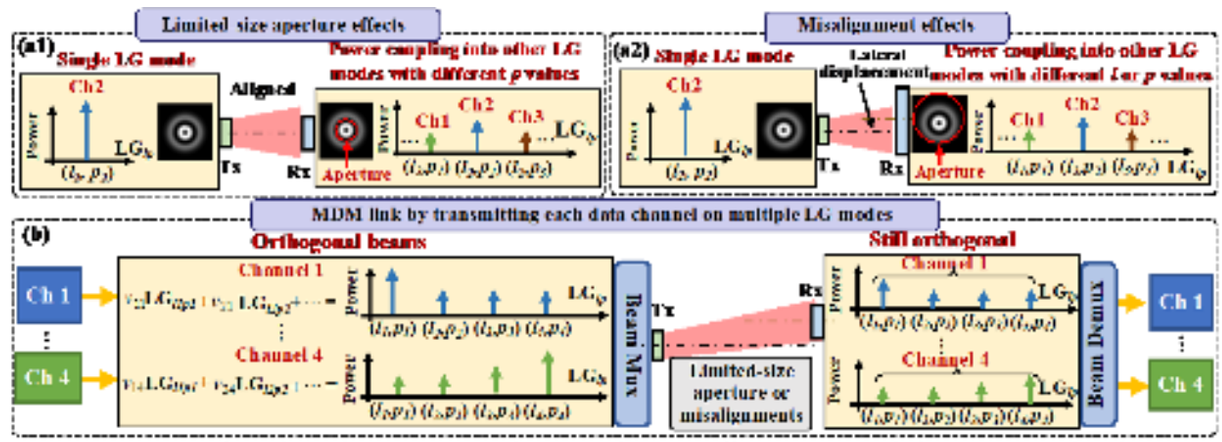

FIG. 19 (a) Concept of (a1) limited-size aperture and (a2) misalignment effects on an FSO link using LG modes. (b) Concept diagram of transmitting each data channel on a designed beam that is a combination of multiple LG modes to mitigate the effects of the limited-size aperture or misalignments in an MDM link. Ch: Channel; Tx: Transmitter; Rx: Receiver. (© 2020 Optical Society of America)

ACCEPTED MANUSCRIPT
APL Photonics
This is the author's peer reviewed, accepted manuscript. However, the online version of record will be different from this version once it has been copyedited and typeset.
PLEASE CITE THIS ARTICLE AS DOI:10.1063/5.0031230
AIP Publishing

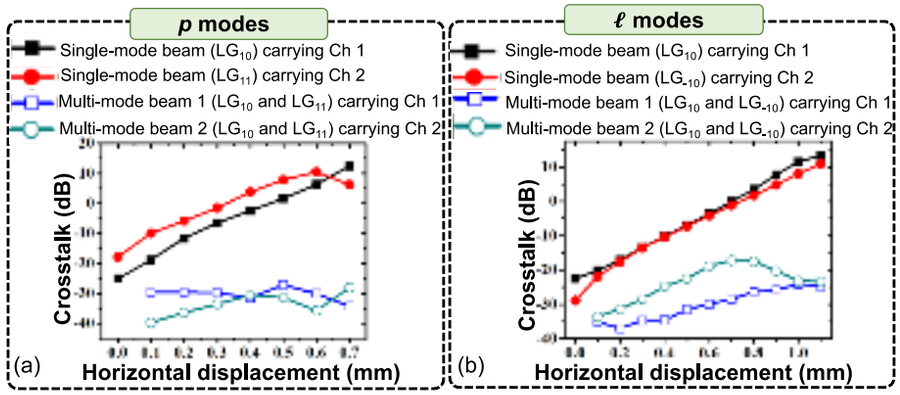

FIG. 20 Experimental results of the simultaneous orthogonalization and shaping of multiple LG beams method for crosstalk mitigation: displacement-induced channel crosstalk under various horizontal displacements when transmitting data channels on (a) pure LG modes with different p values (LG_{10}, LG_{11}) or designed orthogonal beams and (b) pure LG modes with different l values (LG_{10}, LG_{-10}) or designed orthogonal beams. (© 2020 Optical Society of America).

The above approach was experimentally demonstrated in a four-channel multiplexed link with each channel carries a 100-Gbit/s QPSK signal[43]. The results for crosstalk mitigation under horizontal displacements are shown in Fig. 20 as examples. Fig. 20(a) presents that when transmitting data channels on pure LG modes with different p values (LG_{10}, LG_{11}), the crosstalk becomes larger with an increase in the horizontal displacement. However, when using the orthogonal beams (beam 1 and 2) that are generated by using designed complex combinations of LG_{10}, LG_{11} modes, the crosstalk for both channels could be <-27 dB with the displacement. Fig. 20(b) shows the case of LG modes with different l values (LG_{10}, LG_{-10}) under various displacements. The crosstalk of (LG_{10}, or LG_{-10}) increases with the displacement, but for the designed orthogonal beams (composed of LG_{10}, LG_{-10}), it could stay at a relatively low level (<-17 dB) in association with the displacement for both channels. These results indicate that by simultaneously transmitting and receiving orthogonal beams that are composed of multiple LG modes, the performance of an LG-multiplexed link can be potentially improved.

V. OAM multiplexing for FSO airborne communications

The communication capacity needs of manned and unmanned aerial platforms have been increasing dramatically over the past several years, thereby driving the need for higher-capacity links between these platforms and their ground stations[60–63]. OAM multiplexing techniques may be utilized to increase the data capacity and spectral efficiency and to reduce the probability of interception in FSO airborne communications.

A. Challenges for OAM multiplexing for FSO airborne communications

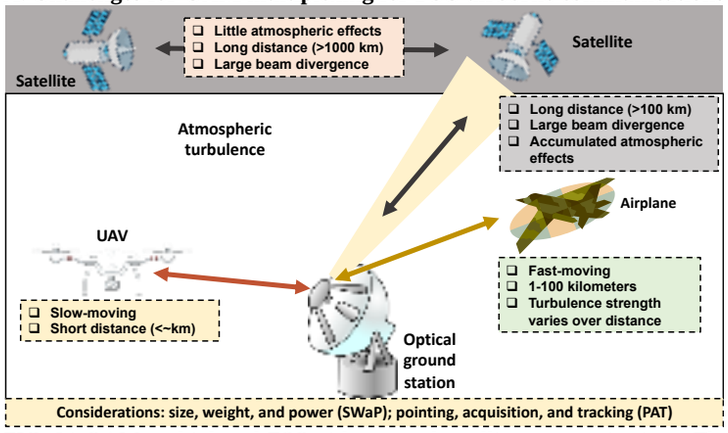

FIG. 21 OAM-multiplexed FSO airborne and satellite communications. The low size, weight and power (SWaP) considerations can be alleviated by advances in the integrated OAM devices. The pointing, acquisition and tracking (PAT) system requirements are determined by the key parameters of the FSO airborne links, such as moving speed and link distance. Moreover, the turbulence effects can degrade the system performance for long-distance links in the atmosphere.

As shown in Fig. 21, there are several scenarios in airborne and satellite FSO communications that require distinct applications and pose specific challenges including:

(i) ***Satellite-to-satellite links*** usually require ultra-long-distance beam propagation (> 1000 km) and careful control over the laser beam divergence. In such a scenario, high sensitivity of the receiver detector is desirable since only a limited proportion of the

ACCEPTED MANUSCRIPT
APL Photonics
This is the author's peer reviewed, accepted manuscript. However, the online version of record will be different from this version once it has been copyedited and typeset.
PLEASE CITE THIS ARTICLE AS DOI:10.1063/5.0031230
AIP Publishing

transmitted beam can reach the receiver[64]. Ultralong links might also necessitate extremely large apertures due to the increased beam divergence of higher order modes[64].

(ii) ***Satellite-to-ground-station links*** generally utilize a laser beam to propagate through the Earth's atmosphere and the accumulated atmospheric turbulence effects would induce severe distortion on the wavefront of the optical beam[64].

(iii) ***Airplane-to-ground links*** involve a fast-moving airplane at a distance range of ~1-100 km. Both the optical beam pointing/tracking and atmospheric turbulence effects are challenges in this scenario[65].

(iv) ***UAV-to-ground-station communications***: a relatively slow-moving unmanned-aerial-vehicle (UAV) is hovering at a distance of < kilometer away from the ground station. UAVs have drawn a lot of attention over the recent years due to their potential for proliferating numerous applications[60,66–68]. In UAV-to-ground-station communications, distances may be relatively short range and a key challenge is to miniaturize the optical hardware.

In addition, these free-space applications share some common desirable characteristics, including: (1) low size, weight and power (SWaP), which can be alleviated by advances in integrated OAM devices[69]; and (2) accurate pointing, acquisition and tracking (PAT) systems, which help limit modal coupling and crosstalk[30].

B. OAM-multiplexed communication links to and from UAV platforms

One example of the aerial platforms is the UAV, such as flying drones that are proliferating for numerous applications[60,66-68,70-72]. As the first example of OAM-multiplexed FSO airborne communications, an 80-Gbit/s OAM-multiplexed FSO link between a flying drone and a ground station was demonstrated[60]. As shown in Fig. 22, the ground station contained an OAM transmitter, an OAM receiver, and a beam tracking system. A retroreflector carried by the UAV was flown up to ~50 m away (i.e., ~100 m round trip) from the ground station to efficiently reflect the OAM beams that were emitted from the transmitter back to the receiver with little distortion.

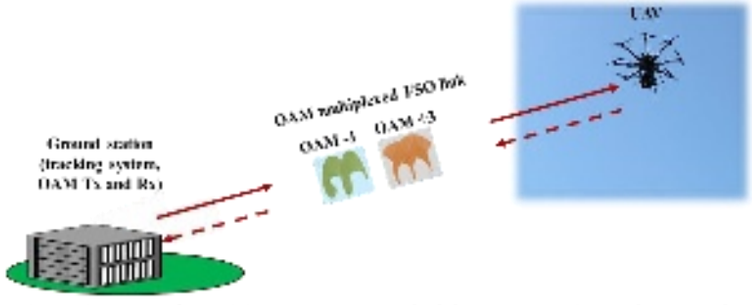

FIG. 22 Concept of an FSO communication link between a UAV and a ground station using OAM multiplexing. The ground station includes the tracking system as well as the OAM transmitter and receiver, and the UAV hovers in the air. Tx: transmitter; Rx: receiver. (© 2017 Macmillan Publishers)

As one example of misalignment issues, the effects of beam jitter on the system performance for OAM-multiplexed UAV platforms were evaluated[60]. In order to evaluate the effects of beam jitter, the statistics of the received beam centroid were measured. Fig. 24 shows the relative positions of the beam when the UAV hovers in the air ~50 m relative to the ground station and ~10 m above the ground with the tracking system on (Fig. 23(a)), moves horizontally in the air at a speed of ~0.1 m/s with the tracking system on (Fig. 23(b)), respectively. The OAM $\ell = +3$ beam was transmitted. The statistics of each scenario were obtained by continuously capturing 1000 intensity profiles of the beam over a 120-second period using an infrared camera. The beam jitter variance was ~0.09 mm^2 when the UAV was hovering and increased to ~0.46 mm^2 when moving, respectively.

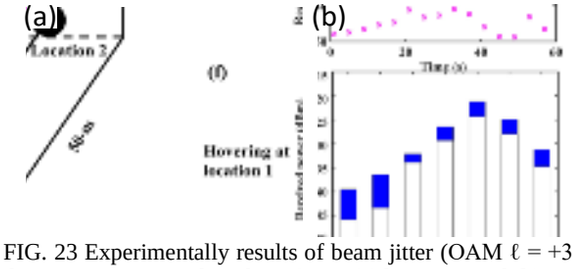

FIG. 23 Experimentally results of beam jitter (OAM $\ell = +3$ beam) in the flight environment: beam displacement with respect to the receiver center when the UAV is (a) hovering and (b) moving at a speed of ~0.1 m/s, respectively. The UAV was at a distance of ~50 m relative to the ground station and ~10 m above the ground. (© 2017 Macmillan Publishers)

C. MIMO for OAM-multiplexed UAV platforms under atmospheric turbulence effects

The atmospheric turbulence might not degrade much the performance of OAM-multiplexed UAV platforms under clean weather condition and over a short distance. However, the effects of atmospheric turbulence would be more significant as transmission

ACCEPTED MANUSCRIPT
APL Photonics
This is the author's peer reviewed, accepted manuscript. However, the online version of record will be different from this version once it has been copyedited and typeset.
PLEASE CITE THIS ARTICLE AS DOI:10.1063/5.0031230
AIP Publishing

distances increase and weather conditions become worse. Due to the stronger distortion induced by the atmospheric turbulence, the received signal carried on a particular OAM mode may include larger power of signals leaked from other channels.

To mitigate atmospheric turbulence in UAV platforms, the MIMO equalization algorithm has been demonstrated to compensate for the inter-channel crosstalk[72]. A rotatable phase plate with a pseudo-random phase distribution was added to the 100-m UAV-to-ground link (the link presented in Fig. 22) to emulate the atmospheric turbulence. A 4 × 4 adaptive MIMO equalizer was implemented in a four-channel OAM multiplexed link and each channel carried 20-Gbit/s QPSK data. Fig. 24(a) illustrates the measured 20-Gbit/s QPSK constellation diagrams and corresponding EVMs for the OAM l = +3 and l = −1 beams without and with the MIMO equalization. The MIMO equalization reduced the EVM from 32% and 54% to 26% and 27% for the OAM l = +3 and l = −1 beams, respectively. Fig. 24(b) shows BERs for both channels as functions of the transmitted power when the UAV was hovering with the phase plate fixed at a random angle. The experimental results indicate that MIMO equalization can help to mitigate the crosstalk caused by turbulence and improve both the EVM and the BER of the signal in an OAM-multiplexed link for flying platforms.

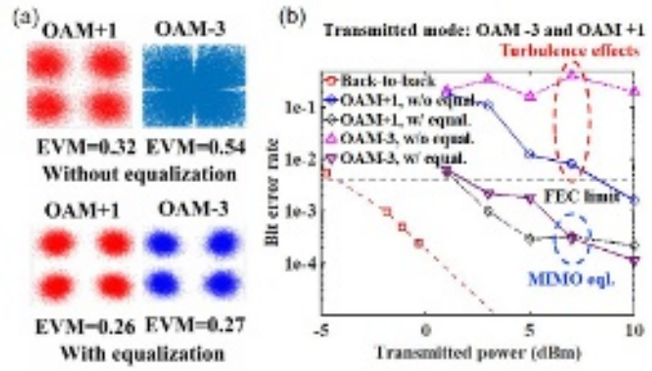

FIG. 24 (a) The measured QPSK constellation diagrams and corresponding EVMs for the OAM l = +3 and l = −1 beams without (upper line) and with (bottom line) the MIMO equalization. (b) Experimentally measured BERs for both channels as functions of transmitted power when the UAV was hovering ~50-m away under turbulence without and with the MIMO equalization. (© 2018 Optical Society of America)

D. OAM beams for optical beam tracking

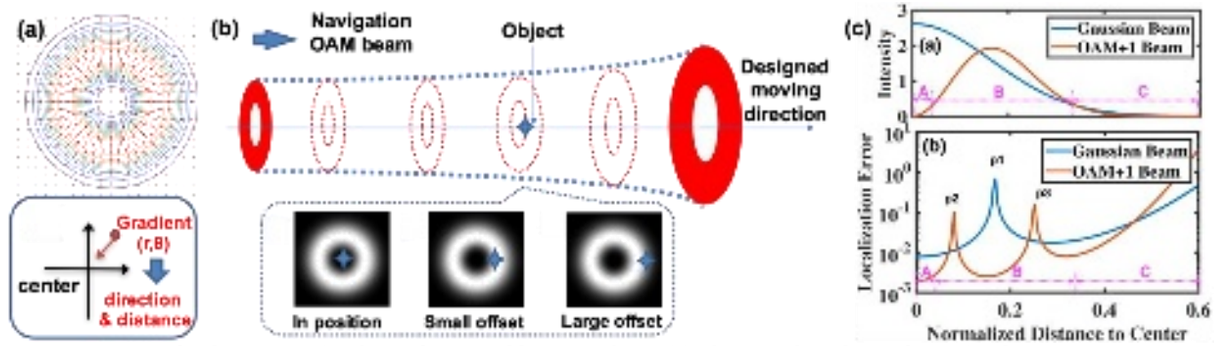

FIG. 25 Concept of utilizing an OAM beam for optical beam tracking: (a) The spatial gradient of an OAM beam as an error signal for beam tracking; (b) Concept of an OAM beam tracking and localization system; (c) Simulation results for the localization error by using the fundamental Gaussian beam and the OAM +1 beam. (© 2017 Optical Society of America)

Beam tracking is considered important for a single-beam non-OAM FSO link, where misalignment between the transmitter and the receiver leads to an increase in power loss and BER[70,73]. For OAM-multiplexed UAV platforms, beam tracking might be even more important[60]. This is because the misalignment issue not only causes power loss but also power coupling among different OAM modes, thereby increasing the inter-channel crosstalk and BER. To maintain the precise alignment between the transmitter and the receiver, a pointing, acquisition, and tracking (PAT) system is typically used in UAV platforms[60].

Beam tracking was demonstrated in single-beam non-OAM FSO links with or without using a probe beam at a separate wavelength[70,73]. Later on, beam tracking was also demonstrated in OAM-multiplexed FSO links using a Gaussian beacon. Such beam tracking systems typically utilize the displacement of the fundamental Gaussian beam as an error signal and utilize a fast-steering mirror (FSM) to correct the misalignment. As illustrated in Figs. 25(a, b), it has been proposed to use spatial gradient of

ACCEPTED MANUSCRIPT
APL Photonics
This is the author's peer reviewed, accepted manuscript. However, the online version of record will be different from this version once it has been copyedited and typeset.
PLEASE CITE THIS ARTICLE AS DOI:10.1063/5.0031230
AIP Publishing

an OAM beam as the error signal for beam tracking[74]. As presented in Fig. 25(c), when there is a displacement between the transmitter and receiver, the spatial gradient of an OAM beam can indicate the amount of displacement. Moreover, due to the unique phase and amplitude structure of an OAM beam, the spatial gradient of the OAM beams could potentially provide a low tracking error.

VI. OAM multiplexing in underwater environment

There is a growing interest in high-capacity underwater wireless communication systems for supporting the significant increase in the demand for data, such as from sensor networks, unmanned underwater vehicles, and submarines[75]. Traditionally, acoustic waves have been used for underwater communications, but this technique has quite limited bandwidth capacity[76]. Alternatively, communication using optical frequencies in the low-attenuation blue-green region can enable higher-capacity underwater transmission links due to the much higher carrier-wave frequency[77].

A. Propagation effects in underwater environment

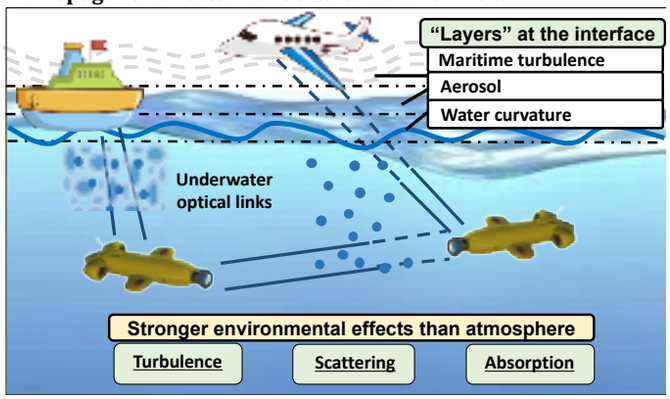

FIG. 26 Challenges in different scenarios for underwater FSO links. Environmental effects include turbulence (e.g., from water currents), scattering (e.g., from a turbid medium), and power loss due to water absorption are stronger than those in atmospheric environment. In addition, transmitting data from above the water to below the water could be an interesting challenge: the structured optical beam may pass through the inhomogeneous media surrounding the interface, including non-uniform aerosols above water, the dynamically changing geometry of the air-water interface, and bubbles/surf below the surface.

Blue-green light exhibits relatively low absorption in water, thereby potentially enabling high-capacity links with a distance of ~100 meters[77]. Note that radio waves simply do not propagate well underwater, and common underwater acoustic links have a very low bit rate. As shown in Fig. 26, maritime and underwater environments pose various challenges, including loss, turbidity, scattering, currents, and turbulence. An interesting challenge is transmitting from above water to below the water, such that the structured optical beam would pass through inhomogeneous media surrounding the interface, including nonuniform aerosols above water, the dynamically changing geometry of the air-water interface, and bubbles/surf below the surface[78-83].

There were several reports of OAM beams' propagation through turbid mediums that include water current and particle scattering effects[78,79]. For example, Fig. 27(a) shows the distorted intensity profiles of OAM beams affected by different environmental effects[79]. The effects of water current, scattering, and turbulence were emulated by using circulation pumps, adding Maalox solution to water, and creating a thermal gradient by mixing cold/hot water. When OAM beams of l = +1 and +3, and a Gaussian beam were transmitted one at a time, it was observed that:

(i) ***In tap water***: the ring-shaped intensity profiles of the OAM beams tend to be maintained after ~ 1-m propagation and are slightly distorted by the water current[79].

(ii) ***With scattering***: there was a small, time-varying change in the intensity profiles, which might be a result of the natural dynamic diffusive movement of the small particles contained in the water[79].

(iii) ***With water current or turbulence***: phase distortion became stronger, such that the phasefront of the OAM beam was distorted[79].

Besides the transmission of a single vortex beam, another work explored the utilization of spatial profiles generated by the coherent combination of multiple concentric optical vortices in the underwater environment[75]. This approach provides an alternative way for utilizing OAM modes in the underwater environment. The intensity profiles of the combinations of concentric optical vortices are presented in Fig. 27(b). Due to the interference between concentric vortices, the resulting beam has a periodic constructive and destructive interference around the center of the beam, i.e., a "petal" pattern. The results show that the "petal" pattern experiences little distortion when the beams propagate through clear water. However, after propagating through turbid water, the intensity profiles of the beams are distorted due to the scattering effects.

ACCEPTED MANUSCRIPT
APL Photonics
This is the author's peer reviewed, accepted manuscript. However, the online version of record will be different from this version once it has been copyedited and typeset.
PLEASE CITE THIS ARTICLE AS DOI:10.1063/5.0031230
AIP Publishing

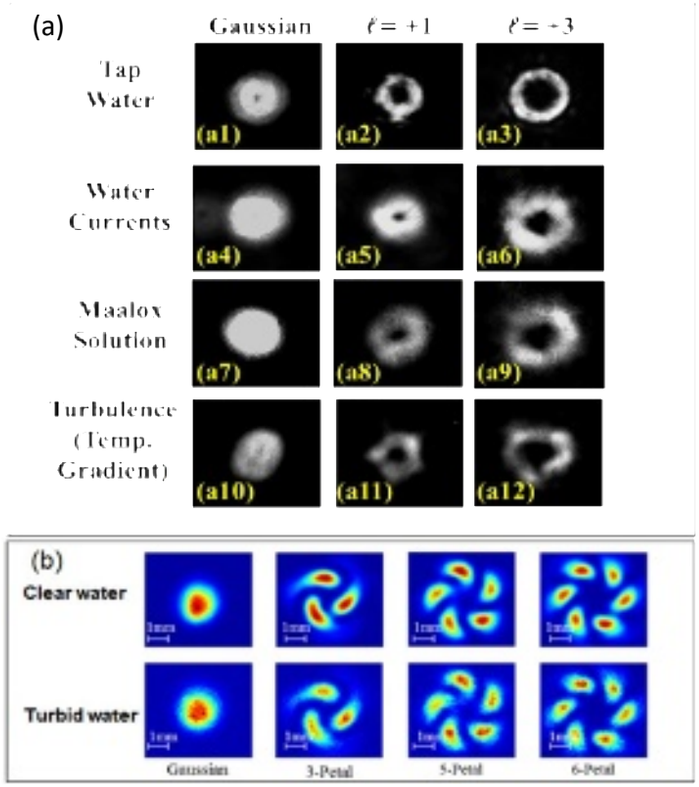

FIG. 27 (a) Measured intensity profiles of OAM beams under various channel degradation effects: (a1-a3) with only tap water, (a4-a6) with water currents, (a7-a9) with the Maalox solution, and (a10-a12) with thermal gradient-induced turbulence. (b) Experimentally measured intensity profiles for the combinations of concentric optical vortices after propagation in clear water (upper line) and turbid water (bottom line). (© 2016 Naval Institute Press) (© 2016 Nature Research)

B. OAM-multiplexed links in underwater environment

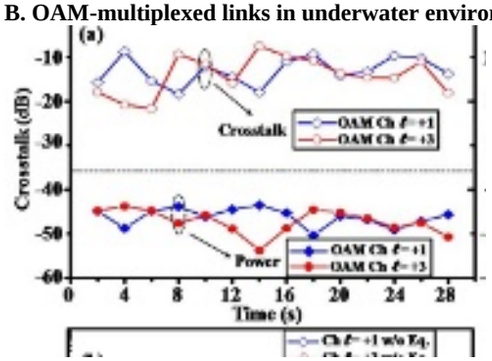

FIG. 28 Experimental results: BER curves of OAM channel l=+1 and l=+3 with and without CMA equalization, each OAM beam carries a 10-Gbit/s on-off keying signal. Thermally induced refractive index inhomogeneity in water causes the BER to reach an error floor. With CMA equalization, BERs improve significantly and are below the FEC limit. Ch.: channel. Eq.: equalization. (© 2016 Nature Research)

In the previous session, we describe propagation effects of OAM-carrying beams in underwater environment. We will present examples of OAM-multiplexed communication links in underwater environment considering the above-discussed effects in this session. For underwater environments there have been several reports on blue-green light non-OAM links with a single-beam and a distance of ~100 meters[77]. To further increase the data capacity in underwater environment, blue-green light OAM-multiplexed links were demonstrated over a few meters in an emulated underwater environment[78,79,83]. A direct way to modulate a blue-green light is to use an internal modulation. For example, by directly modulating the driving current of a 520 nm laser diode, a 1-Gbit/s signal was produced[79]. However, due to the limited bandwidth of the internal modulation of the commercially available laser diodes, the maximal data rate of the green beam was ~1 Gbit/s. To achieve larger data rates in underwater environment, a high-speed modulated light at a lower frequency can be wavelength converted to blue-green light by using second harmonic generation. For

ACCEPTED MANUSCRIPT
APL Photonics
This is the author's peer reviewed, accepted manuscript. However, the online version of record will be different from this version once it has been copyedited and typeset.
PLEASE CITE THIS ARTICLE AS DOI:10.1063/5.0031230
AIP Publishing

example, by using a 10-Gbit/s 1064-nm lithium niobite modulator and a frequency-doubling module, a 10-Gbit/s signal was generated, and the carrier wavelength was converted from 1064 nm to 532 nm[79].

Figure 28 presents the average BER of the channels on the OAM +1 and +3 beams with and without equalization, with each OAM beams carrying a 10-Gbit/s on-off keying signal[79]. To mitigate the thermal-gradient-induced crosstalk in water, the constant modulus algorithm (CMA) equalization is implemented in the DSP. The measured BERs were averaged over one minute of data for two OAM channels ($\ell = +1$ and $+3$) before and after applying the CMA equalization. Due to inter-channel crosstalk, the measured BER curves without 2×2 equalization reached a BER error floor. With the CMA equalization, the BER performance is improved and could reach below the forward error correction (FEC) limit[79]. We note that FEC limit is a BER upper limit under which the FEC method can be performed when coding the channel that can control the errors over unreliable or noisy communication channels.

VII. Novel beams

This section is for the completeness of this review paper besides the discussions for free-space communications. The excitement in the field of novel beams originated by the ability to utilize orthogonal structured optical beams. However, there is much work in the fields of optics and photonics on several types of novel variations of optical beams (e.g., Airy and Bessel types), with more being explored at an exciting pace.

Over the next several years, it would not be surprising if novel beams are used to minimize certain system degrading effects. There have been initial results for some of these concepts, but a partial "wish list" for novel beams could be beams:

(i) that are more resilient to the modal coupling caused by turbulence and turbidity.
(ii) that have limited divergence in free space.
(iii) that are resilient to partial obstruction, such that their phase structure can "self-heal" (e.g., Bessel-type beams).
(iv) whose phase structure can readily be recovered even if the transmitter and receiver are misaligned.

Generally, FSO communication links rely on the line-of-sight (LOS) operation, thus, the obstructions in the beam path are one of the potential challenges. In particular, for OAM communication links that are partially blocked, an OAM beam will produce distortions in its beam profile. This will reduce the orthogonality between the different OAM beams and cause power coupling from the desired OAM mode to neighboring OAM modes, thereby leading to signal fading and channel crosstalk. As one example, Bessel-Gaussian (BG) beams have displayed the unique property to reconstruct or "self-heal" the transverse intensity and phase profiles after experiencing an obstruction. The self-healing property of BG beams is due to the delocalized transport of the beam energy and momentum, which can replace the scattered light by the obstructions[84]. As another example of novel beams, the Airy beam has unique properties including being non-diffracting, self-bending, and self-healing[85]. Due to its curved parabolic trajectory, the Airy beam has been demonstrated to be able to circumvent obstacles in an FSO interconnection link[86-88].

As one example of approximations to true Bessel beams, BG beams are non-diffractive and self-healing over a limited Bessel-range. The self-healing property of the BG beams was utilized to mitigate the degrading effect due to obstruction in short-range FSO OAM communication links[89]. As shown in Fig. 29(a), *N* OAM beams, each carrying a distinct data channel, are spatially multiplexed and transmitted through an axicon to be transformed into BG beams. Within the Bessel-region, the beams are propagation invariant and, therefore, can sustain partial obstructions. At the end of the Bessel-region, an exit axicon that has opposite cone angles is placed to remove the conical phases. Finally, an OAM mode demultiplexer separates each OAM beam. In the experiment, two OAM-multiplexed channels (OAM $l = +1$ and $l = +3$), each carrying 100-Gbit/s QPSK signals were transmitted through a path with obstructions[89]. As an example, the transverse intensity profiles of the obstructed and unobstructed BG beam with $l = +3$ are presented in Fig. 29(b). An obstruction was placed at the beam center, and images of the transverse intensity profiles were taken at various locations along the propagation direction. A comparison between the obstructed and unobstructed beams in the plane of the demultiplexer revealed the self-healing property of the BG beam. Fig. 29(c) illustrates the BER measurement for the unobstructed and obstructed BG beams. Both channels achieve BERs below the FEC limit.

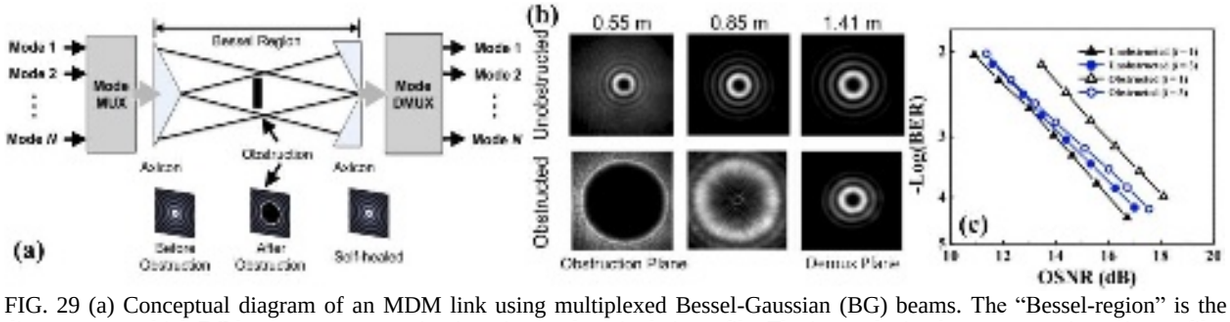

FIG. 29 (a) Conceptual diagram of an MDM link using multiplexed Bessel-Gaussian (BG) beams. The "Bessel-region" is the distance over which BG beams are propagation invariant and retain their profile. The insets depict the transverse intensity profiles of a BG beam before and after being obstructed by an opaque disk and in the receiver plane. (b) Measured transverse intensity

ACCEPTED MANUSCRIPT
APL Photonics
This is the author's peer reviewed, accepted manuscript. However, the online version of record will be different from this version once it has been copyedited and typeset.
PLEASE CITE THIS ARTICLE AS DOI: 10.1063/5.0031230
AIP Publishing

profiles of the obstructed and unobstructed BG beam $l = +3$ after an obstruction of radius 1.5 mm at different locations along the propagation direction. (c) Measured BER for the multiplexed BG beams obstructed by obstructions of radii r_{obs} = 1 mm. (© 2016 Nature Research)

VIII. Utilizing OAM in quantum systems

In the case of a quantum communication system, an individual photon can carry one of many different OAM values; this is similar to digital data taking on one of many different amplitude values and enables OAM-based encoding in quantum systems. If each photon can be encoded with a specific OAM value from *M* possibilities, the photon efficiency in bits/photon can be increased. This has the potential to be quite useful for quantum communication systems which are typically photon "starved" and for which qubits can commonly be encoded on one of only two orthogonal polarization states[90-94]. Figure 30 presents the concept of the OAM-based quantum encoding. Using an OAM mode converter, within each symbol period the coming single Gaussian photon is converted to the respective OAM photon and occupies one of the *M* OAM states. Each photon has a helical phasefront after being processed by the OAM converter. The accumulated intensity structure indicates that it has a ring-like intensity probability distribution[90].

A larger alphabet for each qubit is, in general, highly desirable for enhancing system performance. However, there is much research needed to overcome the challenges in fielding an OAM-encoded quantum communication system, such as: (i) mitigating coupling among orthogonal states, and (ii) developing transmitters that can be tuned rapidly to encode each photon on one of many modes.

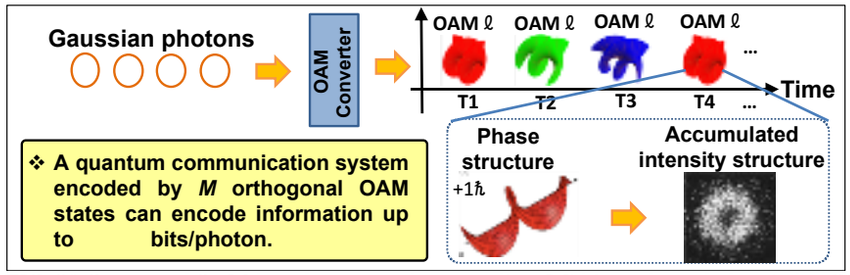

FIG. 30 Concept of OAM-based quantum data encoding. Within each symbol period, a Gaussian photon is converted to one of the M OAM states, resulting in information encoding of up to $\log_2 M$ bit/photon. The accumulated intensity structure image is recorded using a single-photon-sensitivity, low-noise intensified charge coupled device camera[90].

A. AO for quantum OAM encoding systems

Similar to OAM based classical FSO communication links, the system performance degradation due to the atmospheric turbulence is a key challenge also for OAM-based quantum FSO links. Turbulence affects the phasefront of the photon, and thereby, increases the intermodal crosstalk in the quantum communication system.

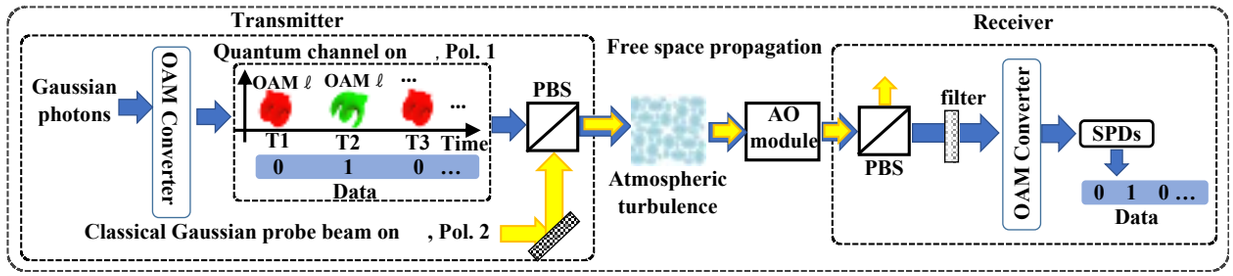

FIG. 31 The concept diagram of an OAM-encoded, FSO quantum communication link through atmospheric turbulence with AO compensation. A classical Gaussian probe beam is transmitted coaxially with the quantum channel for the phase detection in the AO module. The probe beam and the quantum channel have different wavelength, polarization and OAM orders for the efficient separation at the receiver side. SPD: single photon detector; Pol.: polarization; AO: adaptive optics; PBS: polarizing beam splitter.

In order to mitigate the turbulence effect, the AO approach can be applied to OAM-encoded quantum communication links by using a classical Gaussian probe beam (i.e., OAM $\ell = 0$) for the phase detection on a wavefront sensor. As shown in Fig. 31, the AO approach was demonstrated for the compensation of emulated turbulence in an OAM-encoded, FSO quantum communication link at a transmitted rate of 10 Mbit/s[93]. The quantum channel and the classical Gaussian probe beam propagate coaxially through the emulated atmospheric turbulence. Using the distortion information gathered from the classical Gaussian probe beam, the AO system compensates the turbulence effects on the received channel and mitigates the distortion on the OAM-carrying photons. Due to the large power difference between the quantum channel and the classical probe beam (the power of the quantum channel is ~100 dB lower than that of the classical probe beam), one may need to transmit the probe beam with different polarization, wavelength, and OAM order compared to the quantum channel in order to efficiently separate the classical probe beam from the quantum channel at the receiver side.

ACCEPTED MANUSCRIPT
APL Photonics
This is the author's peer reviewed, accepted manuscript. However, the online version of record will be different from this version once it has been copyedited and typeset.
PLEASE CITE THIS ARTICLE AS DOI:10.1063/5.0031230
AIP Publishing

Figure 32 shows the channel transfer matrices (top figures) when sending OAM modes $\{\ell = -3, \ldots, +3\}$ one by one, as well as the photon count ratio (bottom figures) on the received OAM modes (i.e., the ratio of the received photons on the desired OAM modes to the total received photons) when sending only OAM $\ell = 1$ photons in different cases: (from left to right) the back-to-back link (i) without probe and (ii) with the probe, under atmospheric turbulence distortion (iii) without probe, and (iv) with the probe and without AO mitigation, and (v) with the probe and with AO mitigation. Turbulence-induced distortion to the wavefront of OAM-carrying photons increases the probability of OAM photons existing in the undesired orders. Photons are better confined to their desired OAM orders with AO mitigation[93].

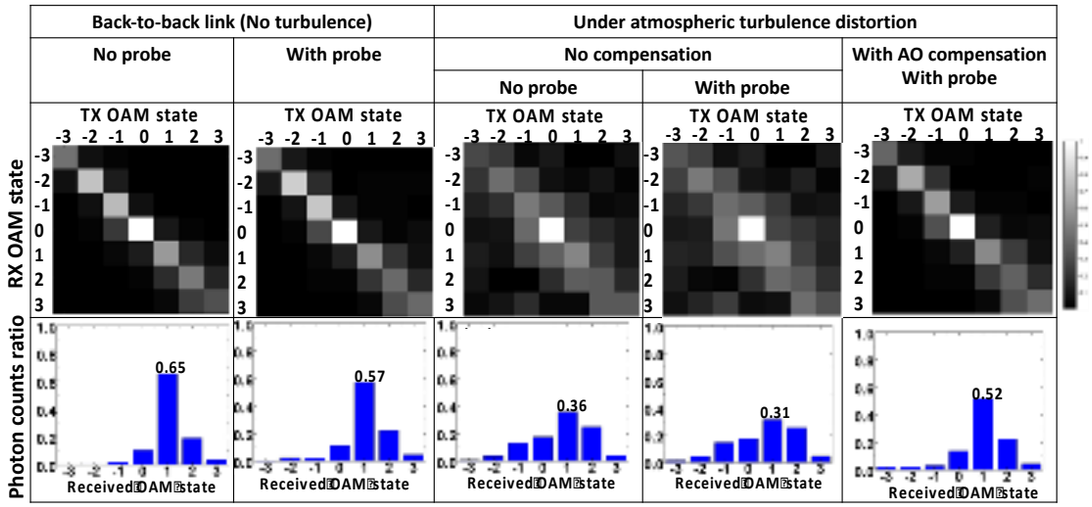

FIG. 32 Experimental results: The performance of AO mitigation in an OAM-based quantum link. (Upper line) Channel transfer matrices when sending OAM modes $\{\ell = -3, \ldots, +3\}$, respectively, for different cases. The numbers are measured in the quantum domain as the ratio of the measured photon counts to the maximum photon counts in this matrix in a unit of dB. (Lower line) The photon counts ratio on received OAM modes $\{\ell = -3, \ldots, +3\}$ when sending only OAM $\ell = 1$ photons for different cases. TX: transmitter; RX: receiver. (© 2019 American Association for the Advancement of Science).

B. OAM-based quantum key distribution

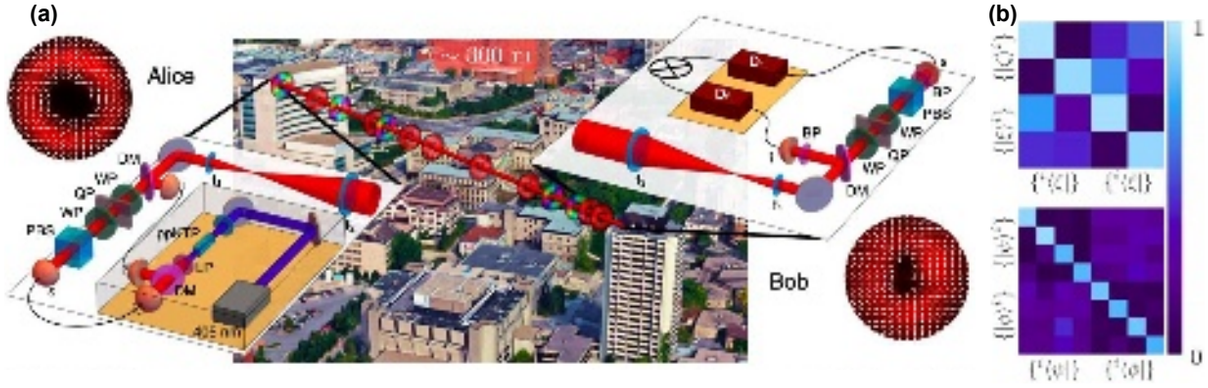

FIG. 33 The 300-m intracity quantum communication link in Ottawa. (a) The schematic diagram of the sender (left) with a single-photon source and Alice's quantum state preparation setup. Alice prepares a state from the OAM modal set or vector modal set using a polarization beam splitter (PBS), wave plates (WP), and a q-plate (QP). Bob, the receiver (right), can perform measurements on the sent states and record the coincidences between the signal and idler photons with detectors D_1 and D_2 in a coincidence logic box. (b) The measured probability-of-detection matrices give quantum bit error rates of 5% and 11% for two and four dimensions, respectively. (© 2017 Optical Society of America)

Quantum cryptography, such as the quantum key distribution (QKD), can be utilized to build secure communication links between many parties. There have been reports of the demonstration of such systems in polarization-based optical systems[95–98]. As another degree of freedom, the OAM state of the light has the potential to enable QKD schemes using a higher-dimensional encoding scheme[99-102]. Fig. 33(a) presents the concept of utilizing high-dimensional OAM-based QKD in a ~300-m FSO quantum communication link[103]. Two sets of mutually unbiased bases (MUBs) including two vector modes and two OAM modes were

ACCEPTED MANUSCRIPT
APL Photonics
This is the author's peer reviewed, accepted manuscript. However, the online version of record will be different from this version once it has been copyedited and typeset.
PLEASE CITE THIS ARTICLE AS DOI:10.1063/5.0031230
AIP Publishing

combined to form four-dimensional quantum states. The transmitter part consists of a single-photon source and the setup of Alice (i.e., transmitter) to prepare states. The receiver part consists of the single-photon detection system and Bob's (i.e., receiver) setup to measure the states. A two- or four-dimensional BB84 protocol was performed under different atmospheric conditions exhibiting moderate turbulence effects. Specifically, Alice prepares the signal photon in one of the MUB states using an appropriate sequence of wave plates and q-plates and combines these with idles photons using a polarization beam splitter (PBS) and spatially magnifies the beams. Bob used a mirrored sequence of wave plates, PBSs, lenses, and q-plates and measured the signal photon by projecting the photon onto one of the states from one of the MUBs[103]. To optimally detect the signal photon, Bob should project onto the same state that Alice sent. Probability-of-detection matrices for the quantum states (Fig. 33(b)) give quantum-bit-error-rates (QBERs) of 5% and 11% in the two- and four-dimensional protocols, respectively, which are below the respective security thresholds.

In typical QKD schemes, a classical key is shared between the two parties[95]. In the past decade, schemes for generating correlated classical keys shared among multiple parties were developed, namely the quantum secret sharing (QSS) protocols[104]. The most common candidate for the experimental implementation of single photon QSS schemes is based on the polarization of light (two dimensions)[105, 106]. A recent work demonstrated a proof-of-concept implementation of a QSS scheme using OAM states with a dimension of 11[107]. As shown in Fig. 34(a), a distributor generates a photon that is a combination of 11 OAM states. Every participant applies their unitary transformation. The final participant sends the qudit state back to the distributor who measures the state. The distributor's secret can be determined through the collaboration of the remaining participants. The detected 11-dimensional probability matrix results in Figs. 34 (b, c) indicate that OAM states offer a higher dimensionality and can be utilized for high-dimensional quantum information processes[107].

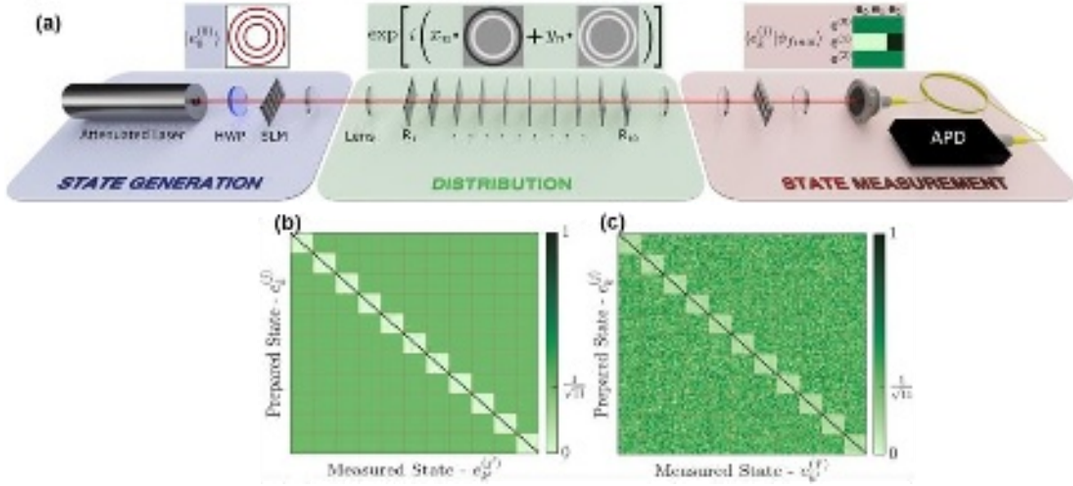

FIG. 34 (a) Conceptual approach for quantum secret sharing using perfect vortex beams, illustrated for dimension d = 3. The distributor generates a photon that comprises d number of concentric rings, with each having a different OAM value. Every participant applies their unitary transformation. The final participant transmits the qudit state back to the distributor who measures the state in the jth mutually unbiased bases, obtaining the outcome showing here as a probabilistic mode projection measurement. (b) Simulated and (c) experimentally measured $11^2 \times 11^2$ detection probability matrix for a high-dimensional quantum secret sharing experiment using 11 OAM states[107]. (© 2020 Wiley)

IX. OAM multiplexing in RF, mm-wave, and THz regimes

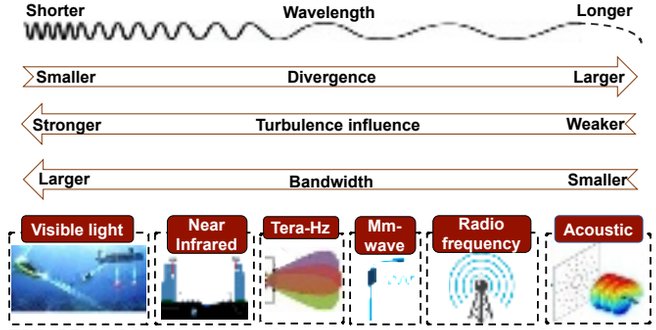

FIG. 35 OAM multiplexing for communications using different carrier-wave frequencies. The orthogonality among different OAM beams does not change with the carrier-wave frequency. Thus, OAM multiplexing can be utilized for any electromagnetic (EM)-wave communication link. EM OAM waves of different wavelengths interact with matters (e.g., propagation media) differently, and have different divergence.

ACCEPTED MANUSCRIPT
APL Photonics
This is the author's peer reviewed, accepted manuscript. However, the online version of record will be different from this version once it has been copyedited and typeset.
PLEASE CITE THIS ARTICLE AS DOI:10.1063/5.0031230
AIP Publishing

Besides using optical beams, free-space communication links can take advantage of mode multiplexing in many other carrier-wave-frequency ranges to increase the system capacity. For example, OAM can manifest in various types of electromagnetic and mechanical waves, and interesting studies have explored the use of OAM in radio frequency, millimeter, acoustic, and THz waves[8, 108–119], as shown in Fig. 35. From a system designer's perspective, there tends to be a trade-off in different frequency ranges:

(i) ***Divergence***: lower frequencies have much higher beam divergence which makes it more challenging to collect enough power of the beam to recover the data channels.

(ii) ***Interaction with matter***: lower frequencies tend to have much lower interaction with matter, such that radio waves are less affected by atmospheric turbulence induced modal coupling than optical waves.

A. OAM-multiplexed links in RF and mm-wave regimes

OAM can be carried by any EM wave with a helical wavefront, and this does not depend on the carrier-wave frequency. Therefore, OAM multiplexing for communications can be applied to the RF regime. The feasibility of using OAM beams to increase system capacity and the spectral efficiency of LOS RF communications is being actively investigated[8, 109-114].

There are exciting developments in the RF and mm-wave OAM application space, and industrial labs are increasingly engaging in R&D to significantly increase the potential capacity of fronthaul and backhaul links[8,109-114]. One proof-of-concept demonstration presented a 32-Gbit/s OAM-multiplexed link containing four OAM modes and two polarizations at a carrier-wave frequency of 28 GHz[8]. As shown in Fig. 36, four different OAM beams with $l = -3, -1, +1$, and $+3$ on each of the two polarizations were generated using spiral phase plates (SPPs) made from high-density polyethylene. Fig. 36(a) shows the horn antenna, SPP for OAM +1, and SPP for OAM +3 at the frequency of 28 GHz. Fig. 36(b) presents the observed intensity profiles for each of the beams and their interferograms with a Gaussian beam. After spatial combining using specially designed beam splitters, the resulting eight multiplexed OAM beams propagated for a distance of ~2.5 m and were separated at the receiver. All eight OAM channels, each carrying a 4-Gbit/s 16-QAM signal, were sequentially recovered, achieving a capacity of 32 Gbit/s and a spectral efficiency of approximately 16 bit/s/Hz.

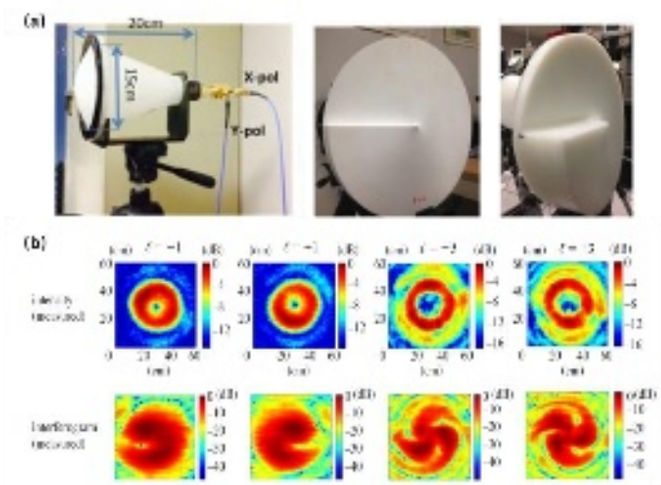

FIG. 36 A 32-Gbit/s data transmission at a 28 GHz carrier frequency by multiplexing four OAM modes and two polarizations[8]. (a) (Left to right) Horn antenna, SPP for OAM +1, and SPP for OAM +3 for generating RF OAM beams. (b) Measured intensity profiles of generated OAM beams and their interferograms. SPP: spiral phase plate. (© 2014 Macmillan Publishers)

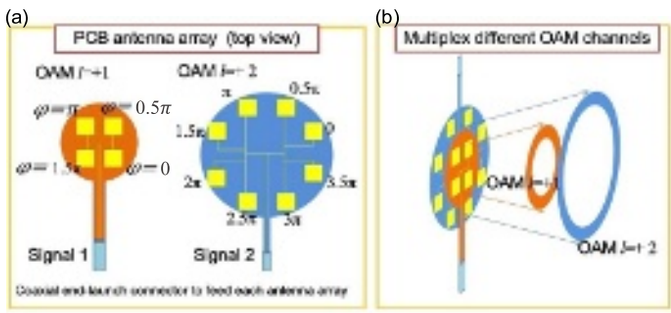

FIG. 37 Concept of using multi-layer patch antenna arrays to multiplex multiple OAM modes. (a) Top view of the stacked patch antenna fabricated on printed-circuit boards (PCBs); (b) Multiple antenna array layers are fed by independent data streams for OAM multiplexing (© 2016 IEEE)

ACCEPTED MANUSCRIPT
APL Photonics
This is the author's peer reviewed, accepted manuscript. However, the online version of record will be different from this version once it has been copyedited and typeset.
PLEASE CITE THIS ARTICLE AS DOI:10.1063/5.0031230
AIP Publishing

The demand for larger bandwidth has gained much interest in OAM-multiplexed links at higher carrier frequencies using different types of OAM generators/receivers[114, 117–125]. For example, a 32-Gbit/s wireless link using OAM and polarization multiplexing was demonstrated at a carrier frequency of 60 GHz[121]. Advances in OAM generators/receivers for higher carrier frequencies include the use of RF antenna arrays that are fabricated on printed-circuit boards (PCBs)[113]. For example, a multiantenna element ring can emit a mm-wave OAM beam by selectively exciting different antenna elements with a differential phase delay[114]. This is shown in Fig. 37(a), the antenna arrays use delay lines of different lengths to set the phase of each patch antenna element in order to generate OAM beams of different orders. Moreover, the concept could be extended to multiplex *N* OAM beams. Multiple concentric rings can be fabricated, resulting in a larger number of multiplexed OAM beams[111, 112]. As presented in Fig. 37(b), multiple antenna array layers can be stacked at the same center for multiplexing when each layer is fed by an independent data stream and emits different OAM beams.

B. OAM-multiplexed links in the THz regime

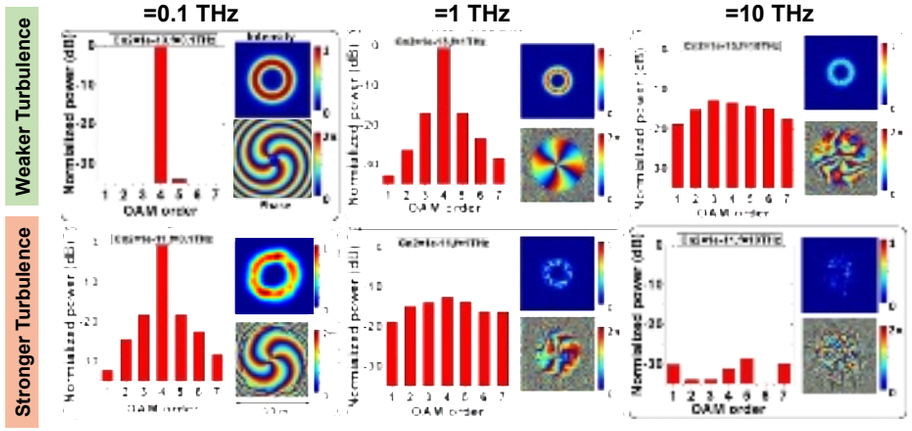

FIG. 38 Simulation results: normalized power distribution, intensity profile and phase profile for different THz OAM modes when transmitting OAM +4 with the same beam waist w_0 = 1 m through a 1-km link. Upper row: weaker turbulence with $C_n^2 = 1 \times 10^{-13}$ m$^{-2/3}$; Lower row: stronger turbulence with $C_n^2 = 1 \times 10^{-11}$ m$^{-2/3}$. C_n^2: atmospheric structure constant. Results of different frequencies (from left to right: f = 0.1 THz, 1 THz, and 10 THz) are presented. (© 2019 IEEE)

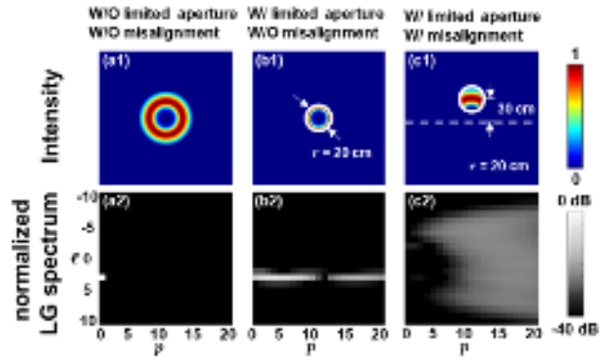

FIG. 39 Simulation results: intensity profiles and normalized 2-D LG spectra of THz OAM beams (a) without the influence of limited aperture size or misalignment, (b) with a limited aperture size of 20 cm in radius and (c) with a limited aperture size of 20-cm radius and a 30-cm misalignment, when transmitting OAM +3 with the beam waist w_0 = 5 cm through a 40-m link. A limited-size aperture would induce modal power coupling to high-order p modes and misalignment would induce modal power coupling to both neighboring ℓ and p modes. (© 2020 IEEE)

The demand for larger channel bandwidths has also created interest in communication systems using THz carrier waves. There is a transmission window with a low atmospheric absorption loss between 200 GHz and 300 GHz, and research has focused on non-OAM communication links in this region. Since OAM multiplexing could further increase the capacity of communication links, it might be valuable to explore THz OAM-multiplexed links.

Since the wavelength of a THz wave is shorter than that of a mm-wave but longer than that of an optical wave, both divergence and turbulence effects might degrade THz OAM links. The fundamental system degrading effects for THz wireless communication links using multiple OAM beams were investigated in simulation[125]. Simulation results in Fig. 38 show that the 0.1-THz OAM beam is distorted only a little bit under strong turbulence (Fig. 38, left panel), while the 1-THz OAM beam experiences a large

ACCEPTED MANUSCRIPT
APL Photonics
This is the author's peer reviewed, accepted manuscript. However, the online version of record will be different from this version once it has been copyedited and typeset.
PLEASE CITE THIS ARTICLE AS DOI:10.1063/5.0031230
AIP Publishing

distortion effect (Figs. 38, middle panel). The 10-THz OAM beam is strongly distorted even under weak turbulence (Fig. 38, right panel). A higher frequency leads to higher power leakage to neighboring modes[28, 125].

The effects of limited-size aperture and misalignment are also investigated by simulation in the THz range[126]. 2-D LG modal decomposition is used to analyze the modal coupling induced by both effects. As Fig. 39(b) shows, the limited aperture causes modal coupling to high-order *p* modes, possibly because the limited-size aperture truncates the beam in the radial direction, but has little influence in the azimuthal direction, so that there is little power coupled to neighboring ℓ modes. However, with the misalignment effect, the beam profile is distorted in both the radial and azimuthal direction, and the simulation results show a modal coupling to both neighboring ℓ and *p* modes (Fig. 39(c)).

C. OAM multiplexing combined with conventional spatial multiplexing

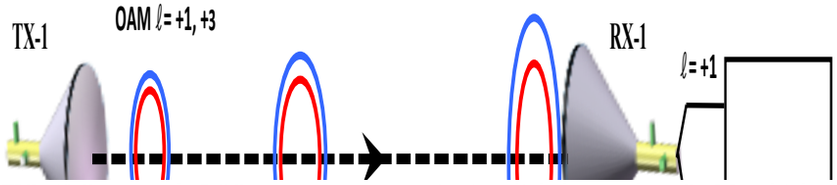

FIG. 40 Concept of a LOS, mm-wave communications link that employs OAM multiplexing over conventional spatial multiplexing. The system consists of two transmitter/receiver apertures, with each transmitter aperture containing two OAM modes. At the receiver, Rx-1(or Rx-2) could receive power from all four OAM modes from the two transmitters, where the power from the two OAM modes transmitted from Tx-2 (or Tx-1) induces crosstalk. Tx: transmitter; Rx: receiver. (© 2017 IEEE)

In general, conventional spatial multiplexing includes multiple spatially separated transmitter/receiver antennas, and the inter-channel crosstalk can be reduced by using MIMO signal processing[127,128]. In comparison, OAM multiplexing employs a pair of transmitter and receiver, and the modal orthogonality among the OAM beams enables little inter-channel crosstalk and efficient (de)multiplexing without signal processing[109,110,129]. A recent work demonstrated the combining of both these two spatial multiplexing techniques to further enhance the system capacity[129]. A 16-Gbit/s mm-wave communication link at 28 GHz using OAM multiplexing combined with conventional spatial multiplexing was demonstrated over a distance of 1.8 meter in the laboratory. Fig. 40 illustrates the combined system configuration containing 2 × 2 antenna apertures. Specifically, each transmitter aperture transmits 2 coaxial OAM beams l = +1 and l = +3, with each carrying a 4-Gbit/s data stream. A 2 × 2 MIMO-based signal processing was used at the receiver to reduce the inter-channel crosstalk. Figs. 41(a, b) show the comparison of the BER performance without and with the MIMO equalization processing. The measured BER curves dropped down and reached below the FEC limit after the MIMO processing.

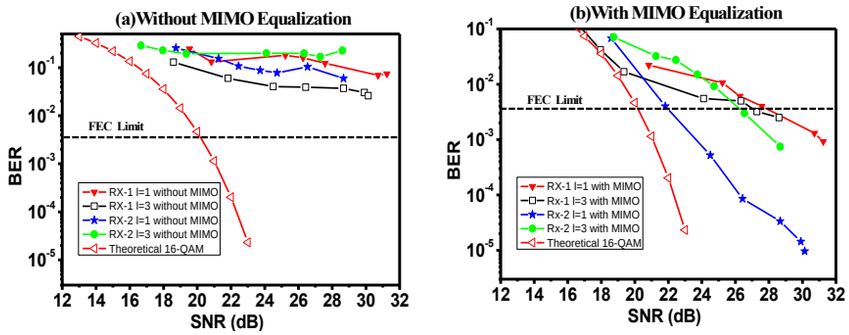

FIG. 41 BER measurements of OAM and MIMO communications (a) without MIMO: BERs were all above the FEC limit, exhibiting the error-floor phenomenon; and (b) with MIMO: BERs for all four OAM channels decreased to be below the FEC limit. (© 2017 IEEE)

A more recent work demonstrated the combination of OAM multiplexing and conventional spatial multiplexing using multiple concentric uniform circular antenna arrays (UCAs) at 28 GHz[130]. As shown in Fig. 42 (a), the UCAs consist of 4 concentric antenna arrays (16 antennas/array) for OAM generation and a single antenna at the center. Each UCA can concurrently transmit or receive five OAM mode signals (0, ±1, ±2) carrying five independent data streams[131]. Thus, the UCAs could support the transmission of 21 data streams in total. At the receiver, another UCAs were utilized to select different OAM modes and receive the multiplexed data channels. Combinations of 16-QAM and 64-QAM with various low-density parity check channel coding rates for FEC successfully yielded a 100-Gbit/s data rate in a wireless communication link over a distance of 10 meters, the setup is shown in Fig. 42(b). Moreover, a more recent work reported a 100-Gbit/s 100-m link by combining OAM multiplexing and polarization multiplexing at 40 GHz frequency band[132].

ACCEPTED MANUSCRIPT
APL Photonics
This is the author's peer reviewed, accepted manuscript. However, the online version of record will be different from this version once it has been copyedited and typeset.
PLEASE CITE THIS ARTICLE AS DOI:10.1063/5.0031230
AIP Publishing

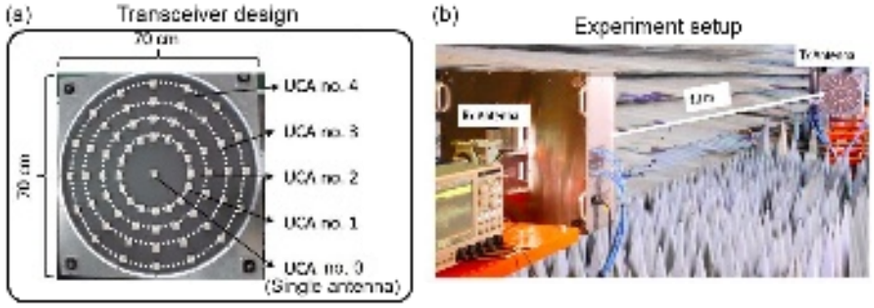

FIG. 42 (a) The structure of multiple concentric uniform circular antenna (UCA) arrays, with each array transmitting and receiving five OAM modes. (b) Experimental setup of a 10-m link using the combination of OAM multiplexing and conventional spatial multiplexing. (©IEEE 2018)

X. OAM in fiber

This section is for the completeness of this review paper besides the discussions for free-space communications. MDM can be implemented in both free-space and fiber, with much of the transmitter and receiver technology being similar. However, the channel medium is different, which gives rise to the following distinctions:

(i) There is no beam divergence in a light-guiding fiber.

(ii) Fiber has inhomogeneities, and coupling can occur among modes, either within a single mode group or between different mode groups, thereby creating deleterious inter-channel crosstalk[5, 133, 134].

The excitement around using MDM for capacity increase originally occurred primarily in the fiber transmission world, especially in research laboratories[16, 19, 135-140]. There were several reports of using linearly polarized (LP) modes as the modal set in fiber. However, since there was significant modal crosstalk when propagating through conventional- central-core few-mode fiber (FMF), MIMO-like DSP was used with impressive results to mitigate crosstalk[135,136]. It should be noted that modal basis sets can typically be represented by a modal combination of other sets. Therefore, it is no surprise that OAM and HG modes have also been used in conventional-type fibers, but significant crosstalk still occurs.

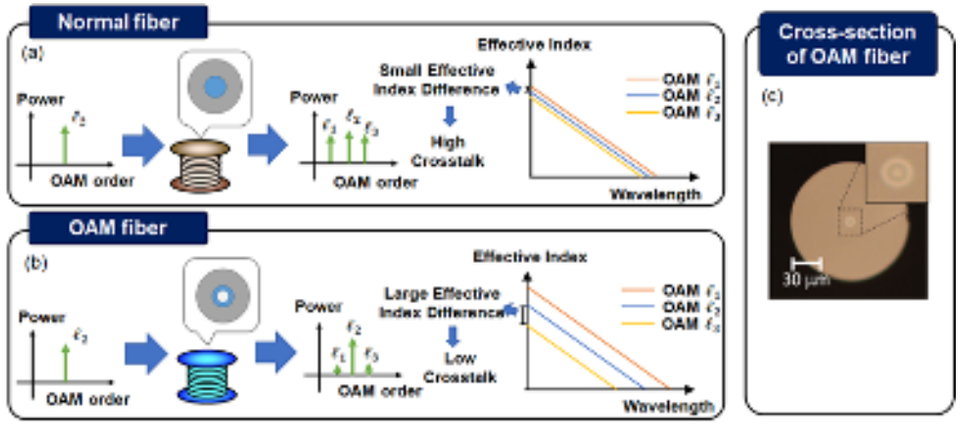

FIG. 43 (a, b) Comparison between (a) the normal fiber and (b) the vortex fiber. The OAM fiber has an annual refractive index profile, leading to a large effective refractive index difference among different OAM modes. Thus, the modal coupling is small during OAM beams' propagation in the special fiber. (c) The cross-section of OAM fiber. (© 2013 AAAS).

OAM has also been used as the modal basis set for fiber transmission, both for central-core and ring-core FMFs[5,16,20,137]. Importantly, the modal coupling itself can be reduced in the optical domain by utilizing specialty fiber that makes the propagation constants of different modes quite different, thus reducing intermodal coupling. Such fibers include ring-core and elliptical-core fiber[20, 137,141], and 10's of modes with low crosstalk have been demonstrated. These specialty fibers have produced exciting results, but they are structurally different than conventional fiber and thus require a little more resolve in order for them to be widely adopted. One design of the vortex fiber is shown in Fig. 43 as an example[69]. This vortex fiber has an annular refractive index profile to provide a large effective refractive index difference among different OAM modes as compared to a normal fiber. Thus, this vortex fiber design could potentially enable the efficient co-propagation and (de)multiplexing of OAM modes with lower inter-modal crosstalk[16,137].

ACCEPTED MANUSCRIPT
APL Photonics
This is the author's peer reviewed, accepted manuscript. However, the online version of record will be different from this version once it has been copyedited and typeset.
PLEASE CITE THIS ARTICLE AS DOI:10.1063/5.0031230
AIP Publishing

Another challenge for achieving MDM in fiber is the power loss due to fiber attenuation which limits the transmission distance. In general, fiber-based amplifiers can be utilized to increase the transmission distance. For an MDM system, two main features are desired for the amplifiers: large mode gain and small difference between gains over different modes. Fig. 44 presents two examples of OAM fiber amplifiers to address the above features. By using the ring-core fiber structure, OAM erbium-doped fiber amplifiers (EDFA)[142, 143] and Raman amplifiers[144] have been demonstrated in these two papers, respectively. As for the performance, the example of OAM EDFA provides a high gain of > 10 dB over a bandwidth of 20 nm while the gain curve is not flat. As a comparison, the example of the OAM Raman amplifier has a low gain of ~ 3 dB with a flat gain curve over a bandwidth of 30 nm.

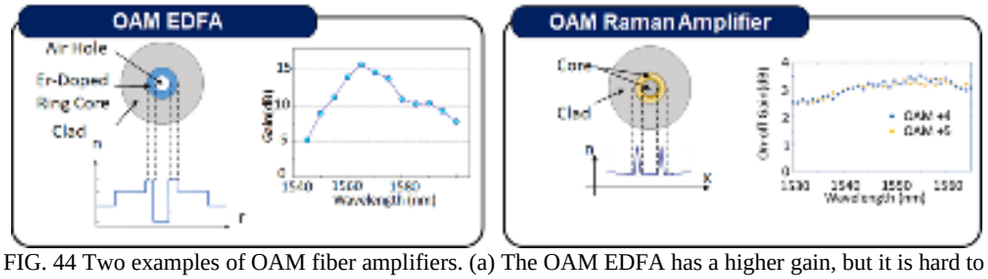

FIG. 44 Two examples of OAM fiber amplifiers. (a) The OAM EDFA has a higher gain, but it is hard to provide a flat gain over a broad bandwidth. (b) The OAM Raman amplifier has a lower gain with a flatter curve over ~ 30 nm. EDFA: Erbium-Doped Fiber Amplifier. (©2017, 2018 Optical Society of America)

XI. Summary perspective

Will OAM be widely deployed in communication systems? Not clear. However, our opinion is that the R&D community is producing excellent advances that, in all likelihood, will be valuable for some important aspects that use structured light.

This paper reviews the use of OAM to potentially enhance the capacity of MDM communication systems. The following points are noteworthy:

(i) The use of OAM multiplexing under more complicated and harsher channel conditions than those described in this paper remains challenging. It would be important to investigate the system performance under these conditions and to develop potential techniques to combat the degradation effects. It would also be valuable to explore the limits of these conditions below which the degradation effects can be efficiently mitigated.

(ii) The future of OAM deployment will rely heavily on the development of a technology ecosystem for OAM generation and multiplexing. Efficient OAM (de)multiplexing using compact and cost-efficient integrated devices would be one important issue[145]. Key desirable features of these integrated devices include[69]: low insertion loss, high amplifier gain, uniform performance for different modes, high modal purity, low modal coupling and intermodal crosstalk, high efficiency for mode conversion, high dynamic range, small size, large wavelength range, and accommodation of high numbers of modes. Other functions that could be advantageous include: (a) fast tunability and reconfigurability covering a range of OAM modes, and (b) integration of an OAM communication system-on-a-chip that incorporates a full transceiver.

(iii) OAM multiplexing could be utilized in different frequency domains. Future OAM systems might use hybrid technologies, and, thus, systems that can be compatible with different OAM multiplexing technologies over different frequency domains may be valuable, including but not limited to the RF, mm-wave, THz, and optical domains[146-148]. Components, including broadband signal emitters/detectors, and frequency converters in different frequency domains, may need to be considered to enable heterogeneous OAM-multiplexed communications. Another consideration could be the frequency channel selections, the key challenges of which include link loss and channel distortion caused by OAM beam divergence and beam interaction with matter (e.g., atmospheric turbulence) in heterogeneous OAM-multiplexed links. In such cases, potential solutions, such as AO and MIMO, could be helpful.

Acknowledgement

We acknowledge the generous supports from Vannevar Bush Faculty Fellowship sponsored by the Basic Research Office of the Assistant Secretary of Defense (ASD) for Research and Engineering (R&E) and funded by the Office of Naval Research (ONR) (N00014-16-1-2813); Defense Security Cooperation Agency (DSCA 4441006051); Air Force Research Laboratory (FA8650-20-C-1105); National Science Foundation (NSF) (ECCS-1509965); Office of Naval Research through a MURI grant (N00014- 20-1-2558); Airbus Institute for Engineering Research; Nippon Telegraph and Telephone Corporation; and Qualcomm Innovation Fellowship (QIF).

Data Availability

The data that support the findings of this study are available from the corresponding author upon reasonable request.

References

[1] L. Allen, M. W. Beijersbergen, R. J. C. Spreeuw, and J. P. Woerdman, Phys. Rev. A **45**, 8185 (1992).
[2] R.L. Phillips and L.C. Andrews, Appl. Opt. **22**, 643 (1983).
[3] A.M. Yao and M.J. Padgett, Adv. Opt. Photon. **3**, 161 (2011).

ACCEPTED MANUSCRIPT
APL Photonics
This is the author's peer reviewed, accepted manuscript. However, the online version of record will be different from this version once it has been copyedited and typeset.
PLEASE CITE THIS ARTICLE AS DOI:10.1063/5.0031230
AIP Publishing

[4] A.E. Willner, H. Huang, Y. Yan, Y. Ren, N. Ahmed, G. Xie, C. Bao, L. Li, Y. Cao, Z. Zhao, J. Wang, M.P.J. Lavery, M. Tur, S. Ramachandran, A.F. Molisch, N. Ashrafi, and S. Ashrafi, Adv. Opt. Photon. **7**, 66 (2015).
[5] D.J. Richardson, J.M. Fini, and L.E. Nelson, Nat. Photonics **7**, 354 (2013).
[6] P.J. Winzer, Nat. Photonics **8**, 345 (2014).
[7] J. Wang, J.-Y. Yang, I.M. Fazal, N. Ahmed, Y. Yan, H. Huang, Y. Ren, Y. Yue, S. Dolinar, M. Tur, and A.E. Willner, Nat. Photonics **6**, 488 (2012).
[8] Y. Yan, G. Xie, M.P.J. Lavery, H. Huang, N. Ahmed, C. Bao, Y. Ren, Y. Cao, L. Li, Z. Zhao, A.F. Molisch, M. Tur, M.J. Padgett, and A.E. Willner, Nat. Commun. **5**, 4876 (2014).
[9] H. Huang, G. Xie, Y. Yan, N. Ahmed, Y. Ren, Y. Yue, D. Rogawski, M.J. Willner, B.I. Erkmen, K.M. Birnbaum, S.J. Dolinar, M.P.J. Lavery, M.J. Padgett, M. Tur, and A.E. Willner, Opt. Lett. **39**, 197 (2014).
[10] J. Wang, S. Li, M. Luo, J. Liu, L. Zhu, C. Li, D. Xie, Q. Yang, S. Yu, J. Sun, X. Zhang, W. Shieh, and A.E. Willner, in *2014 The European Conference on Optical Communication (ECOC)* (2014), pp. 1–3.
[11] A.E. Willner and C. Liu, Nanophotonics, 20200435 (2020).
[12] A.E. Willner, IEEE Spectrum **53**, 34 (2016).
[13] Y. Ren, Z. Wang, P. Liao, L. Li, G. Xie, H. Huang, Z. Zhao, Y. Yan, N. Ahmed, A. Willner, M.P.J. Lavery, N. Ashrafi, S. Ashrafi, R. Bock, M. Tur, I.B. Djordjevic, M.A. Neifeld, and A.E. Willner, Opt. Lett. **41**, 622 (2016).
[14] Y. Zhao, J. Liu, J. Du, S. Li, Y. Luo, A. Wang, L. Zhu, and J. Wang, in *2016 Optical Fiber Communications Conference and Exhibition (OFC)* (2016), pp. 1–3.
[15] M. Krenn, J. Handsteiner, M. Fink, R. Fickler, R. Ursin, M. Malik, and A. Zeilinger, Proc. Natl. Acad. Sci. U.S.A **113**, 13648 (2016).
[16] N. Bozinovic, Y. Yue, Y. Ren, M. Tur, P. Kristensen, H. Huang, A.E. Willner, and S. Ramachandran, Science **340**, 1545 (2013).
[17] K. Pang, H. Song, Z. Zhao, R. Zhang, H. Song, G. Xie, L. Li, C. Liu, J. Du, A.F. Molisch, M. Tur, and A.E. Willner, Opt. Lett. **43**, 3889 (2018).
[18] G. Xie, Y. Ren, Y. Yan, H. Huang, N. Ahmed, L. Li, Z. Zhao, C. Bao, M. Tur, S. Ashrafi, and A.E. Willner, Opt. Lett. **41**, 3447 (2016).
[19] R. Ryf, S. Randel, A.H. Gnauck, C. Bolle, A. Sierra, S. Mumtaz, M. Esmaeelpour, E.C. Burrows, R.-J. Essiambre, P.J. Winzer, D.W. Peckham, A.H. McCurdy, and R. Lingle, Journal of Lightwave Technology **30**, 521 (2012).
[20] B. Ndagano, R. Brüning, M. McLaren, M. Duparré, and A. Forbes, Opt. Express **23**, 17330 (2015).
[21] R. W. Boyd and M. J. Padgett, Private Communication, 2020.
[22] M. J. Padgett, R. W. Boyd, and A. E. Willner.
[23] S. Restuccia, D. Giovannini, G. Gibson, and M. J. Padgett, Opt. Express **24**, 27127 (2016).
[24] L. Li, G. Xie, Y. Yan, Y. Ren, P. Liao, Z. Zhao, N. Ahmed, Z. Wang, C. Bao, A.J. Willner, S. Ashrafi, M. Tur, and A.E. Willner, J. Opt. Soc. Am. B, JOSAB **34**, 1 (2017).
[25] G. Gibson, J. Courtial, M.J. Padgett, M. Vasnetsov, V. Pas'ko, S.M. Barnett, and S. Franke-Arnold, Opt. Express **12**, 5448 (2004).
[26] L. C. Andrews and R. L. Phillips, SPIE, (2005).
[27] G.A. Tyler and R.W. Boyd, Opt. Lett. **34**, 142 (2009).
[28] Y. Ren, H. Huang, G. Xie, N. Ahmed, Y. Yan, B.I. Erkmen, N. Chandrasekaran, M.P.J. Lavery, N.K. Steinhoff, M. Tur, S. Dolinar, M. Neifeld, M.J. Padgett, R.W. Boyd, J.H. Shapiro, and A.E. Willner, Opt. Lett. **38**, 4062 (2013).
[29] S. Fu and C. Gao, Photon. Res. **4**, B1 (2016).
[30] G. Xie, L. Li, Y. Ren, H. Huang, Y. Yan, N. Ahmed, Z. Zhao, M.P.J. Lavery, N. Ashrafi, S. Ashrafi, R. Bock, M. Tur, A.F. Molisch, and A.E. Willner, Optica **2**, 357 (2015).
[31] X. Zhong, Y. Zhao, G. Ren, S. He, and Z. Wu, IEEE Access **6**, 8742 (2018).
[32] Z. Mei and D. Zhao, J. Opt. A: Pure Appl. Opt. **6**, 1005 (2004).
[33] G. Labroille, B. Denolle, P. Jian, P. Genevaux, N. Treps, and J. F. Morizur, Opt. Express **22**, 15599-15607 (2014).
[34] N.K. Fontaine, R. Ryf, H. Chen, D.T. Neilson, K. Kim, and J. Carpenter, Nat. Commun., **10**(1), 1-7 (2019).
[35] Y. Wen, I. Chremmos, Y. Chen, J. Zhu, Y. Zhang, and S. Yu, Phys. Rev. Lett., **120**(19), 193904 (2018).
[36] G.C. Berkhout, M.P. Lavery, J. Courtial, M.W. Beijersbergen, and M.J. Padgett, Phys. Rev. Lett., **105**(15), 153601 (2010).
[37] Z.S. Eznaveh, J.C.A. Zacarias, J.E.A. Lopez, K. Shi, G. Milione, Y. Jung, B.C. Thomsen, D.J. Richardson, N. Fontaine, S.G. Leon-Saval, and R.A. Correa, Opt. Express, **26**(23), 30042-30051 (2018).
[38] J. A. Anguita, M. A. Neifeld, and B. V. Vasic, Appl. Opt. **47**, 2414, (2008).
[39] C. N. Chandrasekaran and J. H. Shapiro, J. Light. Technol. **32**, 1075, (2014).
[40] C. Paterson, Phys. Rev. Lett. **94**, 153901 (2005).
[41] M. Malik, M. O'Sullivan, B. Rodenburg, M. Mirhosseini, J. Leach, M.P.J. Lavery, M.J. Padgett, and R.W. Boyd, Opt. Express **20**, 13195 (2012).
[42] Y. Ren, G. Xie, H. Huang, C. Bao, Y. Yan, N. Ahmed, M.P.J. Lavery, B.I. Erkmen, S. Dolinar, M. Tur, M.A. Neifeld, M.J. Padgett, R.W. Boyd, J.H. Shapiro, and A.E. Willner, Opt. Lett. **39**, 2845 (2014).
[43] K. Pang, S. Haoqian, Xinzhou Su, K. Zou, Z. Zhao, H. Song, A. Almaiman, R. Zhang, C. Liu, N. Hu, S. Zach, N. Cohen, B. Lynn, A.F. Molisch, R.W. Boyd, M. Tur, and A.E. Willner, in *2020 Optical Fiber Communications Conference and Exhibition (OFC)* (2020), pp. 1–3.
[44] G. A. Tyler, Opt. Eng. **52**, 021011, (2012).

ACCEPTED MANUSCRIPT
APL Photonics
This is the author's peer reviewed, accepted manuscript. However, the online version of record will be different from this version once it has been copyedited and typeset.
PLEASE CITE THIS ARTICLE AS DOI:10.1063/5.0031230
AIP Publishing

[45]Y. Ren, G. Xie, H. Huang, N. Ahmed, Y. Yan, L. Li, C. Bao, M. P. J. Lavery, M. Tur, M. A. Neifeld, R. W. Boyd, J. H. Shapiro, and A. E. Willner, Optica **1**, 376, (2014).
[46] N. K. Fontaine, R. Ryf, H. Chen, D. T. Neilson, K. Kim, and J. Carpenter, Nat. Commun. **10**, 1, (2019).
[47] S. Chen, S. Li, Y. Zhao, J. Liu, L. Zhu, A. Wang, J. Du, L. Shen, and J. Wang, Opt. Lett., **41**(20), 4680-4683 (2016).
[48] P. J. Winzer and G. J. Foschini, Opt. Express **19**, 16680, (2011).
[49] B. Clerckx, and C. Oestges, Academic Press, (2013).
[50] H. Huang, Y. Cao, G. Xie, Y. Ren, Y. Yan, C. Bao, N. Ahmed, M. A. Neifeld, S. J. Dolinar, and A. E. Willner, Opt. Lett. **39**, 4360, (2014).
[51]R. Fickler, M. Ginoya, and R. W. Boyd, Phys. Rev. B **95**, 161108 (2017).
[52] I. M. Vellekoop and A. P. Mosk, Phys. Rev. Lett. **101**, 120601 (2008).
[53] R. Zhang, H. Song, Z. Zhao, H. Song, J. Du, C. Liu, K. Pang, L. Li, H. Zhou, A. N. Willner, A. Almaiman, Y. Zhou, R. W. Boyd, B. Lynn, R. Bock, M. Tur, and A. E. Willner, Opt. Lett. **45**, 702–705 (2020).
[54] J.-F. Morizur, L. Nicholls, P. Jian, S. Armstrong, N. Treps, B. Hage, M. Hsu, W. Bowen, J. Janousek, and H.-A. Bachor, J. Opt. Soc. Am. A **27**, 2524–2531 (2010).
[55] H. Song, X. Su, H. Song, R. Zhang, Z. Zhao, C. Liu, K. Pang, N. Hu, A. Almaiman, S. Zach, N. Cohen, A. Molisch, R. Boyd, M. Tur, and A. E. Willner, in 2020 Optical Fiber Communications Conference (OFC) (2020), p. W1G.3.
[56] H. Song, H. Song, R. Zhang, K. Manukyan, L. Li, Z. Zhao, K. Pang, C. Liu, A. Almaiman, R. Bock, B. Lynn, M. Tur, and A.E. Willner, J. Light. Technol. **38**, 82 (2020).
[57] D. A. B. Miller, Science **347**, 1423 (2015).
[58] V. Liu, D. A. B. Miller, and S. Fan, Opt. Express, **20**, 28388 (2012).
[59] C. Yang, C. Xu, W. Ni, Y. Gan, J. Hou, and S. Chen, Opt. Express **25**, 25612 (2017).
[60] L. Li, R. Zhang, Z. Zhao, G. Xie, P. Liao, K. Pang, H. Song, C. Liu, Y. Ren, G. Labroille, P. Jian, D. Starodubov, B. Lynn, Rock, M. Tur, and A.E. Willner, Sci. Rep. **7**, 1 (2017).
[61] J. Cunningham, D. Foulke, T. Goode, D. Baber, B. Gaughan, M. Fletcher, D.W. Young, J.C. Juarez, J.E. Sluz, and J.L. Riggins, in *MILCOM 2009 - 2009 IEEE Military Communications Conference* (2009), pp. 1–7.
[62] S.S. Muhammad, T. Plank, E. Leitgeb, A. Friedl, K. Zettl, T. Javornik, and N. Schmitt, in *2008 6th International Symposium on Communication Systems, Networks and Digital Signal Processing* (2008), pp. 82–86.
[63] R. Fields, C. Lunde, R. Wong, J. Wicker, D. Kozlowski, J. Jordan, B. Hansen, G. Muehlnikel, W. Scheel, U. Sterr, R. Kahle, and R. Meyer, in *Sensors and Systems for Space Applications III* (International Society for Optics and Photonics, 2009), p. 73300Q.
[64] F. Heine, G. Mühlnikel, H. Zech, S. Philipp-May, and R. Meyer, in *2014 7th Advanced Satellite Multimedia Systems Conference and the 13th Signal Processing for Space Communications Workshop (ASMS/SPSC)* (2014), pp. 284–286.
[65] F. Moll, J. Horwath, A. Shrestha, M. Brechtelsbauer, C. Fuchs, L.A. Martín Navajas, A.M. Lozano Souto, and D. Díaz González, IEEE J. Sel. Areas Commun. **33**, 1985 (2015).
[66] K.E. Zarganis and A. Hatziefremidis, J. Opti. and Photonics **3**, 5 (2015).
[67] A. Kaadan, H. Refai, and P. Lopresti, IEEE Trans. Aerosp. Electron. Syst. **52**, 2157 (2016).
[68] A. Kaadan, H.H. Refai, and P.G. LoPresti, J. Light. Technol. **32**, 4785 (2014).
[69] A.E. Willner, in *Conference on Lasers and Electro-Optics (2018), Paper STu3B.1* (Optical Society of America, 2018), p. STu3B.1.
[70] K. Kazaura, K. Omae, T. Suzuki, M. Matsumoto, E. Mutafungwa, T.O. Korhonen, T. Murakami, K. Takahashi, H. Matsumoto, K. Wakamori, and Y. Arimoto, Opt. Express **14**, 4958 (2006).
[71] L. Li, R. Zhang, G. Xie, Y. Ren, Z. Zhao, Z. Wang, C. Liu, H. Song, K. Pang, R. Bock, M. Tur, and A.E. Willner, Opt. Lett. **43**, 2392 (2018).
[72] L. Li, R. Zhang, P. Liao, Y. Cao, H. Song, Y. Zhao, J. Du, Z. Zhao, C. Liu, K. Pang, H. Song, A. Almaiman, D. Starodubov, B. Lynn, R. Bock, M. Tur, A.F. Molisch, and A.E. Willner, Opt. Lett. **44**, 5181 (2019).
[73] E. Ciaramella, Y. Arimoto, G. Contestabile, M. Presi, A. D'Errico, V. Guarino, and M. Matsumoto, IEEE J. Sel. Areas Commun. **27**, 1639 (2009).
[74] G. Xie, L. Li, Y. Ren, Y. Yan, N. Ahmed, Z. Zhao, C. Bao, Z. Wang, C. Liu, H. Song, R. Zhang, K. Pang, S. Ashrafi, M. Tur, and A.E. Willner, Opt. Lett. **42**, 395 (2017).
[75] N. Friedman, *The Naval Institute Guide to World Naval Weapon Systems* (Naval Institute Press, 2006).
[76] M. Stojanovic, IEEE J. Ocean. Eng. **21**, 125 (1996).
[77] J. Wang, C. Lu, S. Li, and Z. Xu, Opt. Express **27**, 12171 (2019).
[78] J. Baghdady, K. Miller, K. Morgan, M. Byrd, S. Osler, R. Ragusa, W. Li, B.M. Cochenour, and E.G. Johnson, Opt. Express **24**, 9794 (2016).
[79] Y. Ren, L. Li, Z. Wang, S.M. Kamali, E. Arbabi, A. Arbabi, Z. Zhao, G. Xie, Y. Cao, N. Ahmed, Y. Yan, C. Liu, A.J. Willner, S. Ashrafi, M. Tur, A. Faraon, and A.E. Willner, Sci. Rep. **6**, 33306 (2016).
[80] A.K. Majumdar, J. Siegenthaler, and P. Land, in Laser Comm. and Prop. through the Atmosphere and Oceans (International Society for Optics and Photonics) **8517**, p. 85170T (2012).
[81] R.F. Lutomirski, in Ocean Optics V (International Society for Optics and Photonics) **160**, pp. 110-122 (1978).
[82] M. Cheng, L. Guo, and Y. Zhang, Opt. Express **23**, 32606-32621 (2015).
[83] Y. Zhao, A. Wang, L. Zhu, W. Lv, J. Xu, S. Li, and J. Wang, Opt. Lett., **42**(22), 4699-4702 (2017).
[84] D. McGloin and K. Dholakia, Contemp. Phys. **46**, 15 (2005).

ACCEPTED MANUSCRIPT
APL Photonics
This is the author's peer reviewed, accepted manuscript. However, the online version of record will be different from this version once it has been copyedited and typeset.
PLEASE CITE THIS ARTICLE AS DOI:10.1063/5.0031230
AIP Publishing

[85] N. K. Efremidis, Z. Chen, M. Segev, and D. N. Christodoulides, Optica **6**, 686-701 (2019).
[86] G. Zhu, Y. Wen, X. Wu, Y. Chen, J. Liu, and S. Yu, Opt. Lett. **43**, 1203-1206 (2018).
[87] L. Zhu, A. Wang, and J. Wang, Sci. Rep. **9**, 1 (2019).
[88] L. Zhu, Z. Yang, S. Fu, Z. Cao, Y. Wang, Y. Qin, and A. M. J. Koonen, J. Light. Technol. **38**, 6474-6480 (2020).
[89] N. Ahmed, Z. Zhao, L. Li, H. Huang, M.P.J. Lavery, P. Liao, Y. Yan, Z. Wang, G. Xie, Y. Ren, A. Almaiman, A.J. Willner, S. Ashrafi, A.F. Molisch, M. Tur, and A.E. Willner, Sci. Rep. **6**, 22082 (2016).
[90] M. Erhard, R. Fickler, M. Krenn, and A. Zeilinger, Light Sci. Appl. **7**, 17146 (2018).
[91] M. Mirhosseini, O.S. Magaña-Loaiza, M.N. O'Sullivan, B. Rodenburg, M. Malik, M.P.J. Lavery, M.J. Padgett, D.J. Gauthier, and R.W. Boyd, New J. Phys. **17**, 033033 (2015).
[92] M. Mafu, A. Dudley, S. Goyal, D. Giovannini, M. McLaren, M.J. Padgett, T. Konrad, F. Petruccione, N. Lütkenhaus, and A. Forbes, Phys. Rev. A **88**, 032305 (2013).
[93] C. Liu, K. Pang, Z. Zhao, P. Liao, R. Zhang, H. Song, Y. Cao, J. Du, L. Li, H. Song, Y. Ren, G. Xie, Y. Zhao, J. Zhao, S.M.H. Rafsanjani, A.N. Willner, J.H. Shapiro, R.W. Boyd, M. Tur, and A.E. Willner, Research **2019**, 1 (2019).
[94] J. Liu, I. Nape, Q. Wang, A. Vallés, J. Wang, and A. Forbes, A, Science Advances, **6**(4), eaay0837 (2020).
[95] C.H. Bennett and G. Brassard, Theoretical Computer Science **560**, 7 (2014).
[96] H. Hübel, M.R. Vanner, T. Lederer, B. Blauensteiner, T. Lorünser, A. Poppe, and A. Zeilinger, Opt. Express **15**, 7853 (2007).
[97] C.-Z. Peng, J. Zhang, D. Yang, W.-B. Gao, H.-X. Ma, H. Yin, H.-P. Zeng, T. Yang, X.-B. Wang, and J.-W. Pan, Phys. Rev. Lett. **98**, 010505 (2007).
[98] S.-K. Liao, W.-Q. Cai, W.-Y. Liu, L. Zhang, Y. Li, J.-G. Ren, J. Yin, Q. Shen, Y. Cao, Z.-P. Li, F.-Z. Li, X.-W. Chen, L.-H. Sun, J.-J. Jia, J.-C. Wu, X.-J. Jiang, J.-F. Wang, Y.-M. Huang, Q. Wang, Y.-L. Zhou, L. Deng, T. Xi, L. Ma, T. Hu, Q. Zhang, Y.-A. Chen, N.-L. Liu, X.-B. Wang, Z.-C. Zhu, C.-Y. Lu, R. Shu, C.-Z. Peng, J.-Y. Wang, and J.-W. Pan, Nature **549**, 43 (2017).
[99] G. Vallone, V. D'Ambrosio, A. Sponselli, S. Slussarenko, L. Marrucci, F. Sciarrino, and P. Villoresi, Phys. Rev. Lett. **113**, 060503 (2014).
[100] F. Bouchard, A. Sit, F. Hufnagel, A. Abbas, Y. Zhang, K. Heshami, R. Fickler, C. Marquardt, G. Leuchs, R. w Boyd, and E. Karimi, Opt. Express **26**, 22563 (2018).
[101] D. Cozzolino, E. Polino, M. Valeri, G. Carvacho, D. Bacco, N. Spagnolo, L.K. Oxenløwe, and F. Sciarrino, Advanced Photonics, **1**(4), 046005 (2019).
[102] H. Cao, S.C. Gao, C. Zhang, J. Wang, D.Y. He, B.H. Liu, Z.W. Zhou, Y.J. Chen, Z.H. Li, S.Y. Yu, J. Romero, Y.F. Huang, C.-F. Li, and G.-C. Guo, Optica, **7**(3), 232-237 (2020).
[103] A. Sit, F. Bouchard, R. Fickler, J. Gagnon-Bischoff, H. Larocque, K. Heshami, D. Elser, C. Peuntinger, K. Günthner, B. Heim, C. Marquardt, G. Leuchs, R.W. Boyd, and E. Karimi, Optica **4**, 1006 (2017).
[104] M. Hillery, V. Bužek, and A. Berthiaume, Phys. Rev. A **59**, 1829 (1999).
[105] W. Tittel, H. Zbinden, and N. Gisin, Phys. Rev. A **63**, 042301 (2001).
[106] Y.-A. Chen, A.-N. Zhang, Z. Zhao, X.-Q. Zhou, C.-Y. Lu, C.-Z. Peng, T. Yang, and J.-W. Pan, Phys. Rev. Lett. **95**, 200502 (2005).
[107] J. Pinnell, I. Nape, M. de Oliveira, N. TabeBordbar, and A. Forbes, Laser Photonics Rev. **14,** 2000012 (2020).
[108] C. Shi, M. Dubois, Y. Wang, and X. Zhang, Proc Natl Acad Sci USA **114**, 7250 (2017).
[109] W. Cheng, H. Zhang, L. Liang, H. Jing, and Z. Li, IEEE Access **6**, 2732 (2018).
[110] D. Lee, H. Sasaki, H. Fukumoto, Y. Yagi, and T. Shimizu, Applied Sciences **9**, 1729 (2019).
[111] H. Sasaki, D. Lee, H. Fukumoto, Y. Yagi, T. Kaho, H. Shiba, and T. Shimizu, in *2018 IEEE Global Communications Conference (GLOBECOM)* (2018), pp. 1–6.
[112] H. Sasaki, Y. Yagi, T. Yamada, and D. Lee, in *2019 IEEE Globecom Workshops (GC Wkshps)* (2019), pp. 1–4.
[113] Z. Zhao, Y. Yan, L. Li, G. Xie, Y. Ren, N. Ahmed, Z. Wang, C. Liu, A.J. Willner, P. Song, H. Hashemi, H. Yao, D. Macfarlane, R. Henderson, N. Ashrafi, S. Ashrafi, S. Talwar, S. Sajuyigbe, M. Tur, Andreas.F. Molisch, and A.E. Willner, in *2016 IEEE International Conference on Communications (ICC)* (2016), pp. 1–6.
[114] G. Xie, Z. Zhao, Y. Yan, L. Li, Y. Ren, N. Ahmed, Y. Cao, A.J. Willner, C. Bao, Z. Wang, C. Liu, M. Ziyadi, S. Talwar, S. Sajuyigbe, S. Ashrafi, M. Tur, A.F. Molisch, and A.E. Willner, Sci. Rep. **6**, 37078 (2016).
[115] X. Wei, L. Zhu, Z. Zhang, K. Wang, J. Liu, and J. Wang, in *CLEO: 2014 (2014), Paper STu2F.2* (Optical Society of America, 2014), p. STu2F.2.
[116] C. Liu, X. Wei, L. Niu, K. Wang, Z. Yang, and J. Liu, Opt. Express **24**, 12534 (2016).
[117] Q. Wu, and R. Zhang, IEEE Trans. Wirel. Commun. **18**, 5394-5409 (2019).
[118] X.G. Zhang, W.X. Jiang, H.L. Jiang, Q. Wang, H.W. Tian, L. Bai, Z.J. Luo, S. Sun, Y. Luo, C.W. Qiu, and T.J. Cui, Nat. Electronics, **3**(3), 165-171 (2020).
[119] C.M. Watts, D. Shrekenhamer, J. Montoya, G. Lipworth, J. Hunt, T. Sleasman, S. Krishna, D.R. Smith, and W.J. Padilla, Nat. Photonics, **8**(8), 605-609 (2014).
[120] X. Hui, S. Zheng, Y. Chen, Y. Hu, X. Jin, H. Chi, and X. Zhang, Sci. Rep. **5**, 10148 (2015).
[121] Y. Yan, L. Li, Z. Zhao, G. Xie, Z. Wang, Y. Ren, N. Ahmed, S. Sajuyigbe, S. Talwar, M. Tur, N. Ashrafi, S. Ashrafi, A.F. Molisch, and A.E. Willner, in *2016 IEEE International Conference on Communications (ICC)* (2016), pp. 1–6.
[122] W. Wei, K. Mahdjoubi, C. Brousseau, and O. Emile, Electron. Lett. **51**, 442 (2015).
[123] Z. Zhao, G. Xie, L. Li, H. Song, C. Liu, K. Pang, R. Zhang, C. Bao, Z. Wang, S. Sajuyigbe, S. Talwar, H. Nikopour, and A.E. Willner, in *GLOBECOM 2017 - 2017 IEEE Global Communications Conference* (2017), pp. 1–6.

ACCEPTED MANUSCRIPT
APL Photonics
This is the author's peer reviewed, accepted manuscript. However, the online version of record will be different from this version once it has been copyedited and typeset.
PLEASE CITE THIS ARTICLE AS DOI:10.1063/5.0031230
AIP Publishing

[124] Z. Zhao, Y. Ren, G. Xie, Y. Yan, L. Li, H. Huang, C. Bao, N. Ahmed, M.P. Lavery, C. Zhang, N. Ashrafi, S. Ashrafi, S. Talwar, S. Sajuyigbe, M. Tur, A.F. Molisch, and A.E. Willner, in *2015 IEEE International Conference on Communications (ICC)* (2015), pp. 1392–1397.
[125] Z. Zhao, R. Zhang, H. Song, K. Pang, A. Almaiman, H. Zhou, H. Song, C. Liu, N. Hu, X. Su, A. Minoofar, S. Zach, N. Cohen, M. Tur, A. Molisch, and A.E. Willner, in *ICC 2020 - 2020 IEEE International Conference on Communications (ICC)* (2020), pp. 1–7.
[126] X. Su, R. Zhang, Z. Zhao, H. Song, A. Minoofar, N. Hu, H. Zhou, K. Zou, K. Pang, H. Song, B. Lynn, S. Zach, N. Cohen, M. Tur, A. Molisch, H. Sasaki, D. Lee and A.E. Willner, in 2020 IEEE Globecom Workshops (GC Wkshps), pp. 1–6 (2020).
[127] R.W. Heath Jr., N. Gonzalez-Prelcic, S. Rangan, W. Roh, and A. Sayeed, IEEE J. Sel. Top. Signal Process. **10**, 436 (2016).
[128] O.E. Ayach, S. Rajagopal, S. Abu-Surra, Z. Pi, and R.W. Heath, IEEE Trans. Wirel. Commun. **13**, 1499 (2014).
[129] Y. Ren, L. Li, G. Xie, Y. Yan, Y. Cao, H. Huang, N. Ahmed, Z. Zhao, P. Liao, C. Zhang, G. Caire, A.F. Molisch, M. Tur, and A.E. Willner, IEEE Trans. Wirel. Commun. **16**, 3151 (2017).
[130] H. Sasaki, D. Lee, H. Fukumoto, Y. Yagi, T. Kaho, H. Shiba, and T. Shimizu, in 2018 IEEE Global Communications Conference (GLOBECOM), pp. 1-6 (2018).
[131] B. Palacin, K. Sharshavina, K. Nguyen, and N. Capet, in the 8th European Conference on Antennas and Propagation (EuCAP 2014), pp. 2814-2818 (2014).
[132] H. Sasaki, Y. Yagi, T. Yamada, T. Semoto, and D. Lee, in 2020 IEEE International Conference on Communications Workshops (ICC Workshops), pp. 1-6. (2020).
[133] R. Zhang, H. Song, H. Song, Z. Zhao, G. Milione, K. Pang, J. Du, L. Li, K. Zou, H. Zhou, C. Liu, K. Manukyan, N. Hu, A. Almaiman, J. Stone, M.-J. Li, B. Lynn, R. W. Boyd, M. Tur, and A. E. Willner, Opt. Lett. **45**, 3577 (2020).
[134] J. Carpenter, B. C. Thomsen, T. D. Wilkinson, J. Light. Technol. **30**, 3946 (2012).
[135] K. Kitayama and N.-P. Diamantopoulos, IEEE Commun. Mag. **55**, 163 (2017).
[136] S. Randel, R. Ryf, A. Sierra, P.J. Winzer, A.H. Gnauck, C.A. Bolle, R.-J. Essiambre, D.W. Peckham, A. McCurdy, and R. Lingle, Opt. Express **19**, 16697 (2011).
[137] C. Brunet, P. Vaity, Y. Messaddeq, S. LaRochelle, and L.A. Rusch, Opt. Express **22**, 26117 (2014).
[138] S. Bae, Y. Jung, B.G. Kim, and Y.C. Chung, IEEE Photon. Technol. **31**, 739 (2019).
[139] J. Zhang, J. Liu, L. Shen, L. Zhang, J. Luo, J. Liu, and S. Yu, Photon. Res., **8**(7), 1236-1242 (2020).
[140] J. Liu, S.M. Li, L. Zhu, A.D. Wang, S. Chen, C. Klitis, C. Du, Q. Mo, M. Sorel, S.Y. Yu, X.L. Cai and J. Wang, Light Sci. Appl., **7**(3), 17148-17148 (2018).
[141] N. Riesen, J.D. Love, and J.W. Arkwright, IEEE Photon. Technol. **24**, 344 (2012).
[142] Y. Jung, Q. Kang, R. Sidharthan, D. Ho, S. Yoo, P. Gregg, S. Ramachandran, S.-U. Alam, and D.J. Richardson, J. Light. Technol. **35**, 430 (2017).
[143] J. Liu, S. Chen, H. Wang, S. Zheng, L. Zhu, A. Wang, L. Wang, C. Du, and J. Wang, Research **2020**, 7623751 (2020).
[144] L. Zhu, J. Li, G. Zhu, L. Wang, C. Cai, A. Wang, S. Li, M. Tang, Z. He, S. Yu, S. Yu, C. Du, W. Luo, J. Liu, J. Du, and J. Wang, in *Optical Fiber Communication Conference (2018), Paper W4C.4* (Optical Society of America, 2018), p. W4C.4.
[145] N. Zhou, S. Zheng, X. Cao, Y. Zhao, S. Gao, Y. Zhu, M. He, X. Cai, and J. Wang, Science Advances, **5**(5), eaau9593 (2019).
[146] F. Nadeem, V. Kvicera, M. S. Awan, E. Leitgeb, S. S. Muhammad, and G. Kandus, IEEE J. Sel. Areas Commun. **27**, 1687-1697 (2009).
[147] A. Trichili, M. A. Cox, B. S. Ooi, and Mohamed-Slim Alouini, J. Opt. Soc. Am. B **37**, A184-A201 (2020).
[148] F. Ahdi, and S. Subramaniam, In 2011 IEEE Global Telecommunications Conference (GLOBECOM 2011), pp. 1-6. (2011).

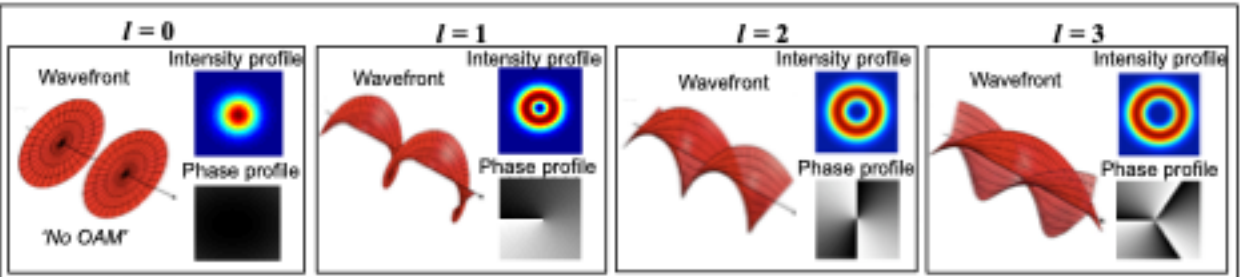

$\phi(r, \phi) = \exp(il\phi)$ (l = ... -3, -2, -1 ,+1, +2, +3 ....) **# of states possible = infinite** , ... (theoretically)

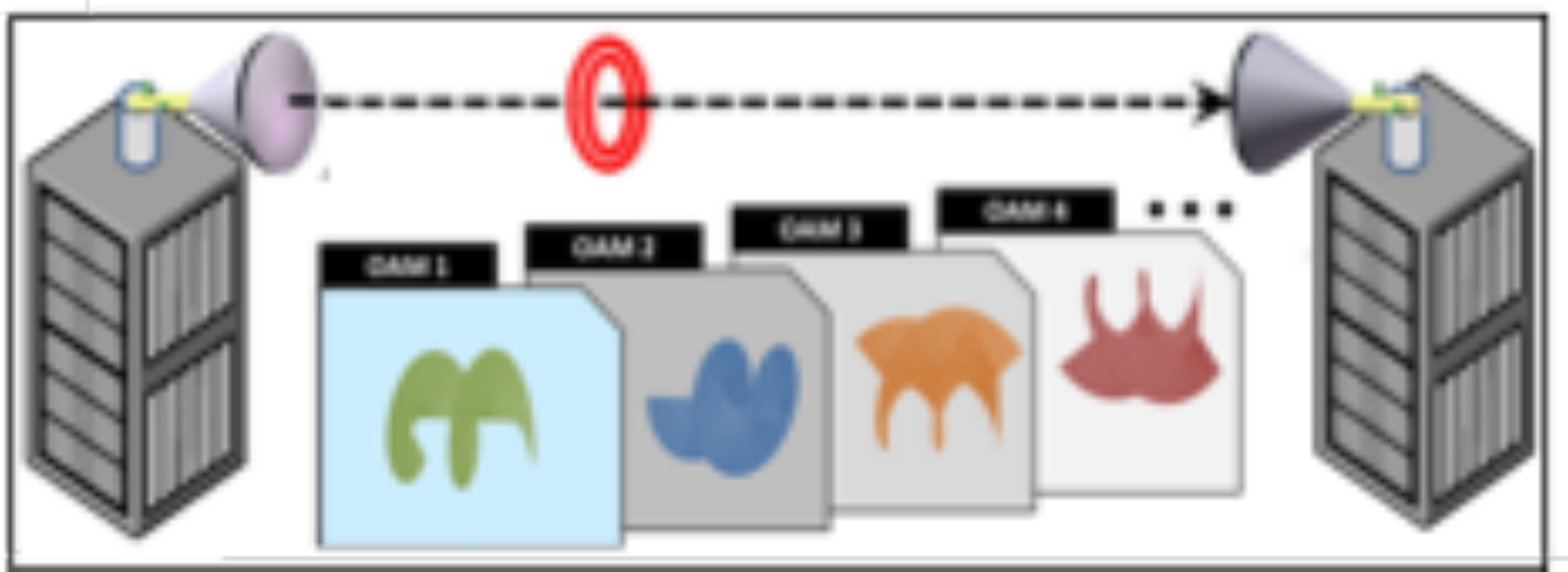
CAM 1
CAM 2
CAM 3
CAM 4

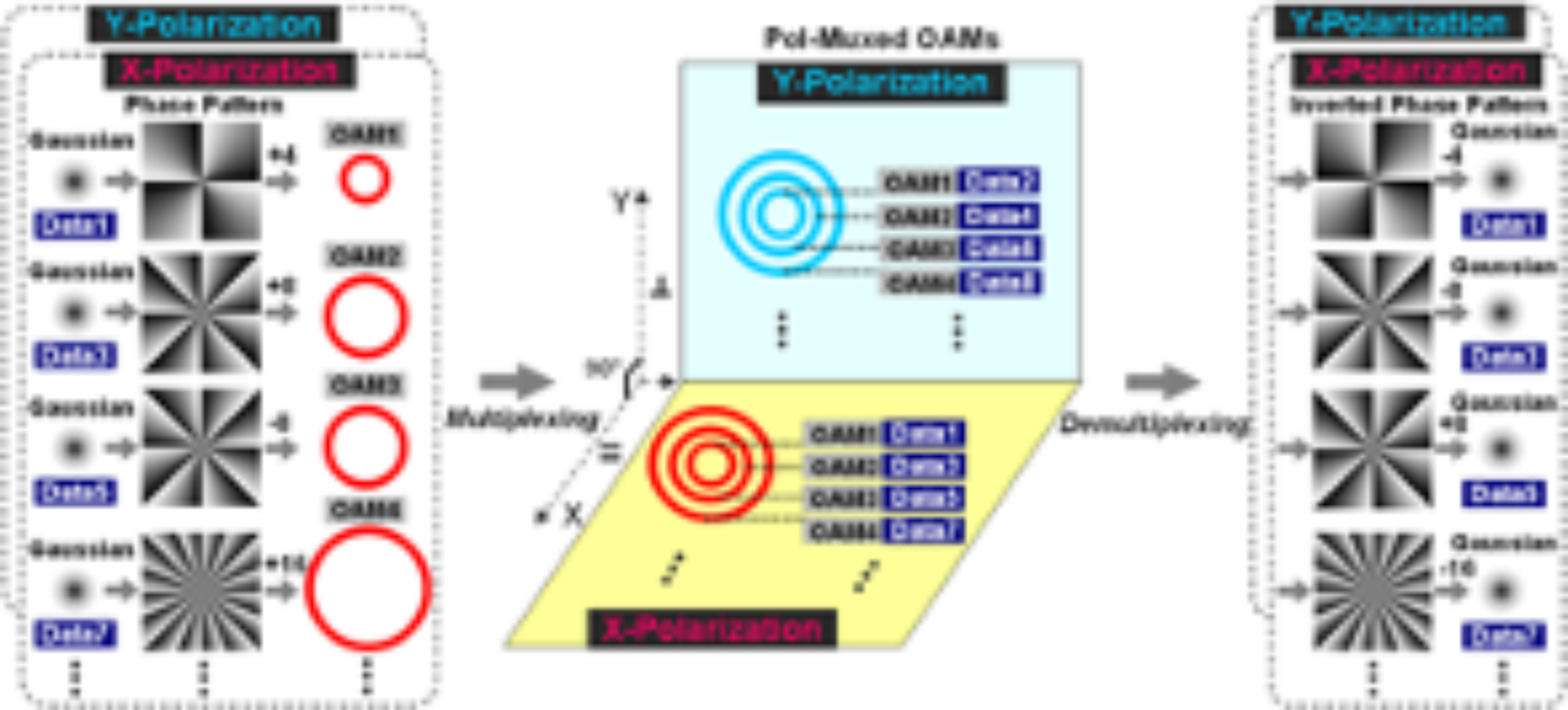
Y-Polarization
X-Polarization
Phase Pattern
Gaussian
+4
Data1
OAM1
Gaussian
+8
Data3
OAM2
Gaussian
-8
Data5
OAM3
Gaussian
+16
Data7
OAM4
Pol-Muxed OAMs
Y-Polarization
OAM1 Data2
OAM2 Data4
OAM3 Data6
OAM4 Data8
Y
90°
X
Multiplexing
OAM1 Data1
OAM2 Data3
OAM3 Data5
OAM4 Data7
X-Polarization
Demultiplexing
Y-Polarization
X-Polarization
Inverted Phase Pattern
Gaussian
-4
Data1
Gaussian
-8
Data3
Gaussian
+8
Data5
Gaussian
-16
Data7

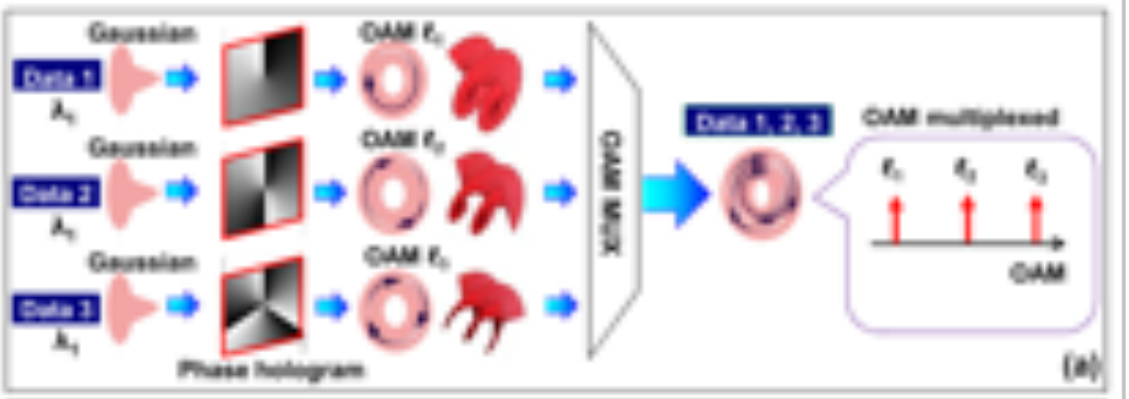
Gaussian
Data 1
Data 2
Data 3
Phase hologram
OAM MUX
Data 1, 2, 3
OAM multiplexed
OAM
(a)

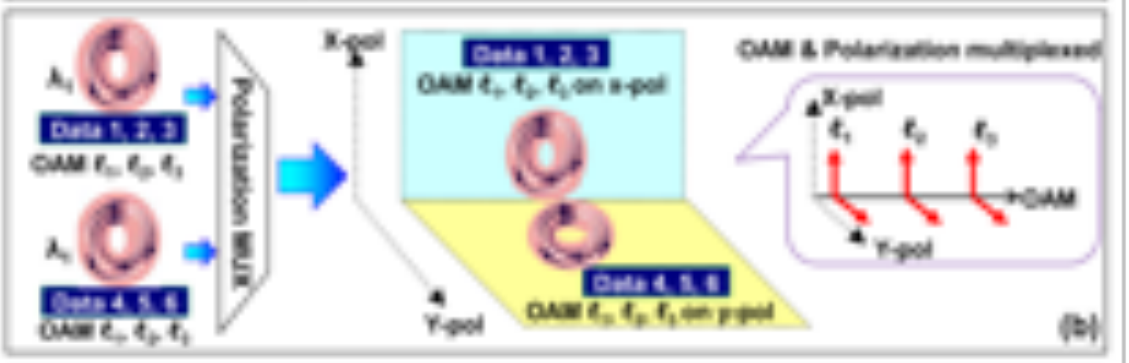
Data 1, 2, 3
Data 4, 5, 6
Polarization MUX
X-pol
Y-pol
OAM & Polarization multiplexed
OAM
(b)

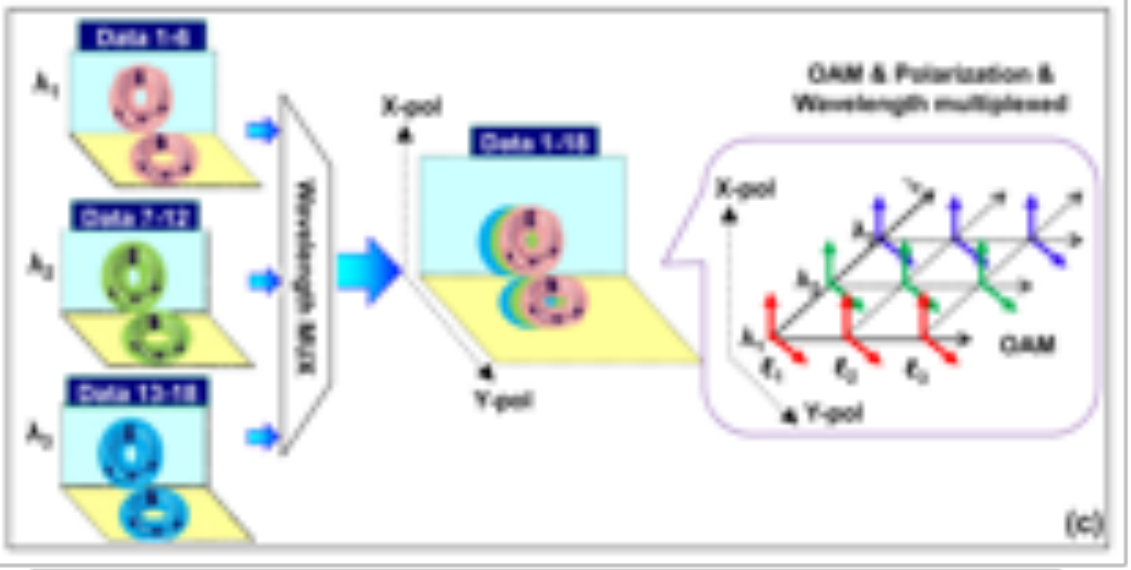
Data 1-6
Data 7-12
Data 13-18
Wavelength MUX
X-pol
Y-pol
OAM & Polarization & Wavelength multiplexed
OAM
(c)

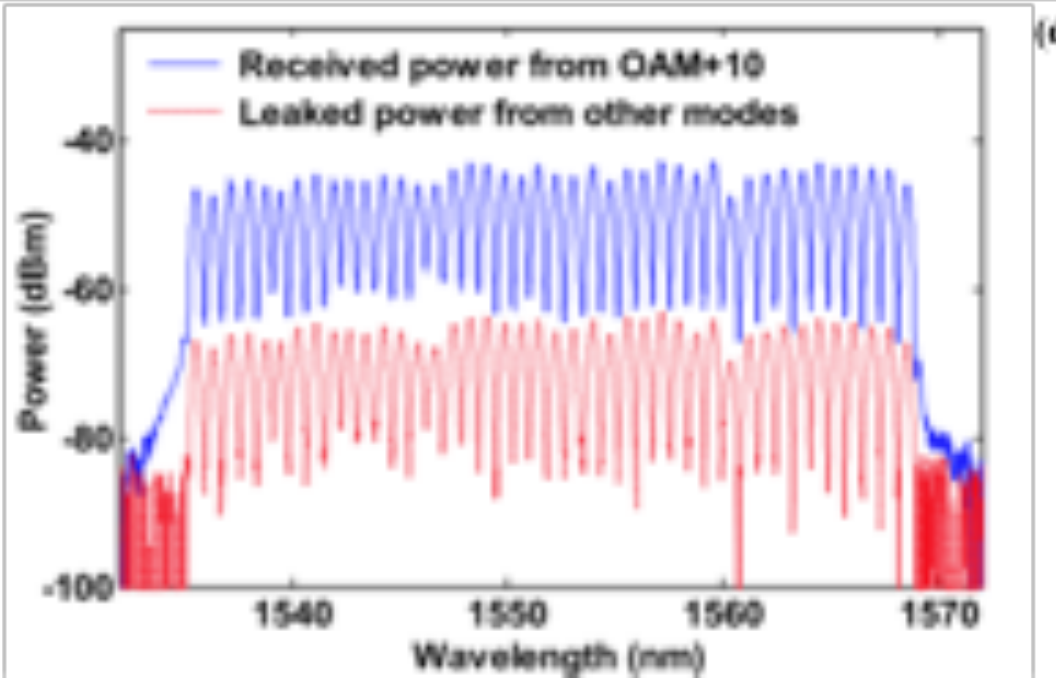
(d)
Received power from OAM+10
Leaked power from other modes
Power (dBm)
-40
-60
-80
-100
1540
1550
1560
1570
Wavelength (nm)

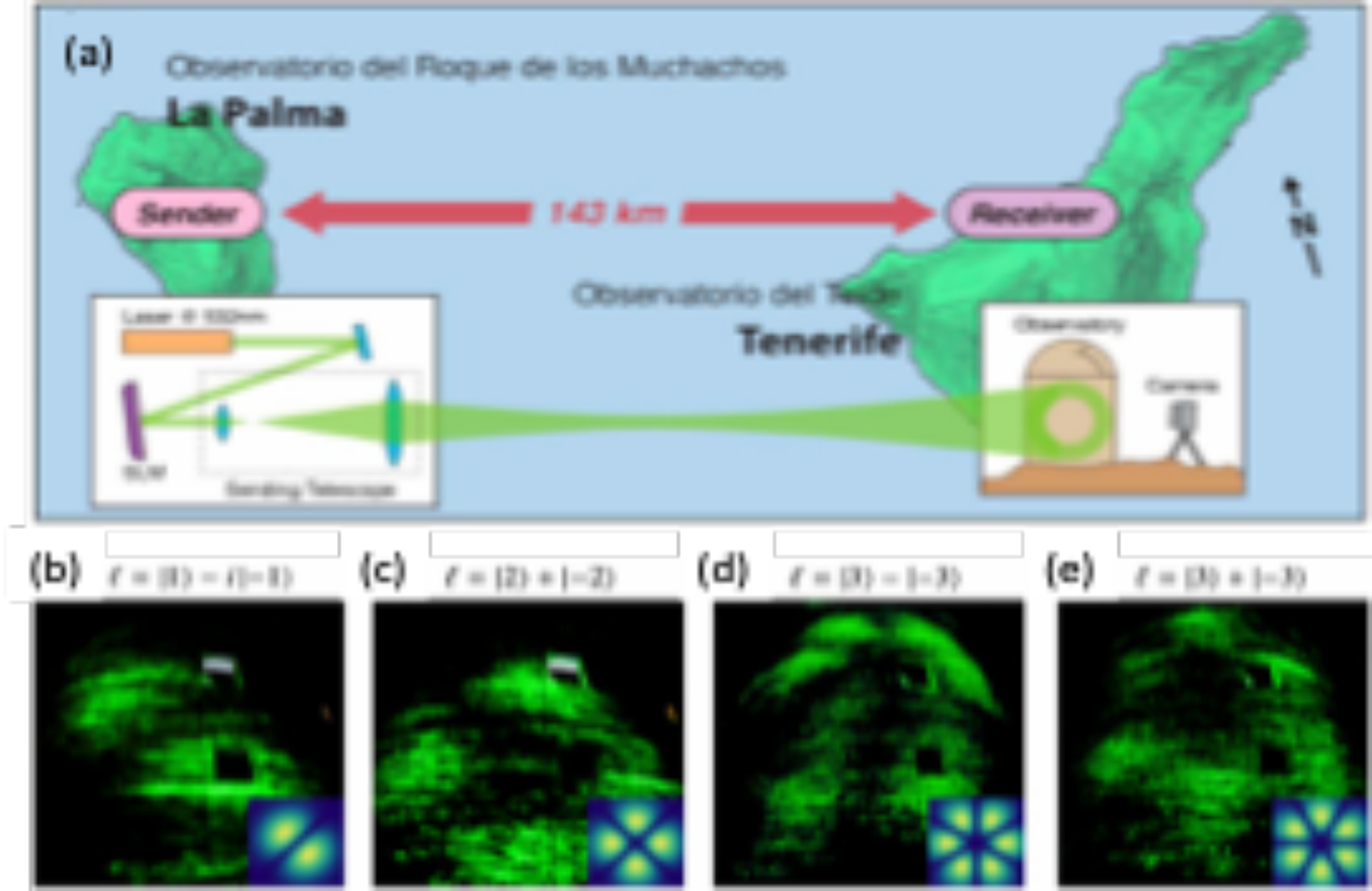
(a)
Observatorio del Roque de los Muchachos
La Palma
Sender
143 km
Receiver
Observatorio del Teide
Tenerife
Observatory
Camera
(b)
(c)
(d)
(e)

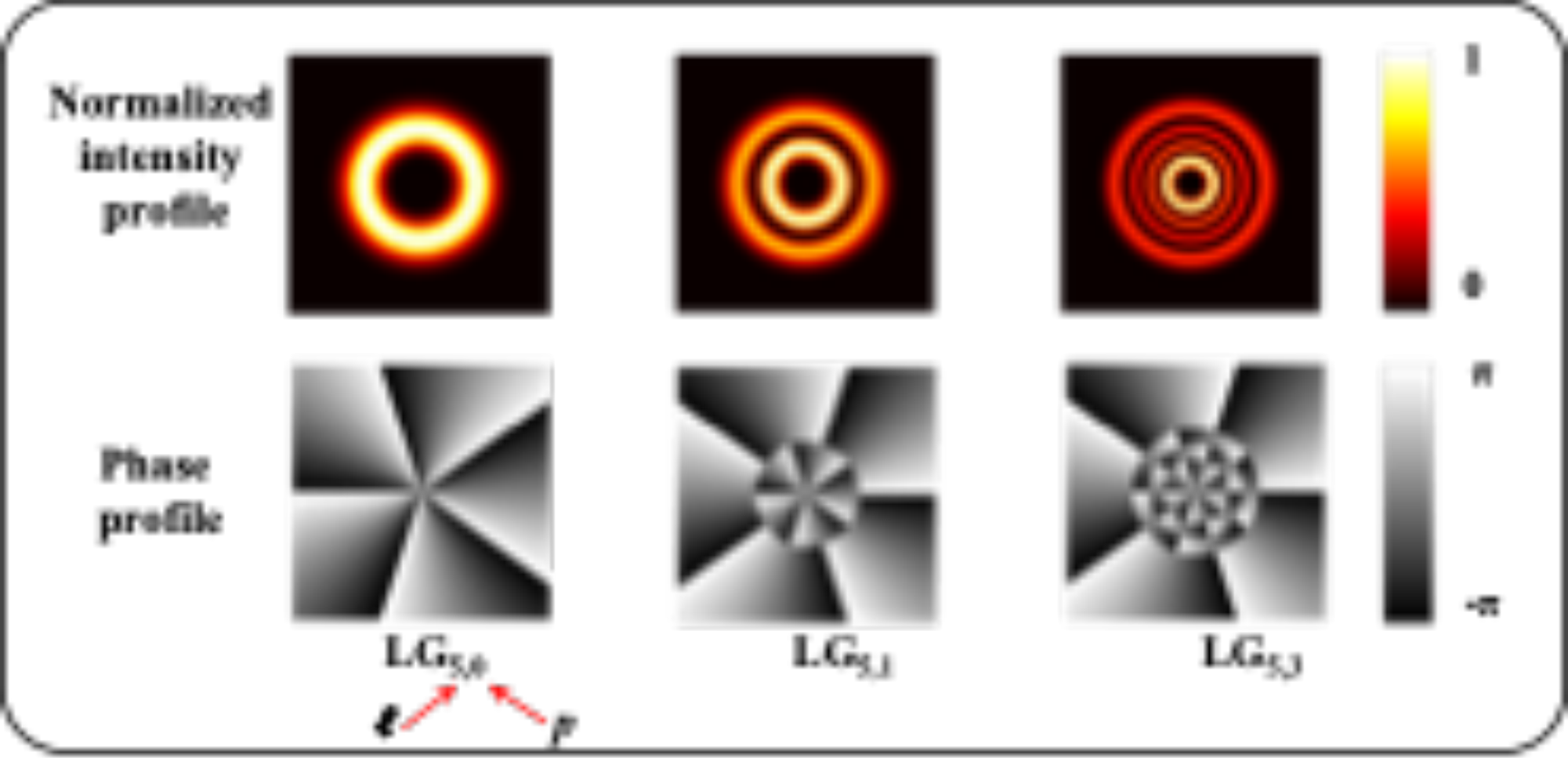
Normalized intensity profile
Phase profile
1
0
π
-π
$LG_{5,0}$
$LG_{5,1}$
$LG_{5,3}$
ℓ
p

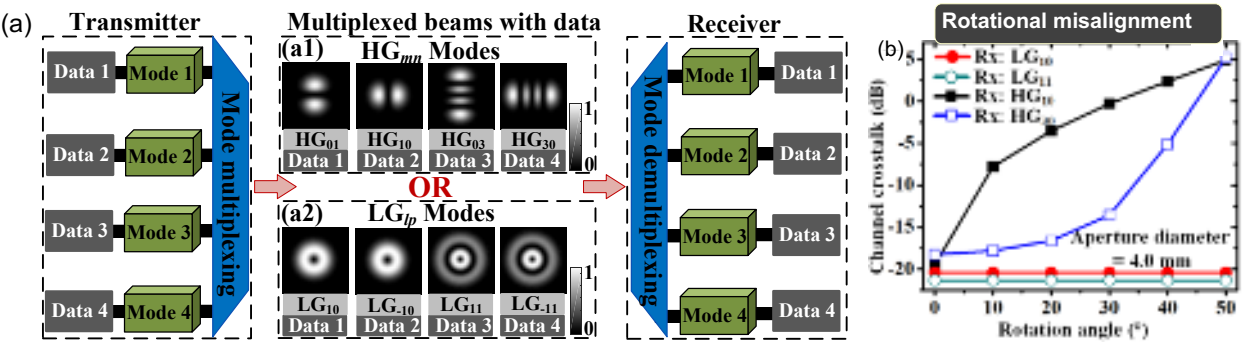
(a)
Transmitter
Data 1
Mode 1
Data 2
Mode 2
Data 3
Mode 3
Data 4
Mode 4
Mode multiplexing
Multiplexed beams with data
(a1) HGmn Modes
HG01
Data 1
HG10
Data 2
HG03
Data 3
HG30
Data 4
1
0
OR
(a2) LGlp Modes
LG10
Data 1
LG-10
Data 2
LG11
Data 3
LG-11
Data 4
1
0
Receiver
Mode demultiplexing
Mode 1
Data 1
Mode 2
Data 2
Mode 3
Data 3
Mode 4
Data 4
(b)
Rotational misalignment
Rx: LG10
Rx: LG11
Rx: HG10
Rx: HG30
Aperture diameter
= 4.0 mm
Channel crosstalk (dB)
5
0
-5
-10
-15
-20
0
10
20
30
40
50
Rotation angle (°)


Potential challenges for OAM-multiplexed free-space communication links
Turbulence
Turbulence can cause phase distortion.
Induce dynamic modal coupling and channel crosstalk.
Misalignment
An off-axis, limited-size receiver aperture will not recover the full phase change.
Induce channel crosstalk and power loss.
Divergence
Higher OAM orders diverge faster.
A limited-size receiver aperture can induce power loss and modal coupling.
Mode Mux/Demux
Scalable unitary transformation methods are required.

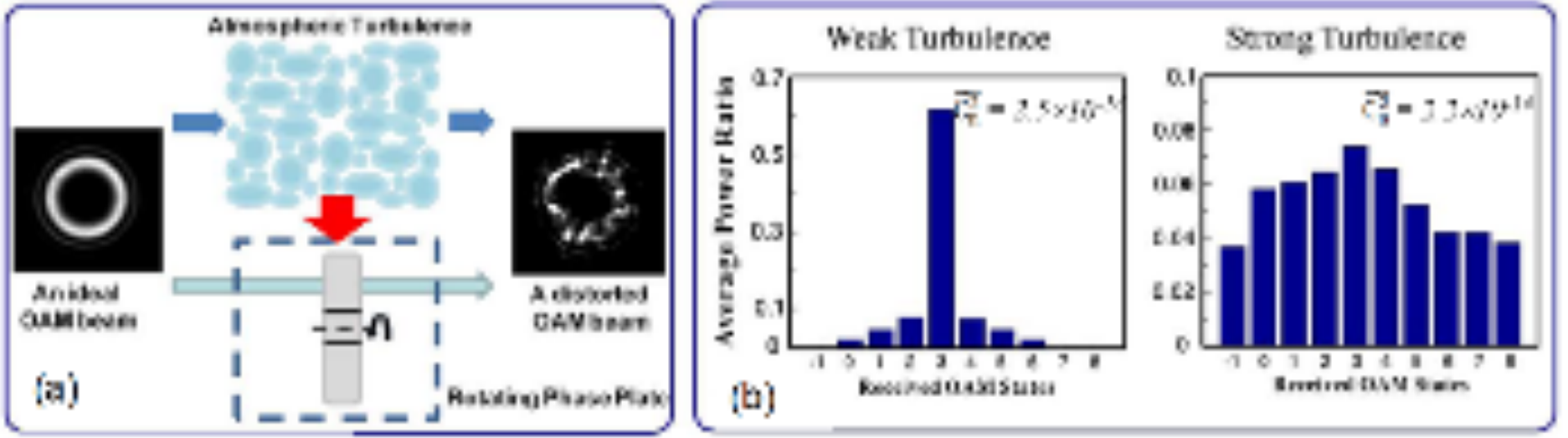
Atmosphere Turbulence
An ideal OAM beam
A distorted OAM beam
(a)
Reloading Phase Plate
Weak Turbulence
Strong Turbulence
Average Power Ratio
(b)

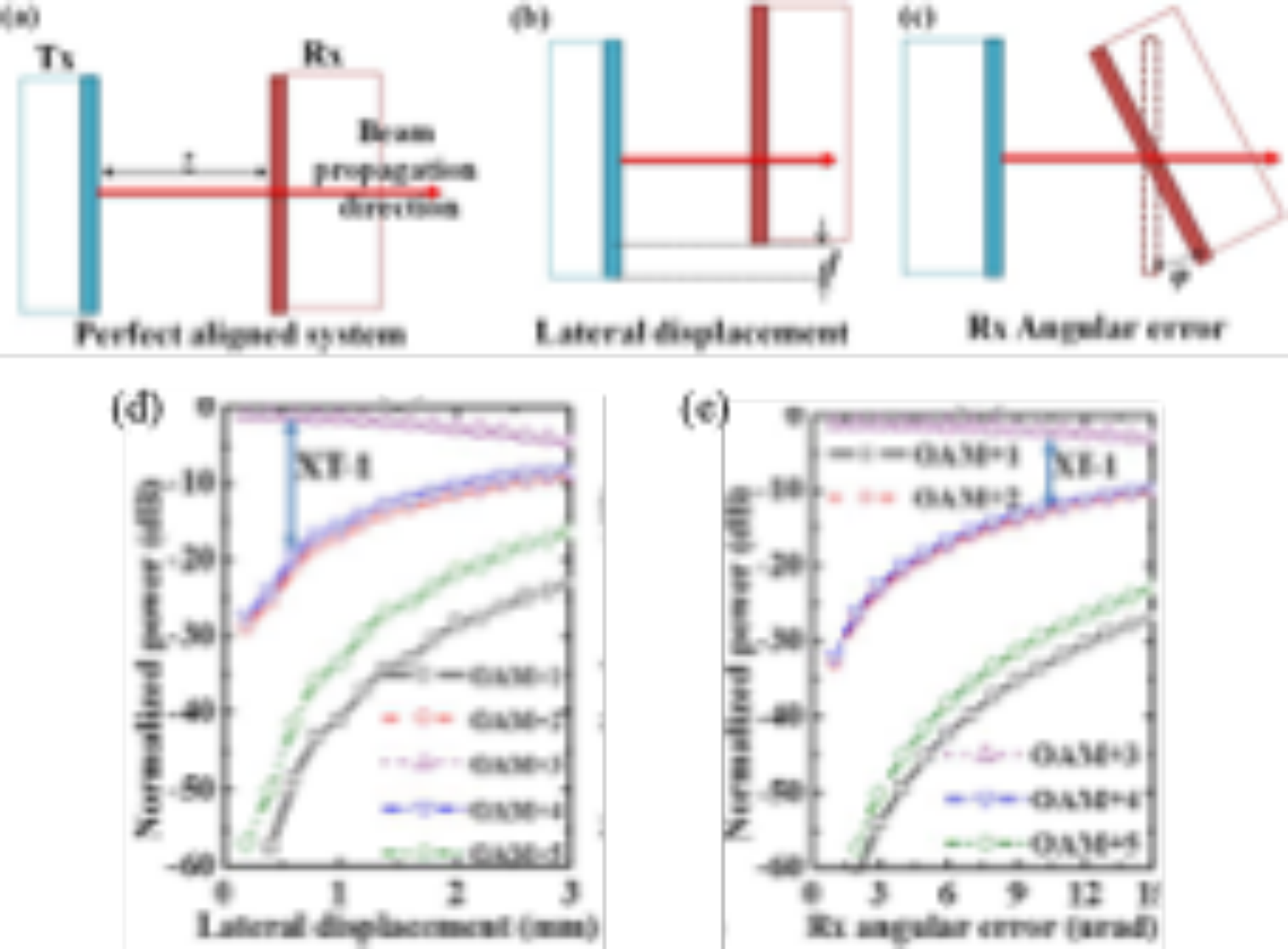
(a)
Tx
Rx
z
Beam propagation direction
Perfect aligned system
(b)
Lateral displacement
(c)
Rx Angular error
(d)
XE-1
Normalized power (dB)
0
-10
-20
-30
-40
-50
-60
0
1
2
3
Lateral displacement (mm)
(e)
GA3E+1
GA3E+2
GA3E+3
GA3E+4
GA3E+5
XE-1
Normalized power (dB)
0
3
6
9
12
Rx angular error (arad)

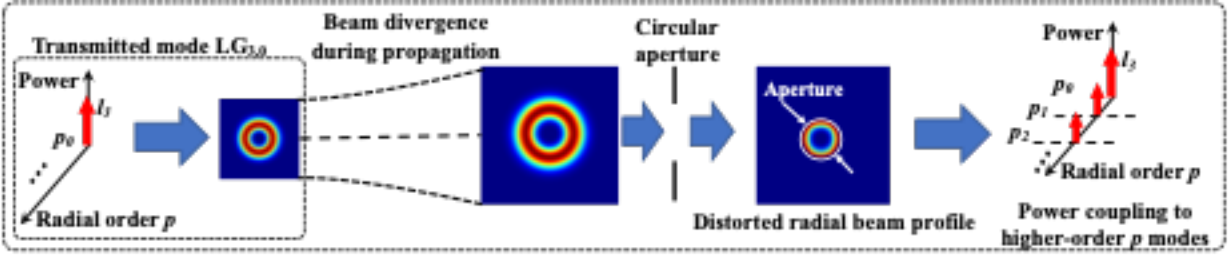
Transmitted mode LG3,0
Power
I_3
p_0
Radial order p
Beam divergence during propagation
Circular aperture
Aperture
Distorted radial beam profile
Power
I_3
p_0
p_1
p_2
Radial order p
Power coupling to higher-order p modes

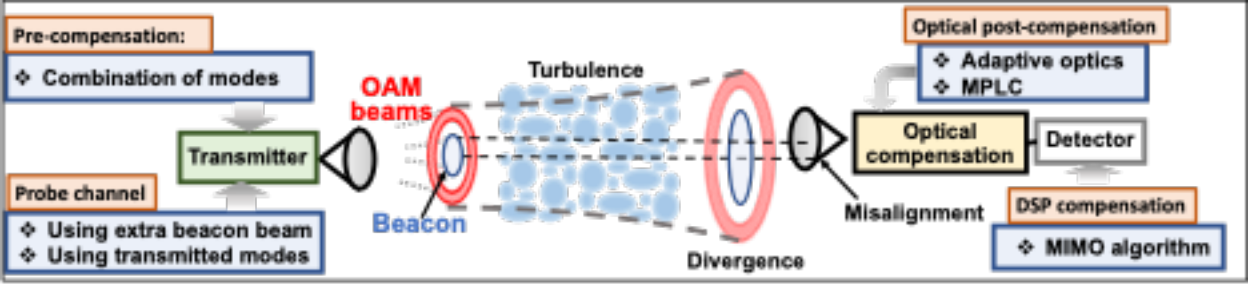
Pre-compensation:
Combination of modes
Transmitter
Probe channel
Using extra beacon beam
Using transmitted modes
OAM beams
Beacon
Turbulence
Divergence
Optical post-compensation
Adaptive optics
MPLC
Optical compensation
Detector
Misalignment
DSP compensation
MIMO algorithm

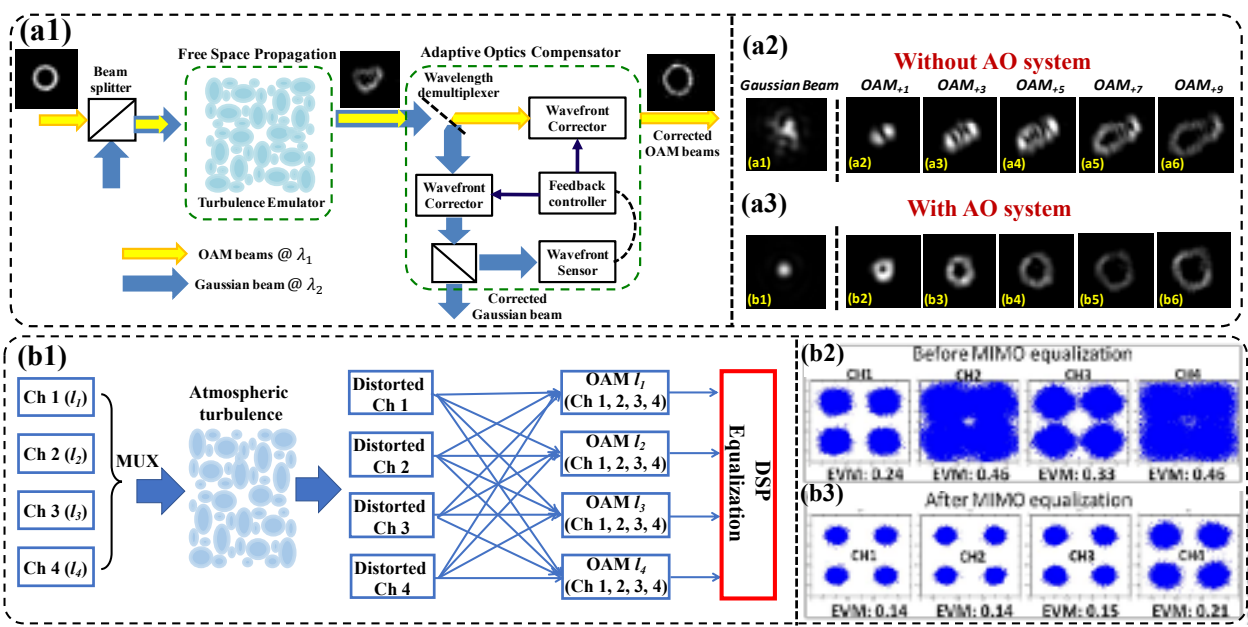
(a1)
Beam splitter
Free Space Propagation
Turbulence Emulator
Adaptive Optics Compensator
Wavelength demultiplexer
Wavefront Corrector
Feedback controller
Wavefront Corrector
Wavefront Sensor
Corrected OAM beams
Corrected Gaussian beam
OAM beams @ λ_1
Gaussian beam @ λ_2
(a2)
Without AO system
Gaussian Beam
OAM_{+1}
OAM_{+3}
OAM_{+5}
OAM_{+7}
OAM_{+9}
(a1)
(a2)
(a3)
(a4)
(a5)
(a6)
(a3)
With AO system
(b1)
(b2)
(b3)
(b4)
(b5)
(b6)
(b1)
Ch 1 (l_1)
Ch 2 (l_2)
Ch 3 (l_3)
Ch 4 (l_4)
MUX
Atmospheric turbulence
Distorted Ch 1
Distorted Ch 2
Distorted Ch 3
Distorted Ch 4
OAM l_1 (Ch 1, 2, 3, 4)
OAM l_2 (Ch 1, 2, 3, 4)
OAM l_3 (Ch 1, 2, 3, 4)
OAM l_4 (Ch 1, 2, 3, 4)
DSP Equalization
(b2)
Before MIMO equalization
CH1
CH2
CH3
CH4
EVM: 0.24
EVM: 0.46
EVM: 0.33
EVM: 0.46
(b3)
After MIMO equalization
CH1
CH2
CH3
CH4
EVM: 0.14
EVM: 0.14
EVM: 0.15
EVM: 0.21

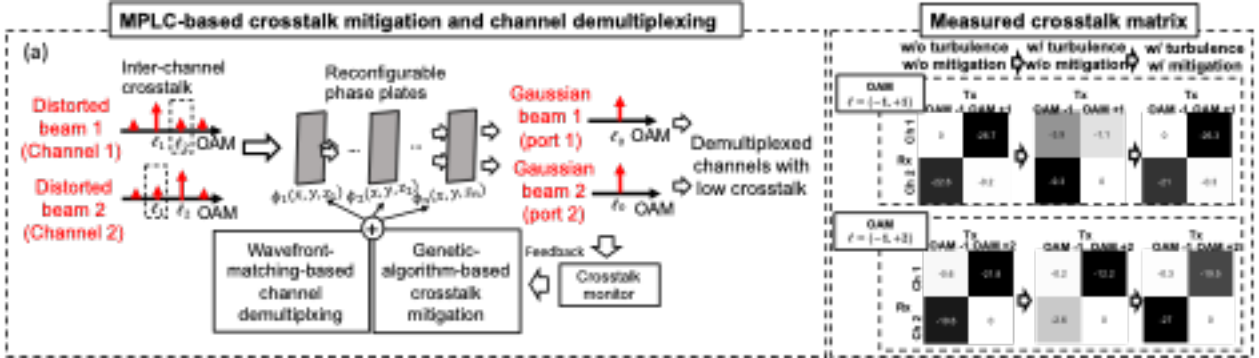
MPLC-based crosstalk mitigation and channel demultiplexing
(a)
Inter-channel crosstalk
Distorted beam 1 (Channel 1)
Distorted beam 2 (Channel 2)
OAM
Reconfigurable phase plates
Gaussian beam 1 (port 1)
Gaussian beam 2 (port 2)
Demultiplexed channels with low crosstalk
Wavefront-matching-based channel demultiplxing
Genetic-algorithm-based crosstalk mitigation
Feedback
Crosstalk monitor
Measured crosstalk matrix
w/o turbulence w/o mitigation
w/ turbulence w/o mitigation
w/ turbulence w/ mitigation
OAM
Tx
Rx
Ch 1
Ch 2


Crosstalk Mitigation Methods for OAM Multiplexed Communication Links
Adaptive optics
Use wavefront sensor and SLM
Transmit each channel on one mode
MIMO DSP
Electronic DSP method
Transmit each channel on one mode
MPLC-based method
Simultaneous crosstalk mitigation and channel demultiplexing
Scalable
Low inherent loss
Mode-combination-based method
In-fiber power measurement
Transmit each channel on multiple modes
Simple system

LG mode decomposition

Complex LG spectrum of structured light

$$U(x,y) = \sum_{\ell p} C_{\ell p} LG_{\ell p}(x,y)$$

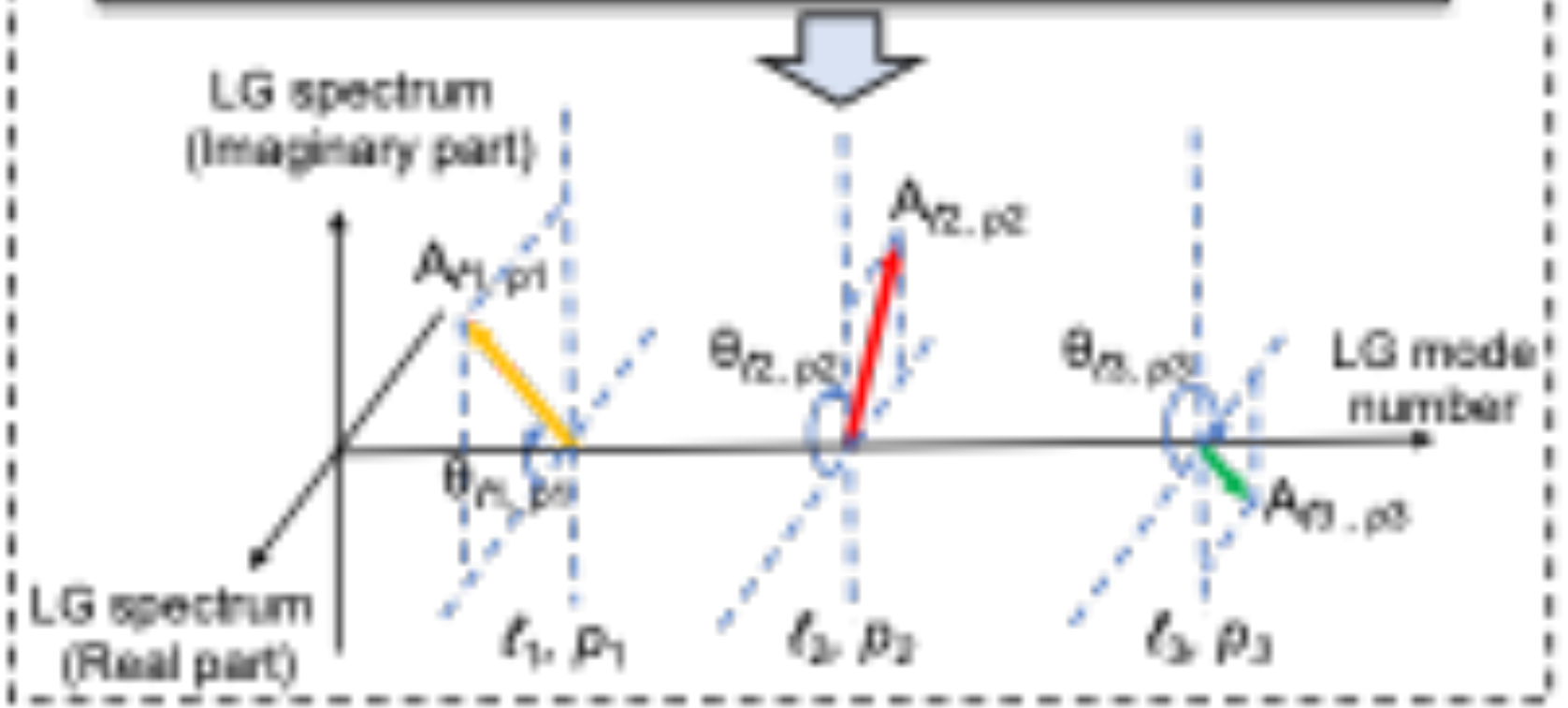

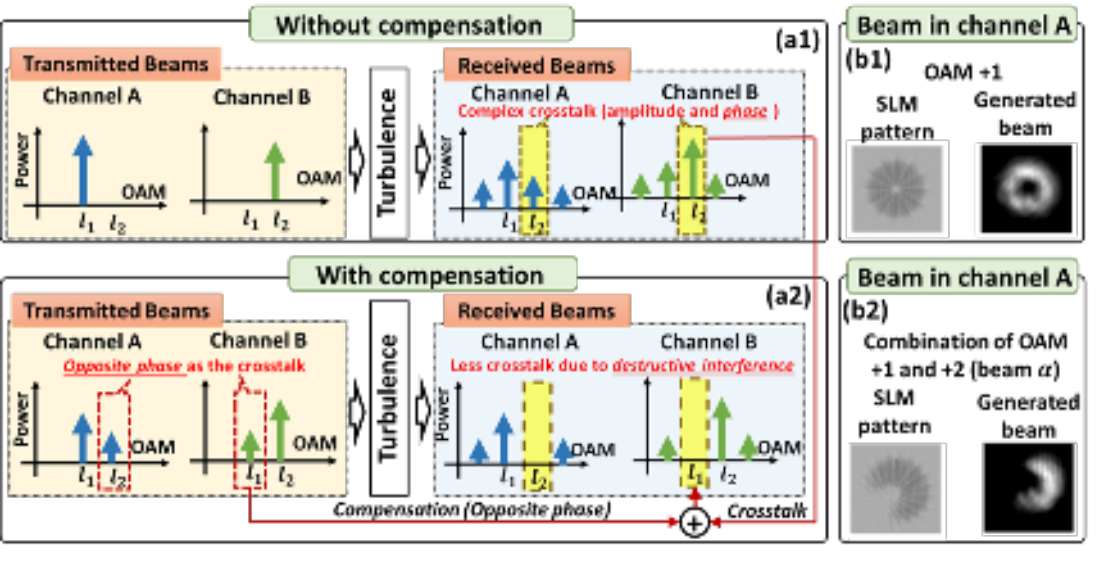
Without compensation
(a1)
Transmitted Beams
Channel A
Channel B
Power
OAM
l_1 l_2
Turbulence
Received Beams
Channel A
Channel B
Complex crosstalk (amplitude and phase)
Beam in channel A
(b1)
OAM +1
SLM pattern
Generated beam
With compensation
(a2)
Transmitted Beams
Channel A
Channel B
Opposite phase as the crosstalk
Received Beams
Channel A
Channel B
Less crosstalk due to destructive interference
Compensation (Opposite phase)
Crosstalk
Beam in channel A
(b2)
Combination of OAM +1 and +2 (beam α)
SLM pattern
Generated beam

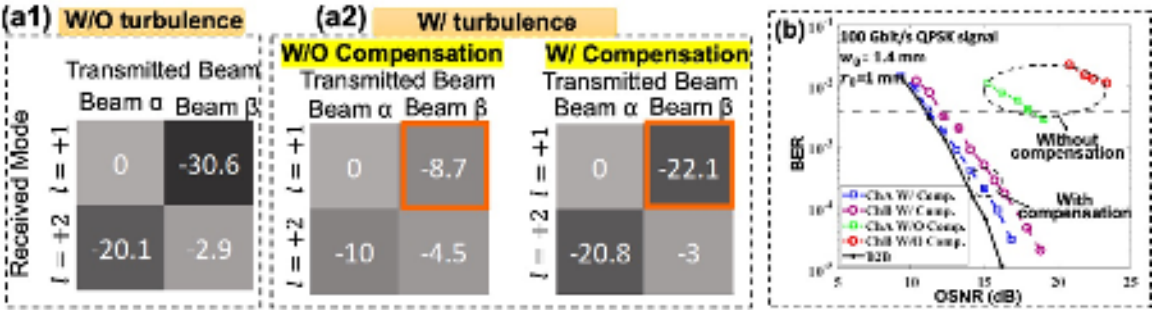
(a1) W/O turbulence
Transmitted Beam
Beam α
Beam β
Received Mode
l = +1
l = +2
0
-30.6
-20.1
-2.9
(a2)
W/O Compensation
Transmitted Beam
Beam α
Beam β
l = +1
l = +2
0
-8.7
-10
-4.5
W/ Compensation
Transmitted Beam
Beam α
Beam β
l = +1
l = +2
0
-22.1
-20.8
-3
(b)
100 Gbit/s QPSK signal
w0 = 1.4 mm
r0=1 mm
Without compensation
With compensation
Cha. W/ Comp.
Chil W/ Comp.
Cha. W/O Comp.
Chil W/O Comp.
B2B
BER
OSNR (dB)

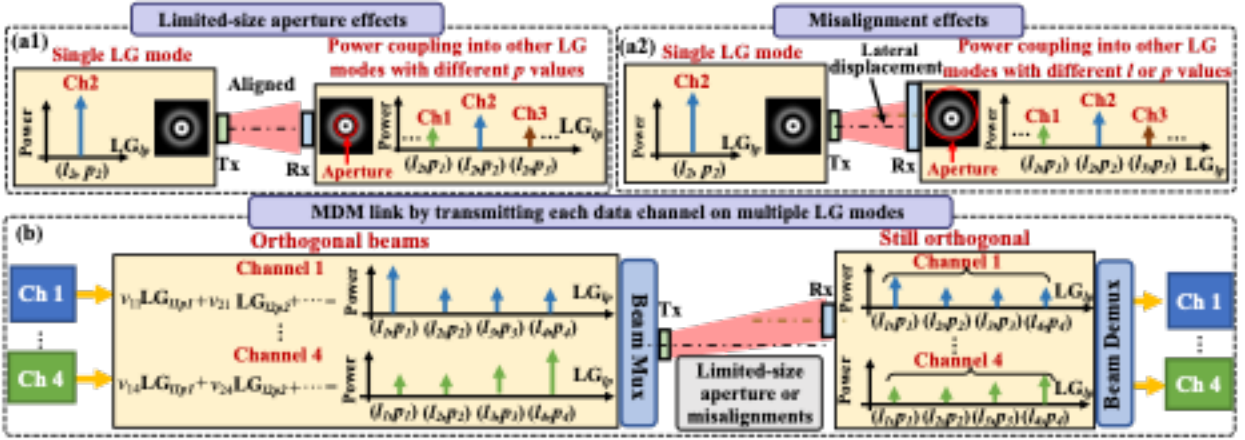
Limited-size aperture effects
(a1)
Single LG mode
Ch2
Power
LG_{l_2}
(l_2, p_2)
Aligned
Tx
Rx
Aperture
Power coupling into other LG modes with different p values
Ch1
Ch2
Ch3
LG_{l_p}
(l_2p_1) (l_2p_2) (l_2p_3)
Misalignment effects
(a2)
Single LG mode
Lateral displacement
Power coupling into other LG modes with different l or p values
MDM link by transmitting each data channel on multiple LG modes
(b)
Orthogonal beams
Channel 1
Channel 4
$v_{11}LG_{l_1p_1}+v_{21}LG_{l_2p_2}+\cdots=$
$v_{14}LG_{l_1p_1}+v_{24}LG_{l_2p_2}+\cdots=$
(l_1p_1) (l_2p_2) (l_3p_3) (l_4p_4)
Ch 1
Ch 4
Beam Mux
Tx
Rx
Limited-size aperture or misalignments
Still orthogonal
Beam Demux

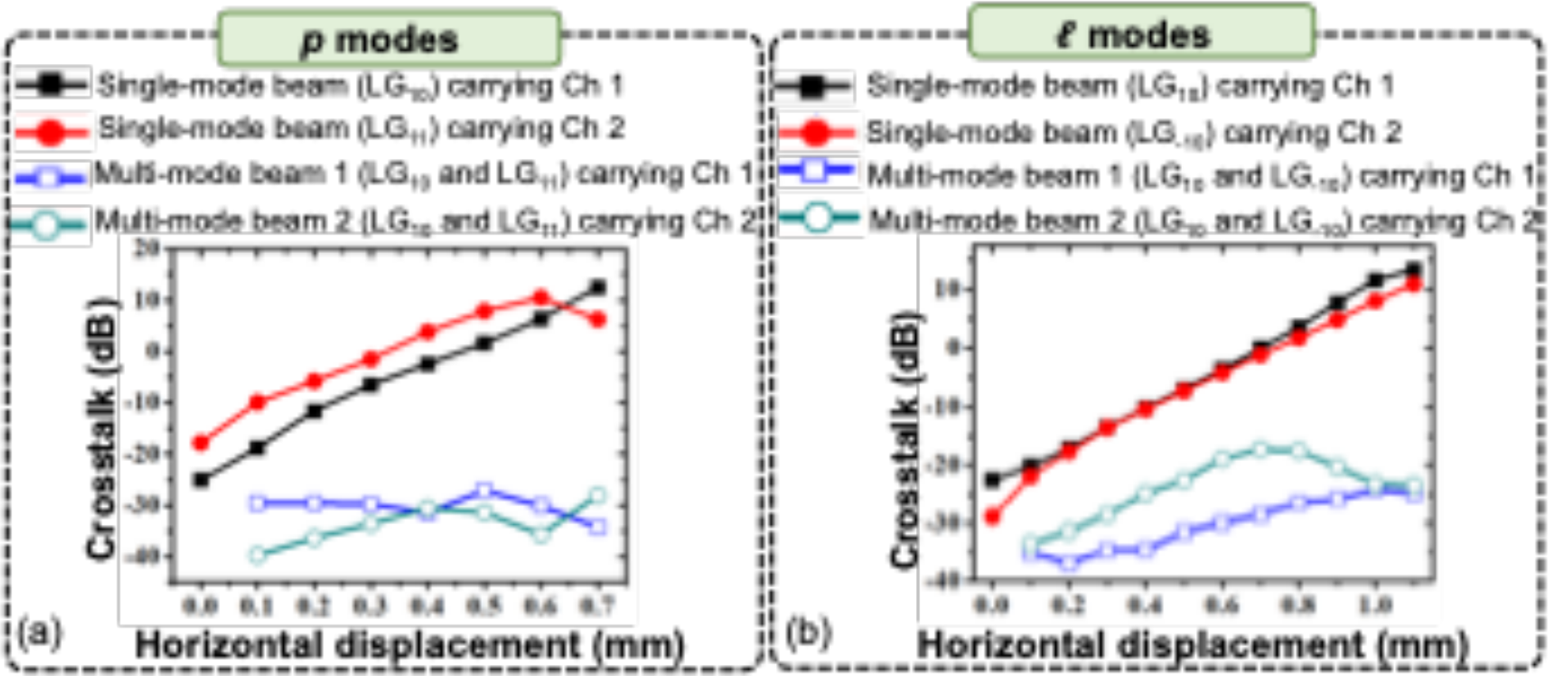
p modes
Single-mode beam (LG00) carrying Ch 1
Single-mode beam (LG11) carrying Ch 2
Multi-mode beam 1 (LG13 and LG11) carrying Ch 1
Multi-mode beam 2 (LG15 and LG11) carrying Ch 2
Crosstalk (dB)
Horizontal displacement (mm)
(a)
ℓ modes
Single-mode beam (LG1,0) carrying Ch 1
Single-mode beam (LG-1,0) carrying Ch 2
Multi-mode beam 1 (LG1,0 and LG-1,0) carrying Ch 1
Multi-mode beam 2 (LG3,0 and LG-3,0) carrying Ch 2
Crosstalk (dB)
Horizontal displacement (mm)
(b)

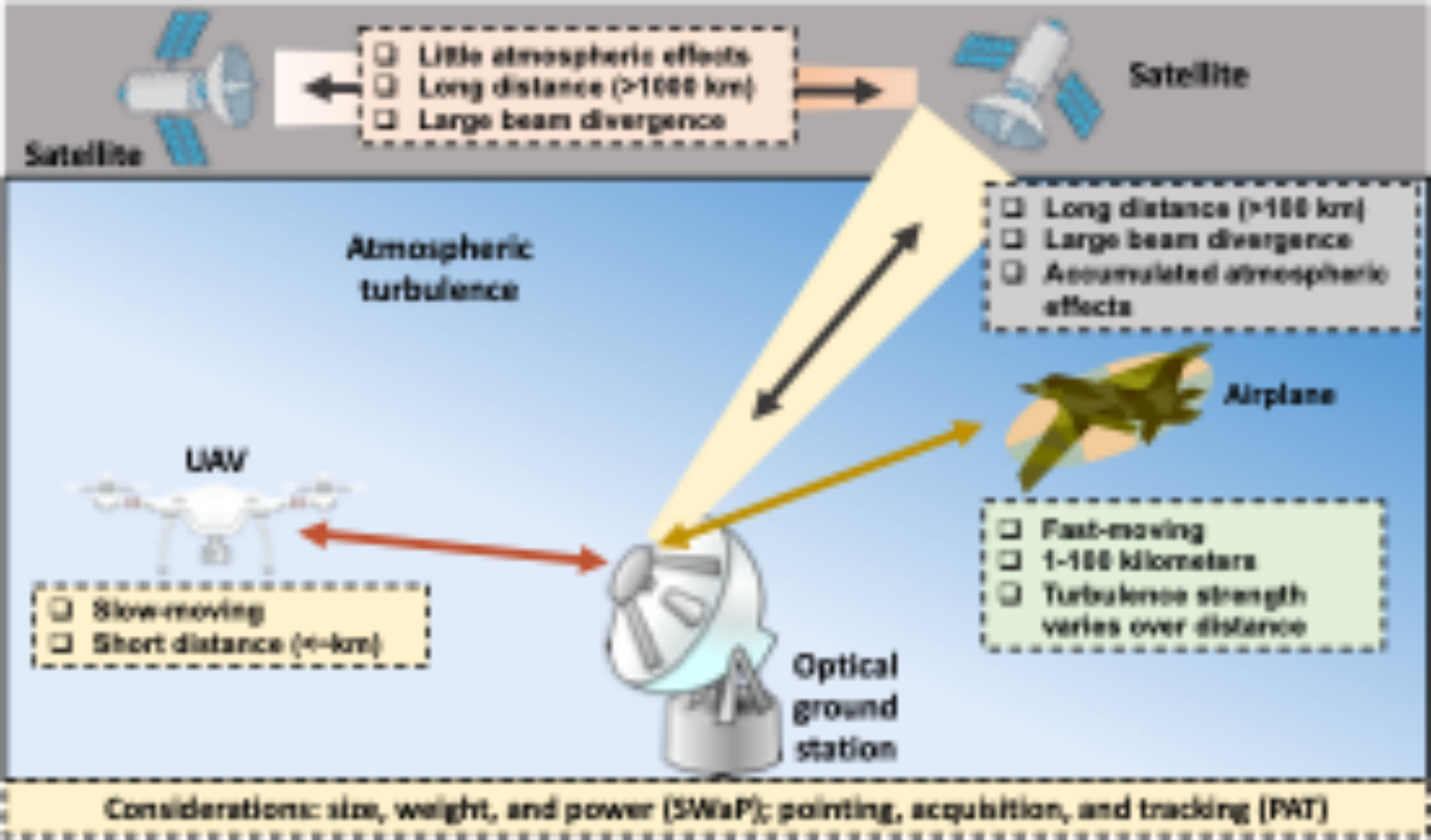
Satellite
Little atmospheric effects
Long distance (>1000 km)
Large beam divergence
Satellite
Long distance (>100 km)
Large beam divergence
Accumulated atmospheric effects
Atmospheric turbulence
Airplane
UAV
Fast-moving
1-100 kilometers
Turbulence strength varies over distance
Slow-moving
Short distance (<~km)
Optical ground station
Considerations: size, weight, and power (SWaP); pointing, acquisition, and tracking (PAT)

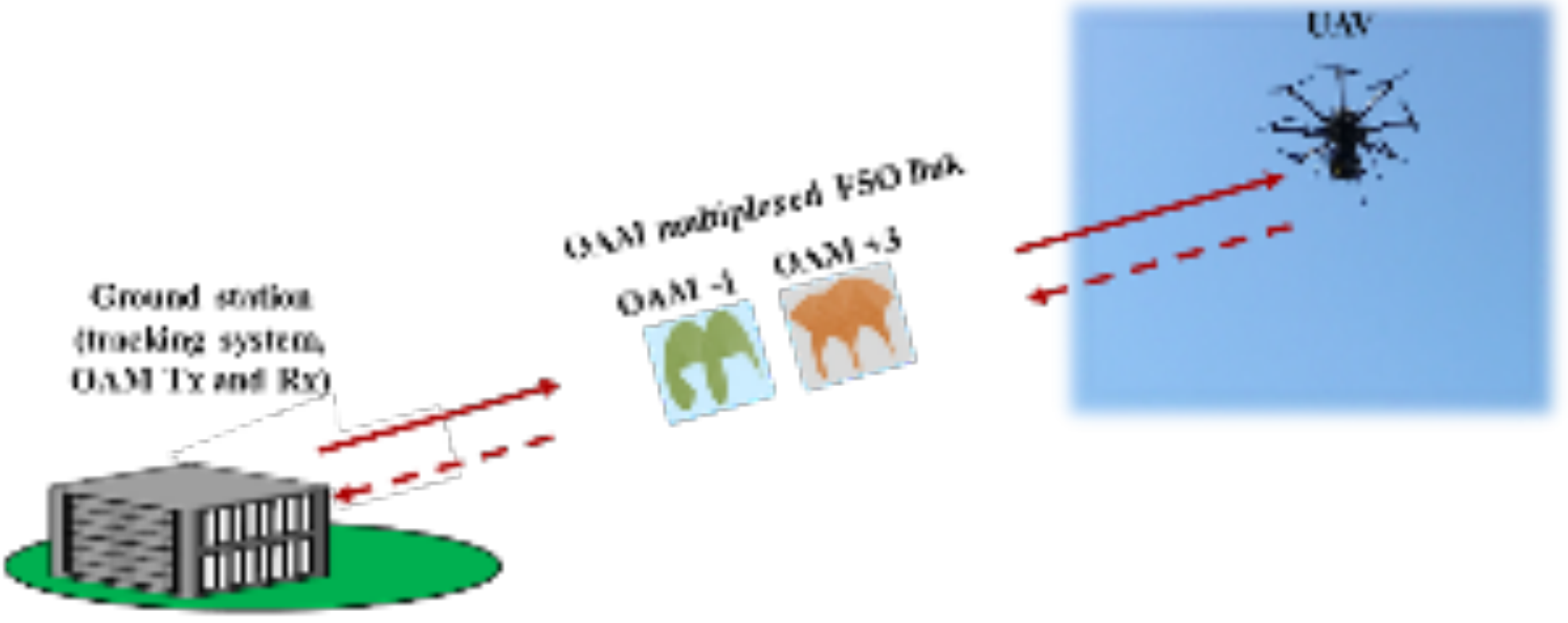
UAV
OAM multiplexed FSO link
OAM -3
OAM +3
Ground station
(tracking system,
OAM Tx and Rx)

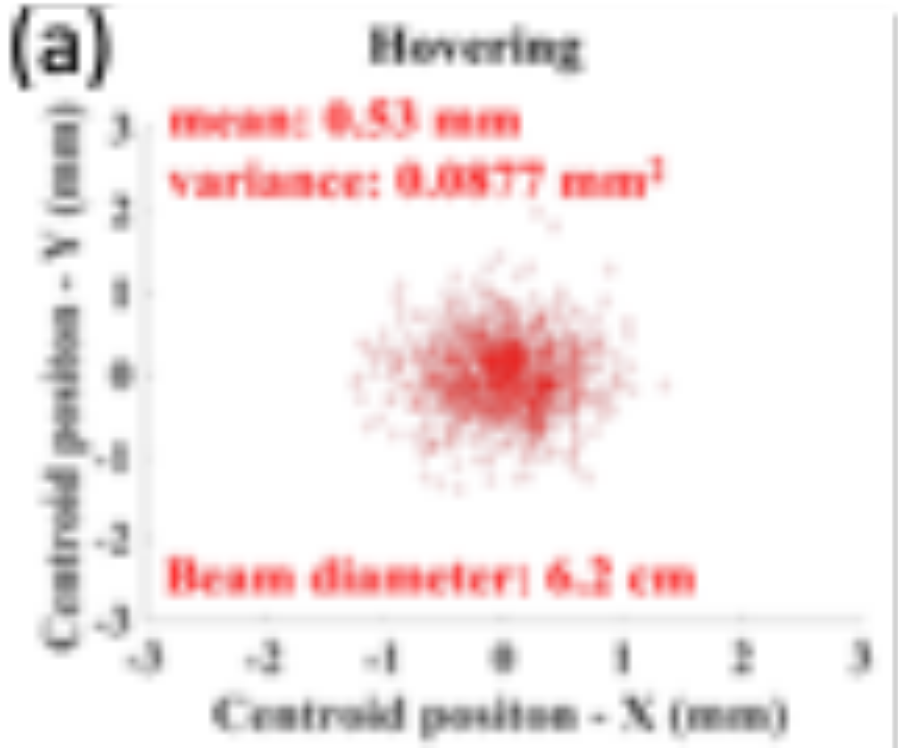
(a)
Hovering
mean: 0.53 mm
variance: 0.0877 mm²
Beam diameter: 6.2 cm
Centroid position - Y (mm)
Centroid positon - X (mm)

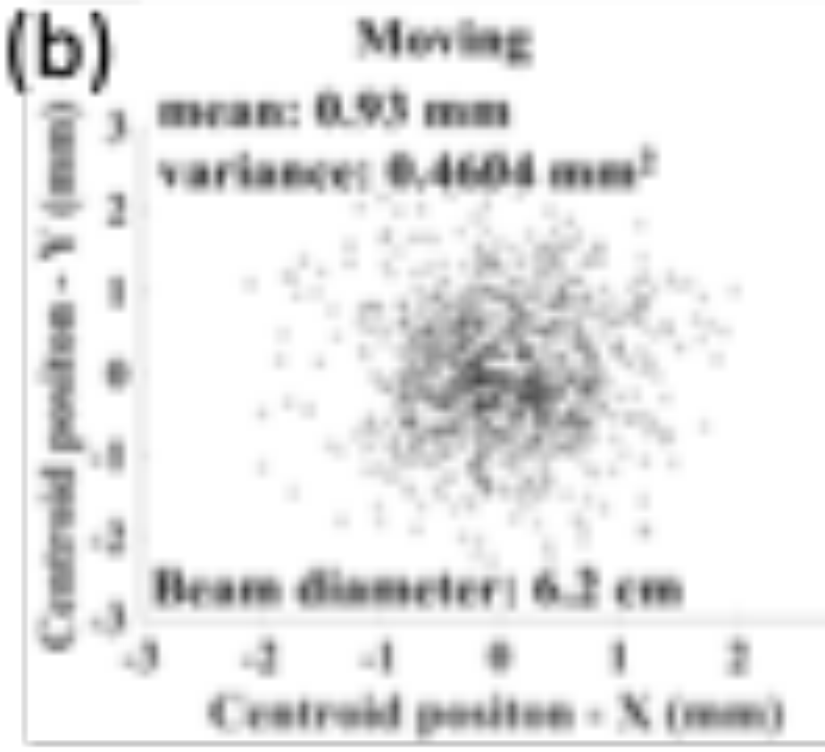
(b)
Moving
mean: 0.93 mm
variance: 0.4604 mm²
Beam diameter: 6.2 cm
Centroid position - Y (mm)
Centroid positon - X (mm)

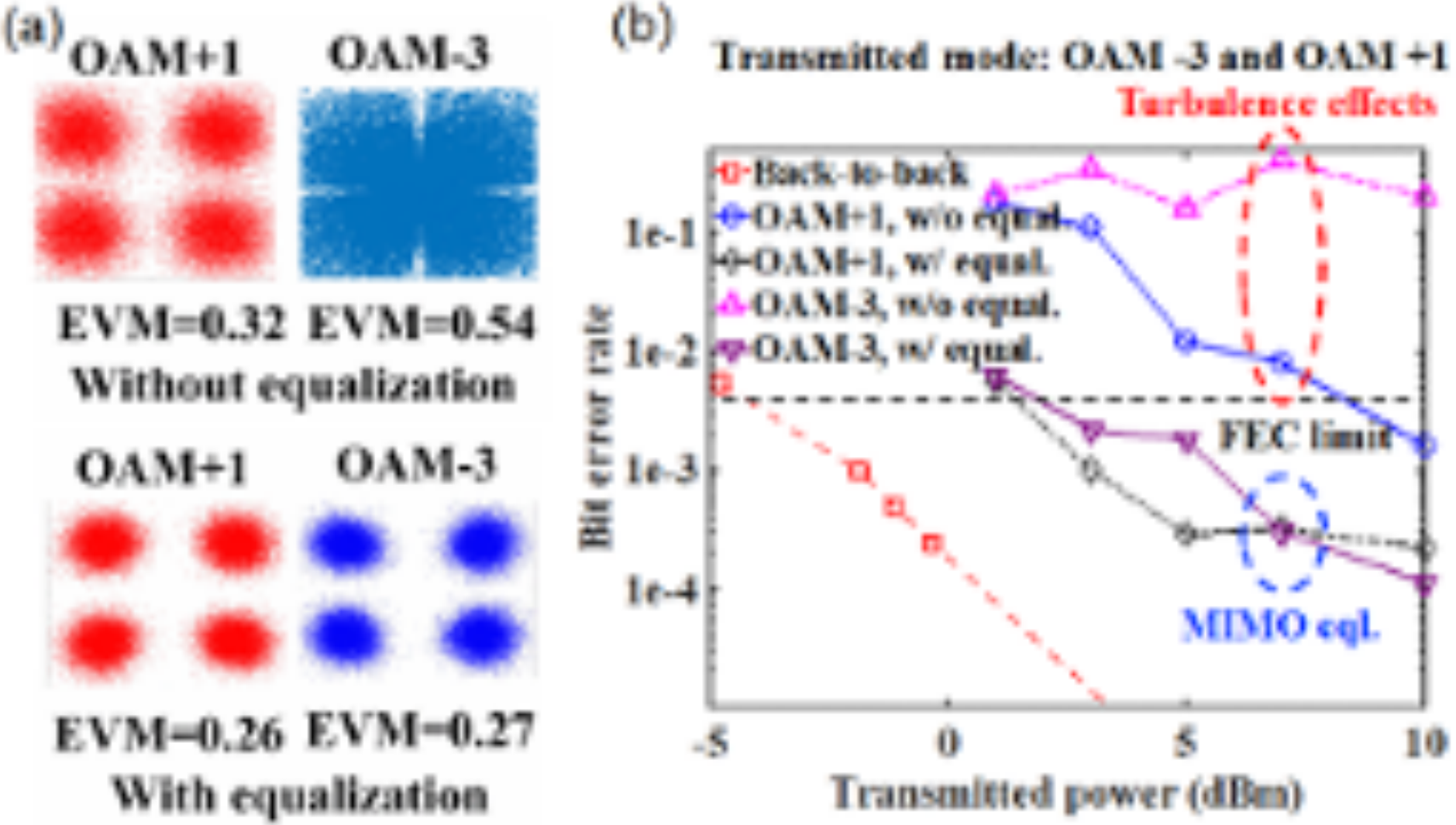
(a)
OAM+1
OAM-3
EVM=0.32
EVM=0.54
Without equalization
OAM+1
OAM-3
EVM=0.26
EVM=0.27
With equalization
(b)
Transmitted mode: OAM -3 and OAM +1
Turbulence effects
Back-to-back
OAM+1, w/o equal.
OAM+1, w/ equal.
OAM-3, w/o equal.
OAM-3, w/ equal.
FEC limit
MIMO eql.
Bit error rate
1e-1
1e-2
1e-3
1e-4
-5
0
5
10
Transmitted power (dBm)

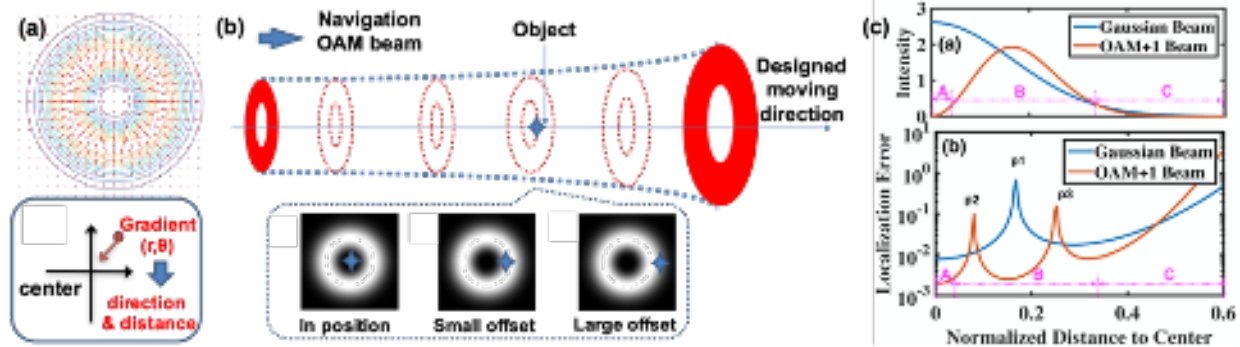
(a)
Gradient
(r,θ)
center
direction
& distance
(b)
Navigation
OAM beam
Object
Designed
moving
direction
In position
Small offset
Large offset
(c)
Gaussian Beam
OAM+1 Beam
Intensity
(a)
A
B
C
(b)
Localization Error
ρ1
ρ2
ρ3
Normalized Distance to Center

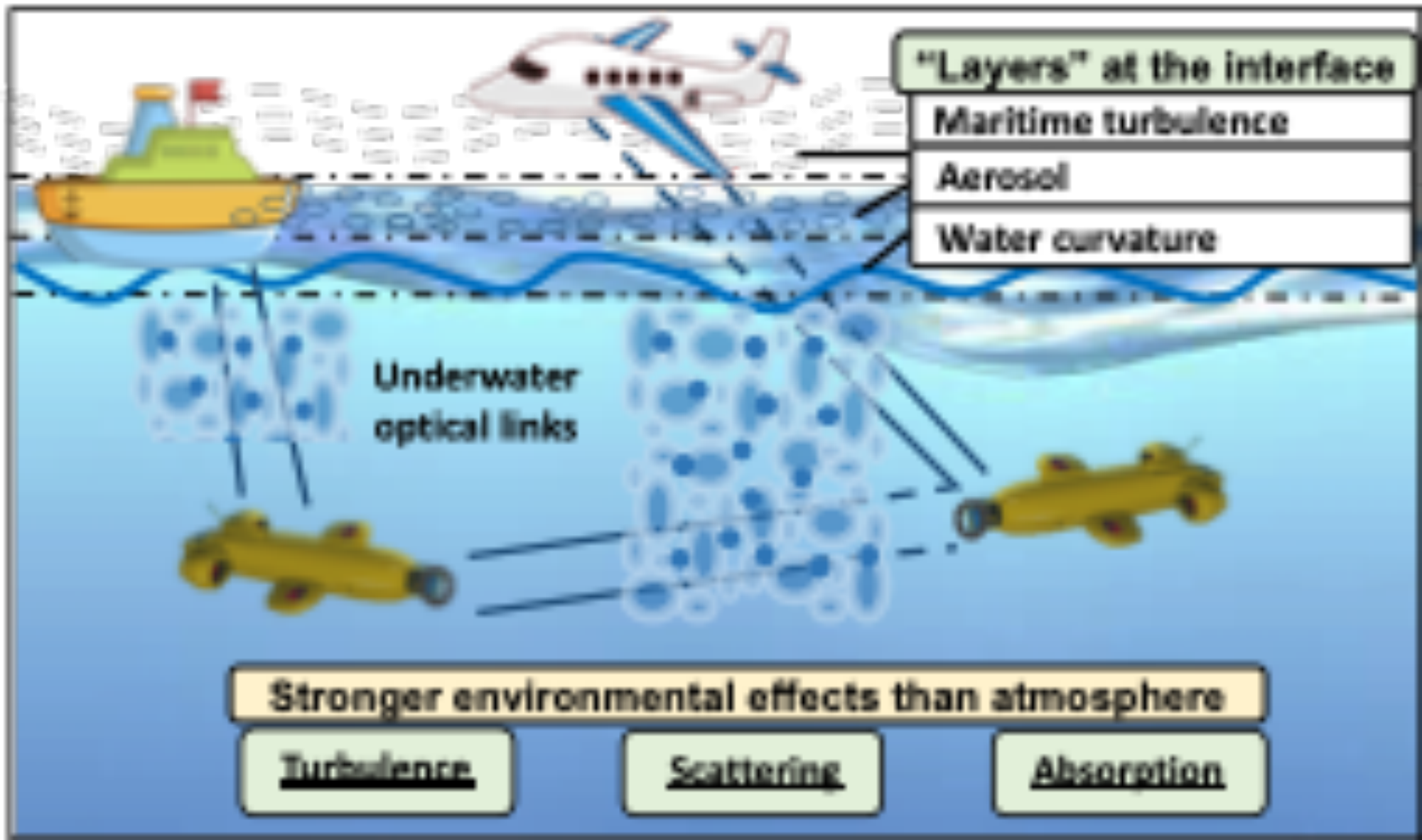
"Layers" at the interface
Maritime turbulence
Aerosol
Water curvature
Underwater optical links
Stronger environmental effects than atmosphere
Turbulence
Scattering
Absorption

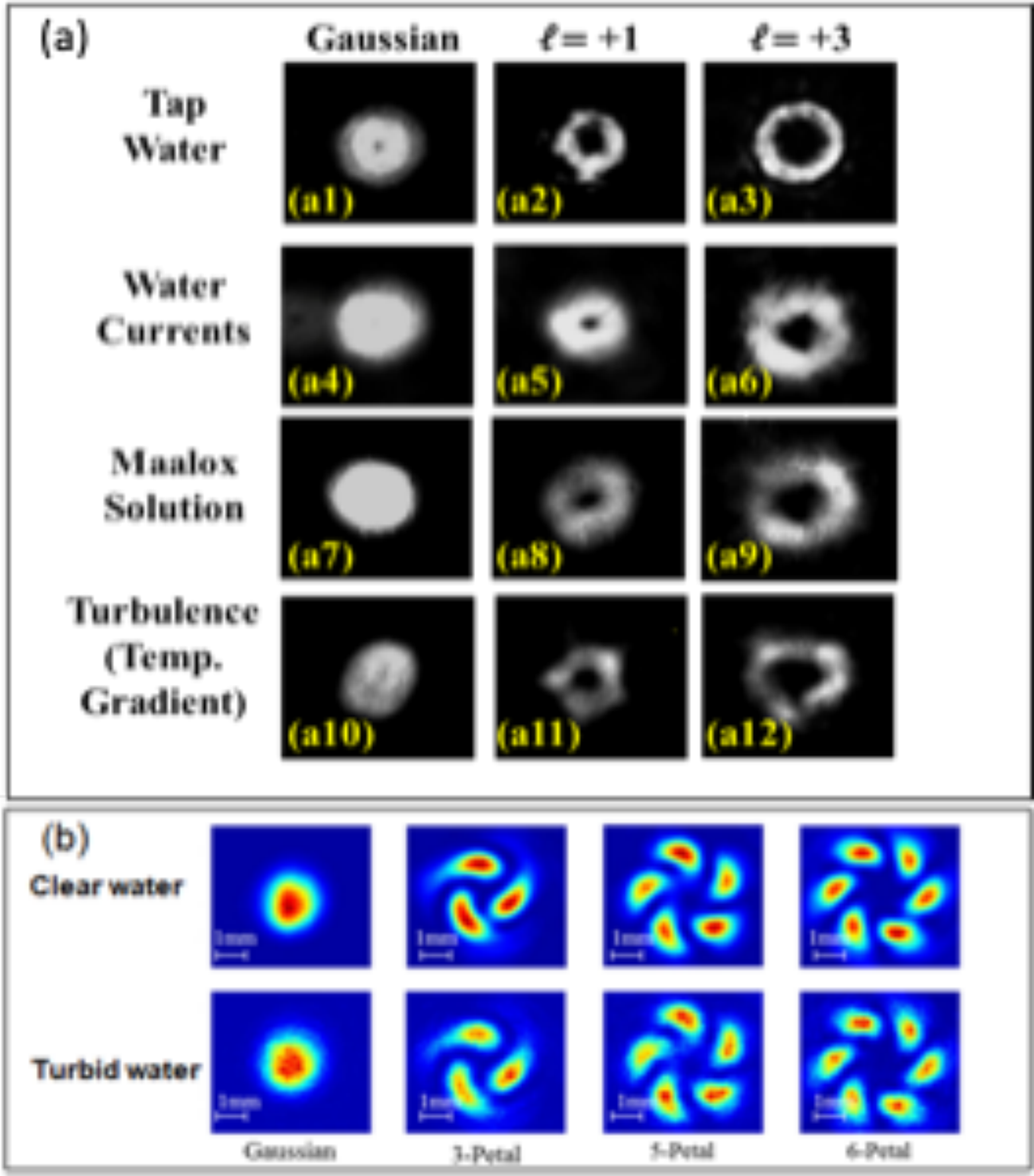
(a)
Gaussian
ℓ = +1
ℓ = +3
Tap Water
(a1)
(a2)
(a3)
Water Currents
(a4)
(a5)
(a6)
Maalox Solution
(a7)
(a8)
(a9)
Turbulence (Temp. Gradient)
(a10)
(a11)
(a12)
(b)
Clear water
Turbid water
Gaussian
3-Petal
5-Petal
6-Petal

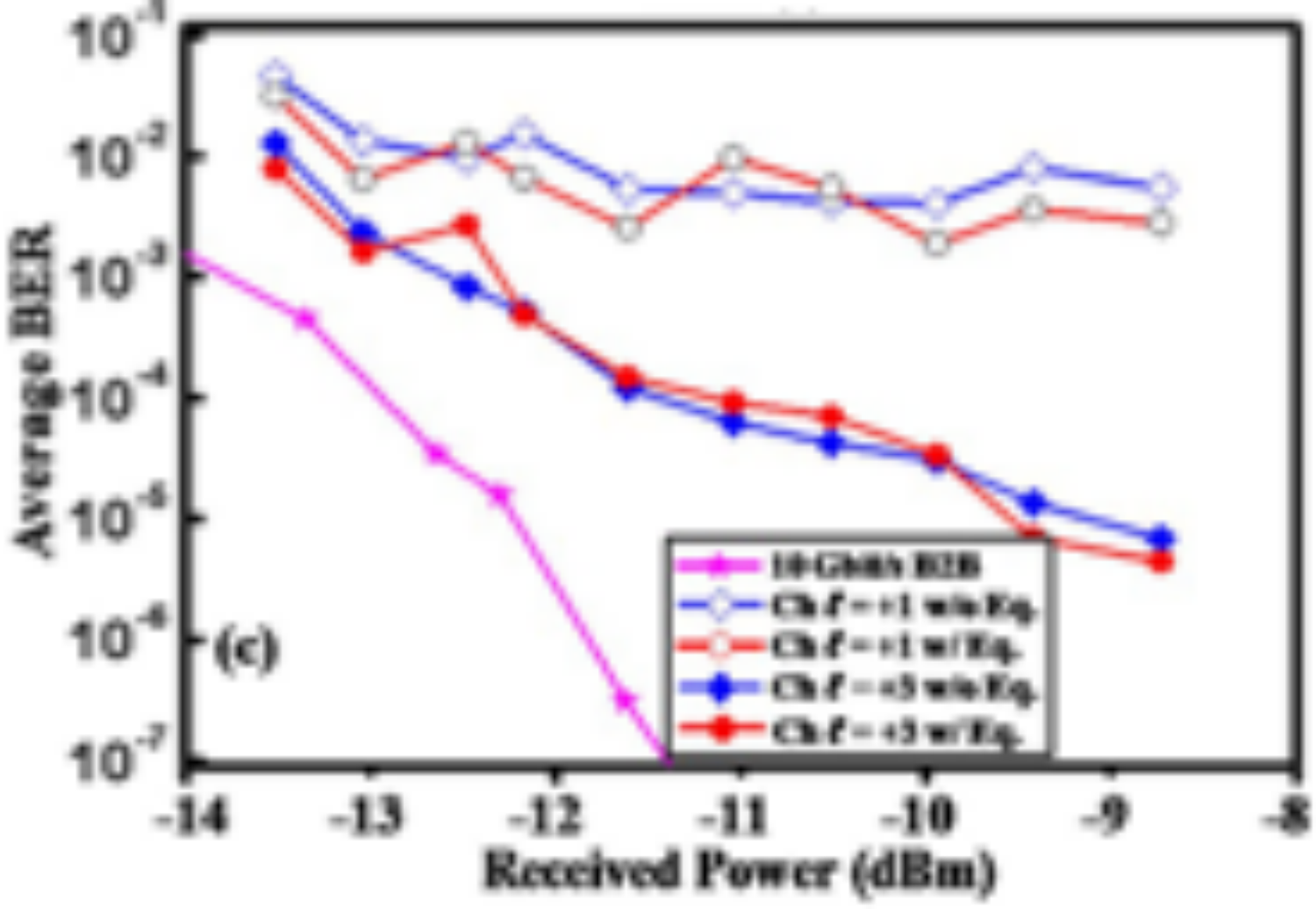
Average BER
Received Power (dBm)
(c)
10 Gbit/s B2B
Ch.f = +1 w/o Eq.
Ch.f = +1 w/ Eq.
Ch.f = +3 w/o Eq.
Ch.f = +3 w/ Eq.

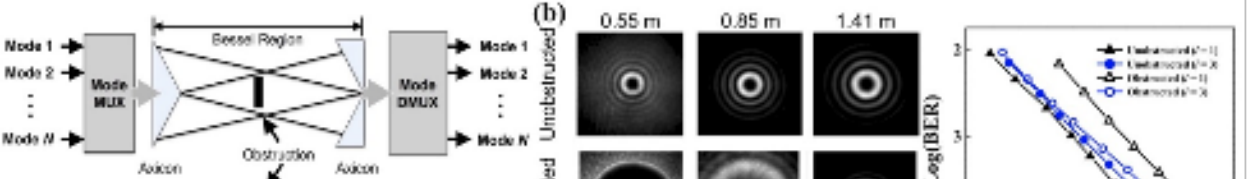
Mode 1
Mode 2
Mode N
Mode MUX
Bessel Region
Mode DMUX
Mode 1
Mode 2
Mode N
Axicon
Obstruction
Axicon
(a)
Before Obstruction
After Obstruction
Self-healed
(b)
0.55 m
0.85 m
1.41 m
Unobstructed
Obstructed
Obstruction Plane
Sensor Plane
(c)
-Log(BER)
OSNR (dB)

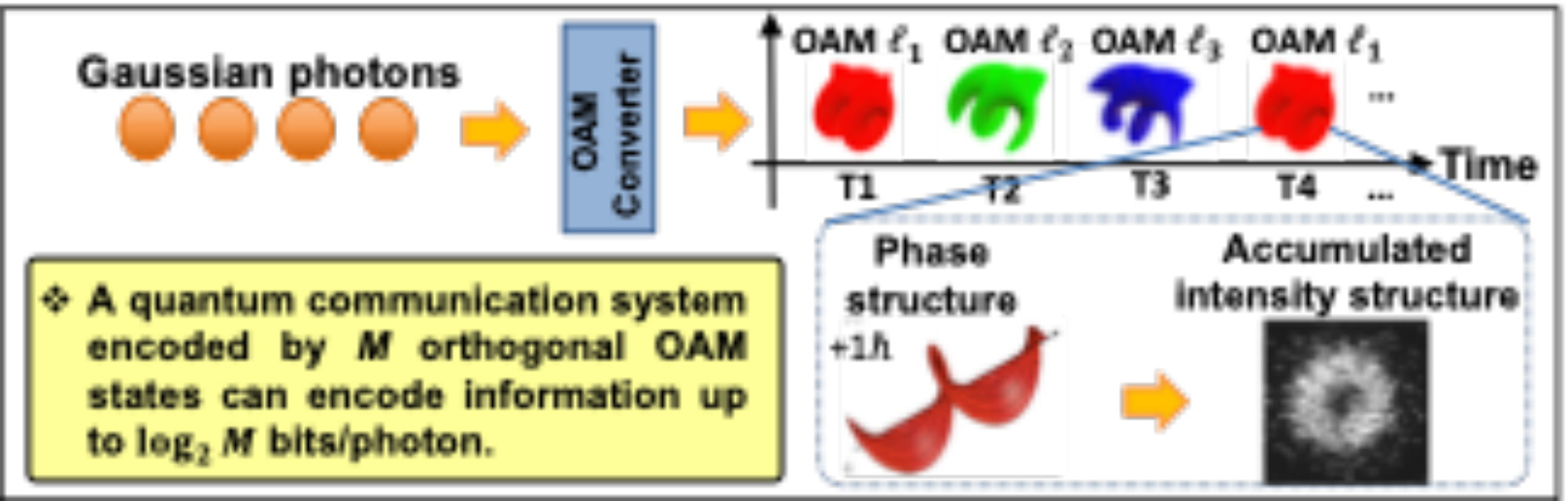
Gaussian photons
OAM Converter
OAM ℓ_1
OAM ℓ_2
OAM ℓ_3
OAM ℓ_1
...
Time
T1
T2
T3
T4
...
Phase structure
+1ħ
Accumulated intensity structure
❖ A quantum communication system encoded by M orthogonal OAM states can encode information up to $\log_2 M$ bits/photon.

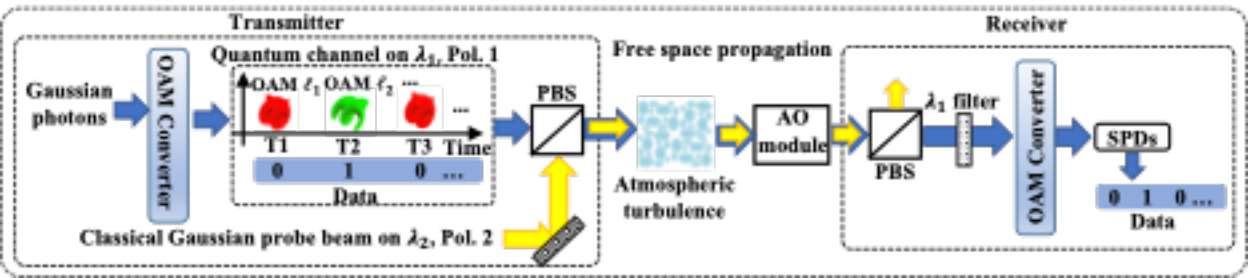
Transmitter
Gaussian photons
OAM Convertor
Quantum channel on λ_1, Pol. 1
OAM ℓ_1
OAM ℓ_2
...
T1
T2
T3
Time
0 1 0 ...
Data
PBS
Classical Gaussian probe beam on λ_2, Pol. 2
Free space propagation
Atmospheric turbulence
AO module
Receiver
PBS
λ_1 filter
OAM Converter
SPDs
0 1 0 ...
Data

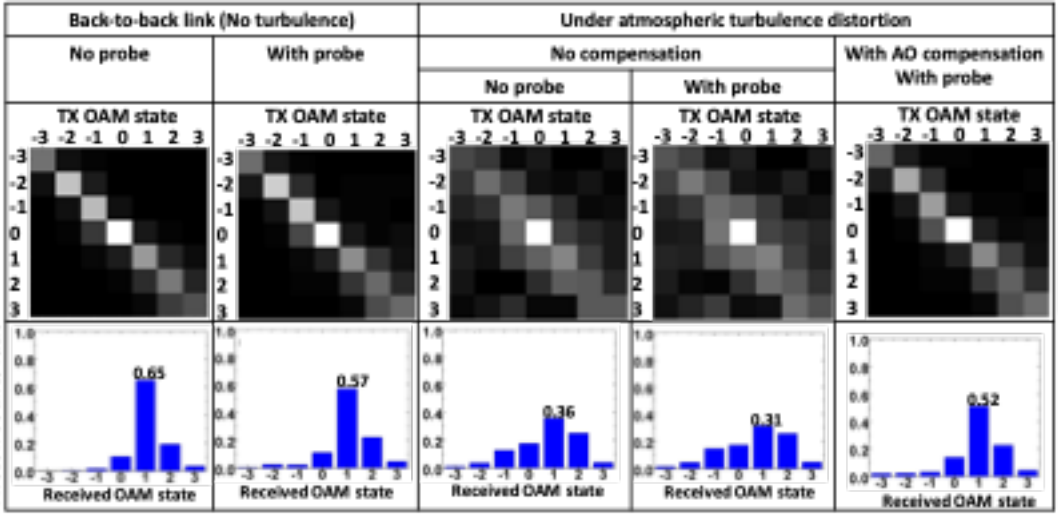
Back-to-back link (No turbulence)
Under atmospheric turbulence distortion
No probe
With probe
No compensation
With AO compensation
No probe
With probe
With probe
TX OAM state
-3 -2 -1 0 1 2 3
RX OAM state
Photon counts ratio
0.65
0.57
0.36
0.31
0.52
Received OAM state

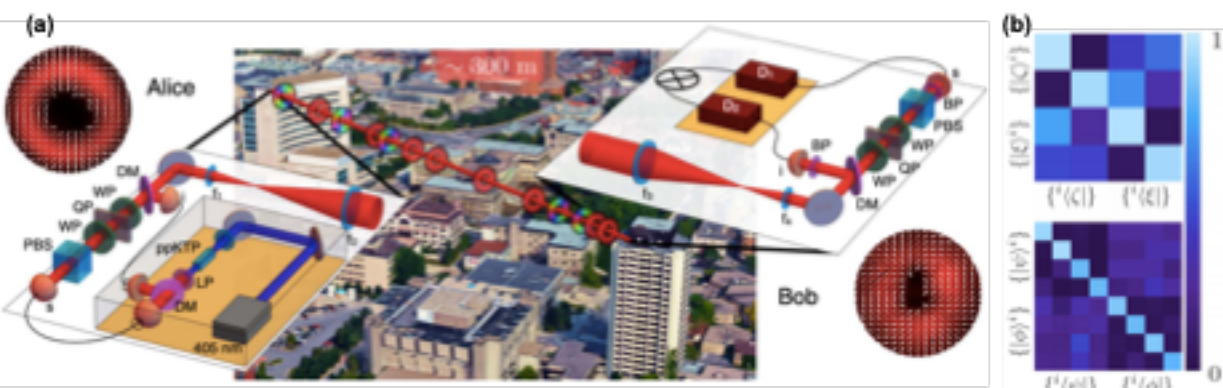
(a)
Alice
Bob
DM
QP
WP
PBS
s
ppKTP
LP
405 nm
BP
i
(b)
1
0

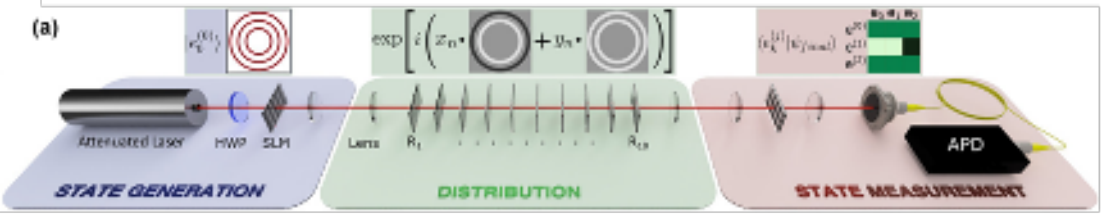
(a)
Attenuated Laser
HWP
SLM
Lens
APD
STATE GENERATION
DISTRIBUTION
STATE MEASUREMENT

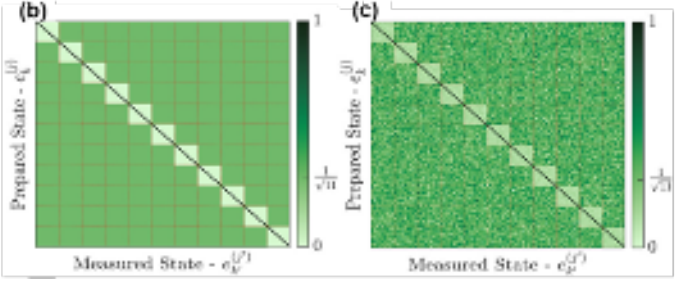
(b)
(c)
Prepared State
Measured State
1
0

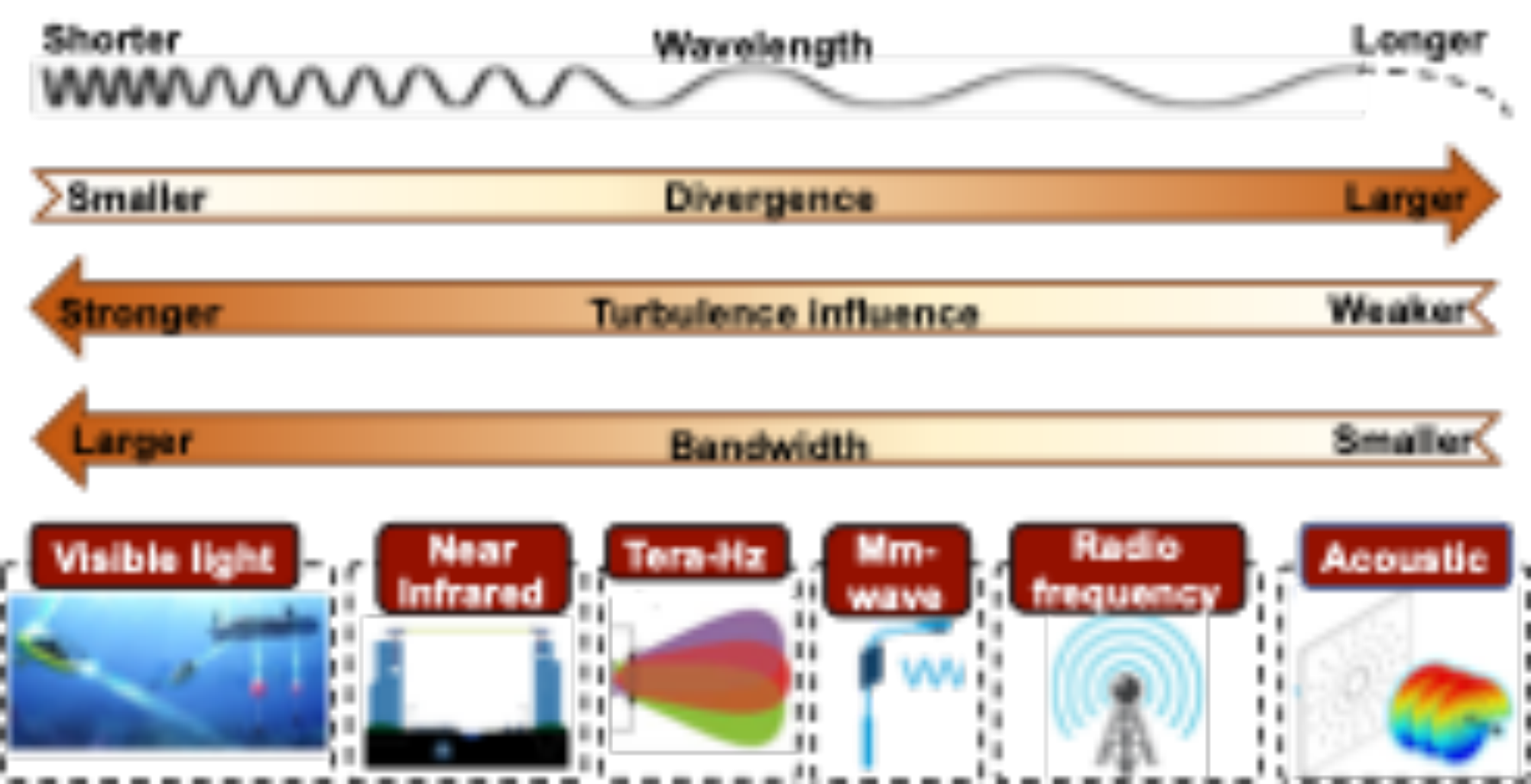
Shorter
Wavelength
Longer
Smaller
Divergence
Larger
Stronger
Turbulence influence
Weaker
Larger
Bandwidth
Smaller
Visible light
Near infrared
Tera-Hz
Mm-wave
Radio frequency
Acoustic

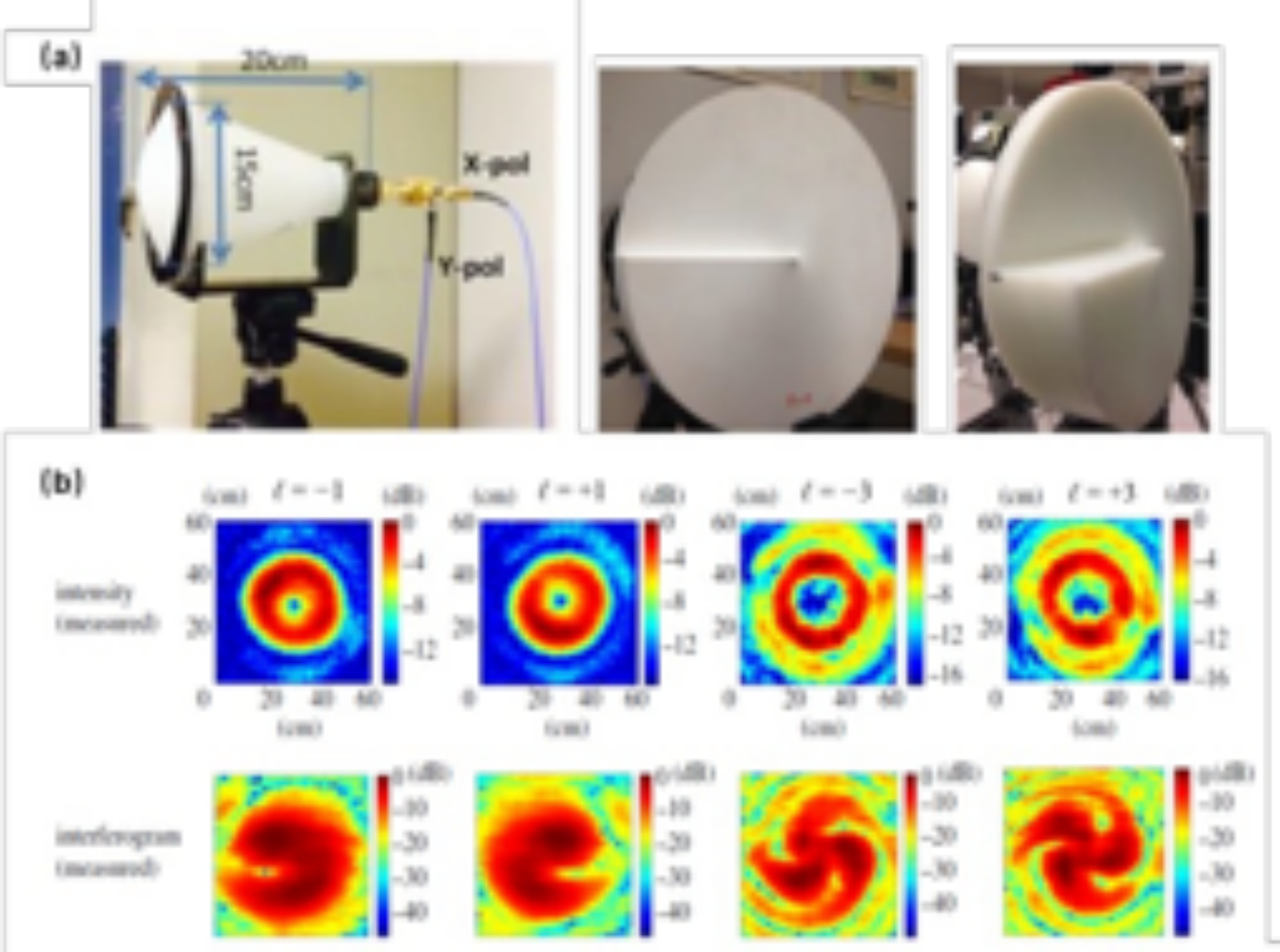
(a)
20cm
15cm
X-pol
Y-pol
(b)
intensity
(measured)
interferogram
(measured)
(cm)
(dB)
$\ell = -1$
$\ell = +1$
$\ell = -3$
$\ell = +3$

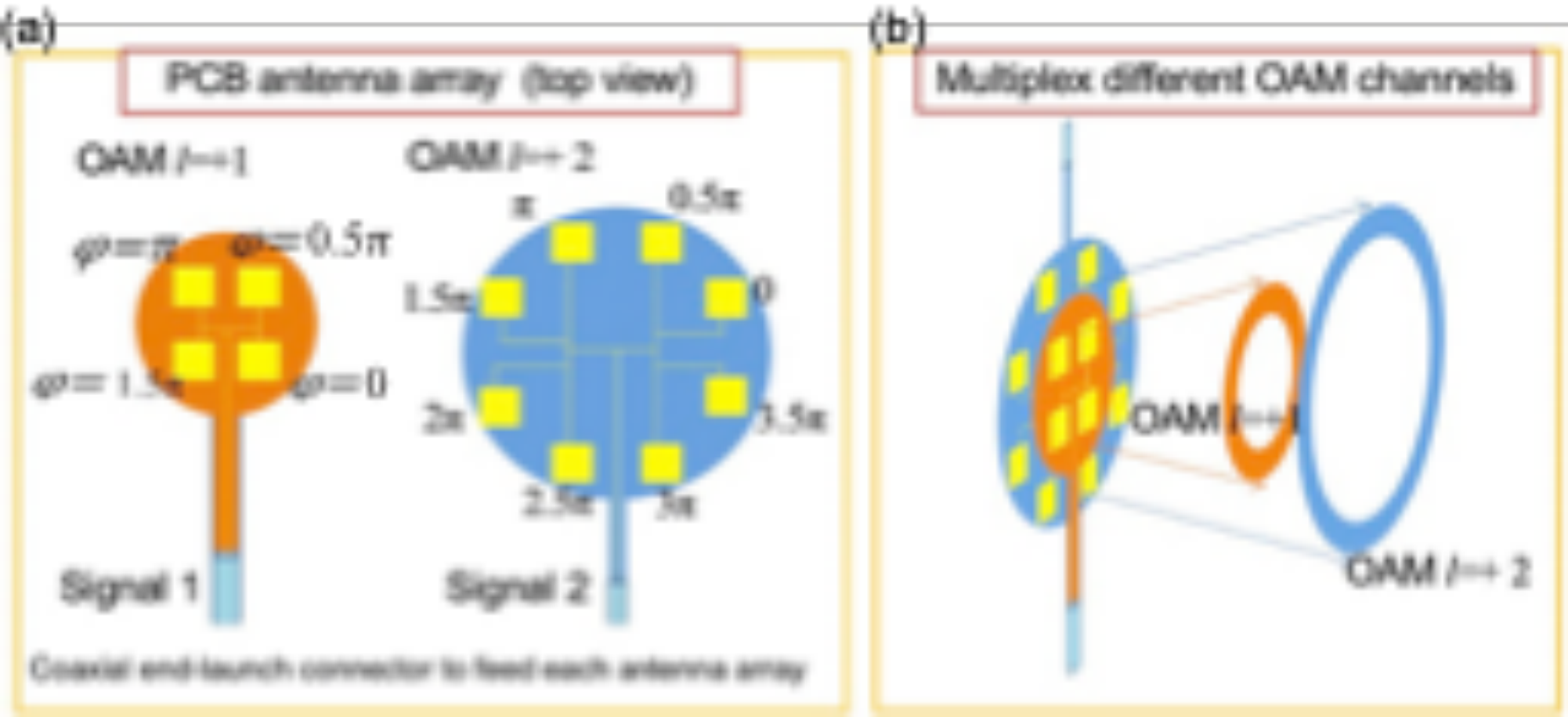
(a)
PCB antenna array (top view)
OAM l=+1
OAM l=+2
φ=π
φ=0.5π
φ=0
Signal 1
Signal 2
π
0.5π
1.5π
0
2π
3.5π
2.5π
3π
Coaxial end-launch connector to feed each antenna array
(b)
Multiplex different OAM channels
OAM l=+1
OAM l=+2

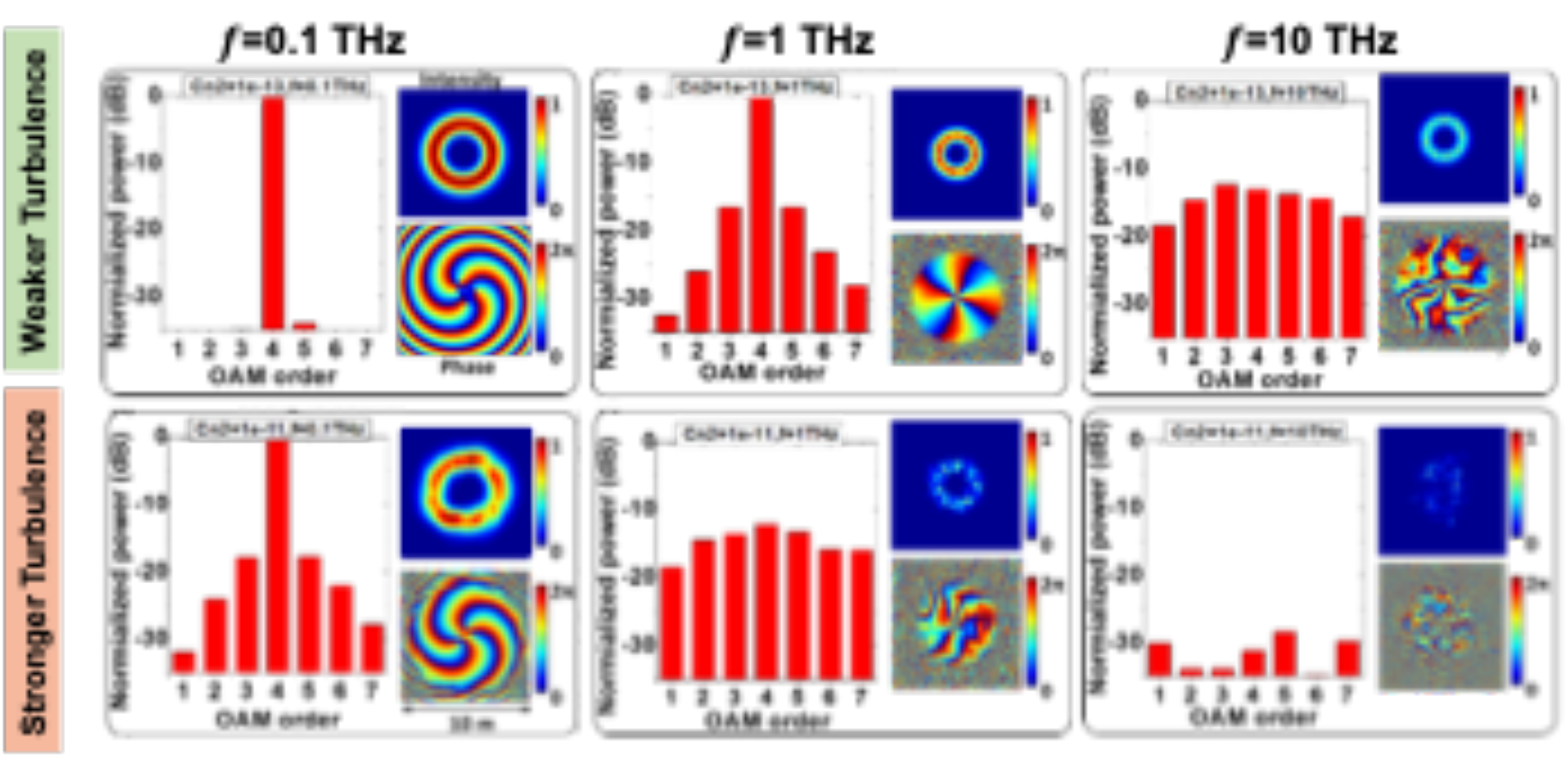
f=0.1 THz
f=1 THz
f=10 THz
Weaker Turbulence
Stronger Turbulence
Normalized power (dB)
OAM order
Phase
10 m

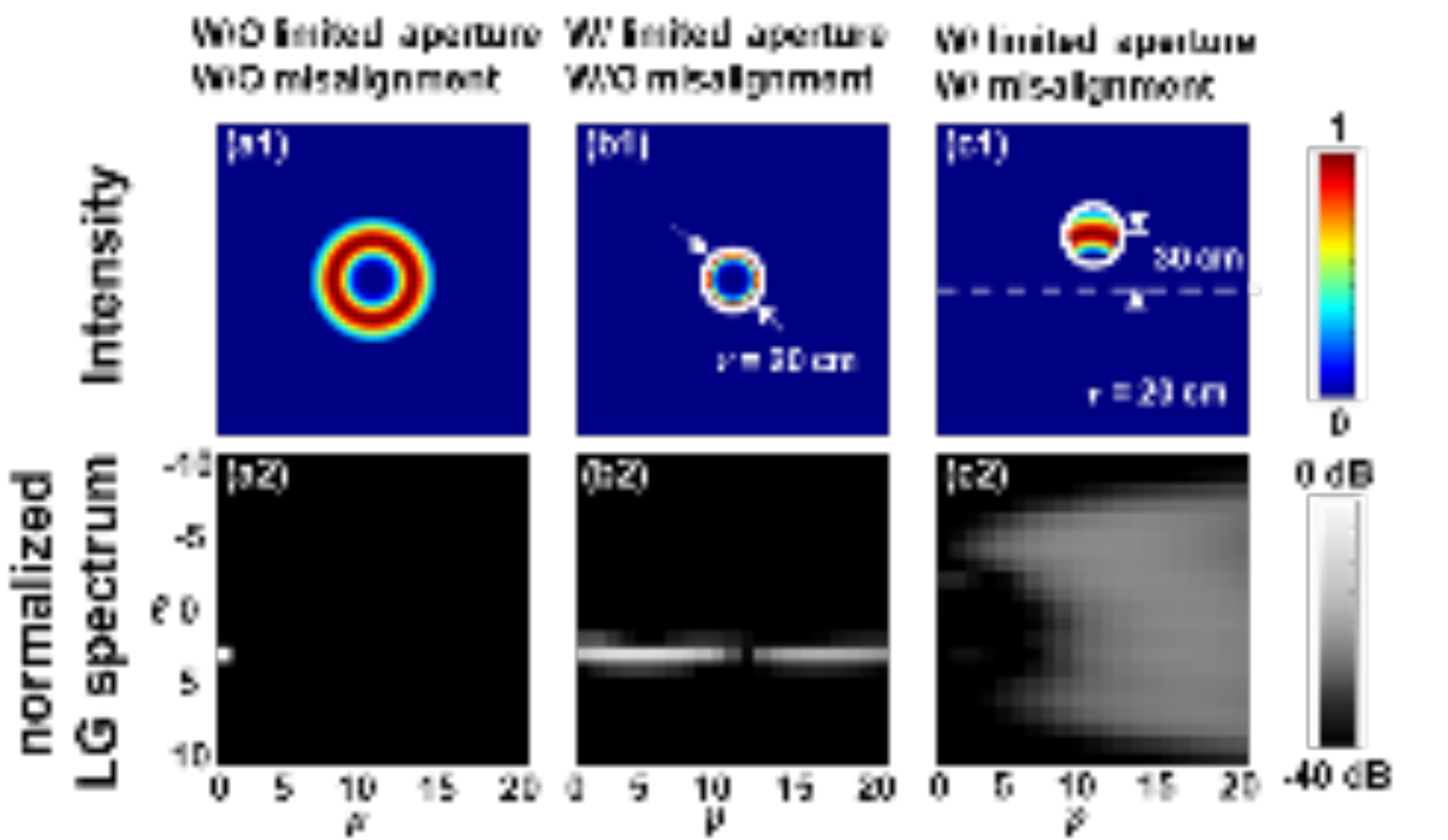
W/O limited aperture
W/O misalignment
W/ limited aperture
W/O misalignment
W/ limited aperture
W/ misalignment
Intensity
normalized LG spectrum
(a1)
(b1)
(c1)
r = 20 cm
r = 20 cm
(a2)
(b2)
(c2)
1
0
0 dB
-40 dB
-10
-5
0
5
10
0
5
10
15
20
p
l

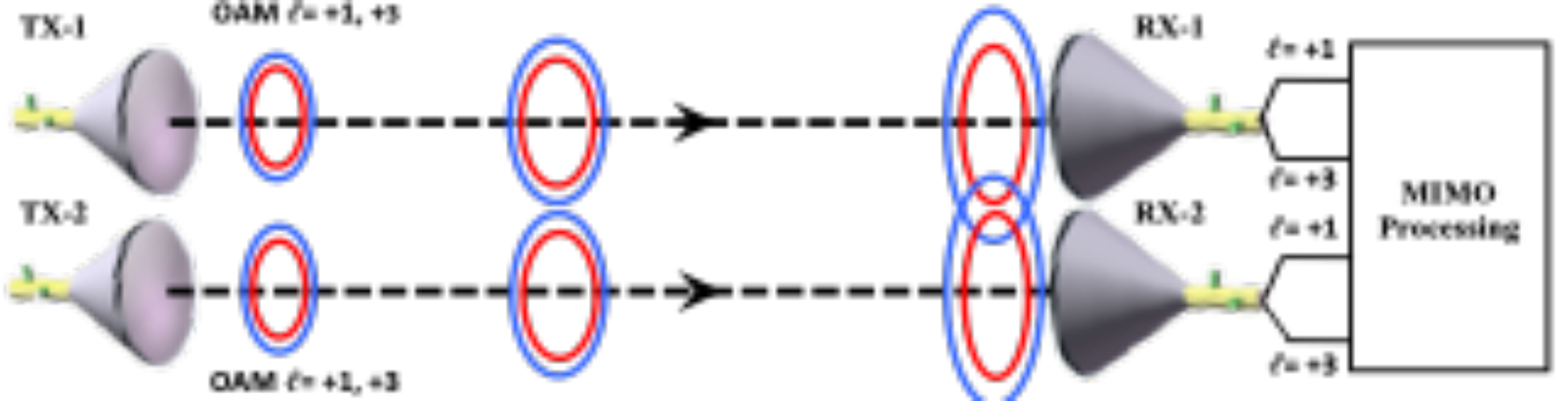
TX-1
OAM ℓ = +1, +3
TX-2
OAM ℓ = +1, +3
RX-1
RX-2
ℓ = +1
ℓ = +3
ℓ = +1
ℓ = +3
MIMO
Processing

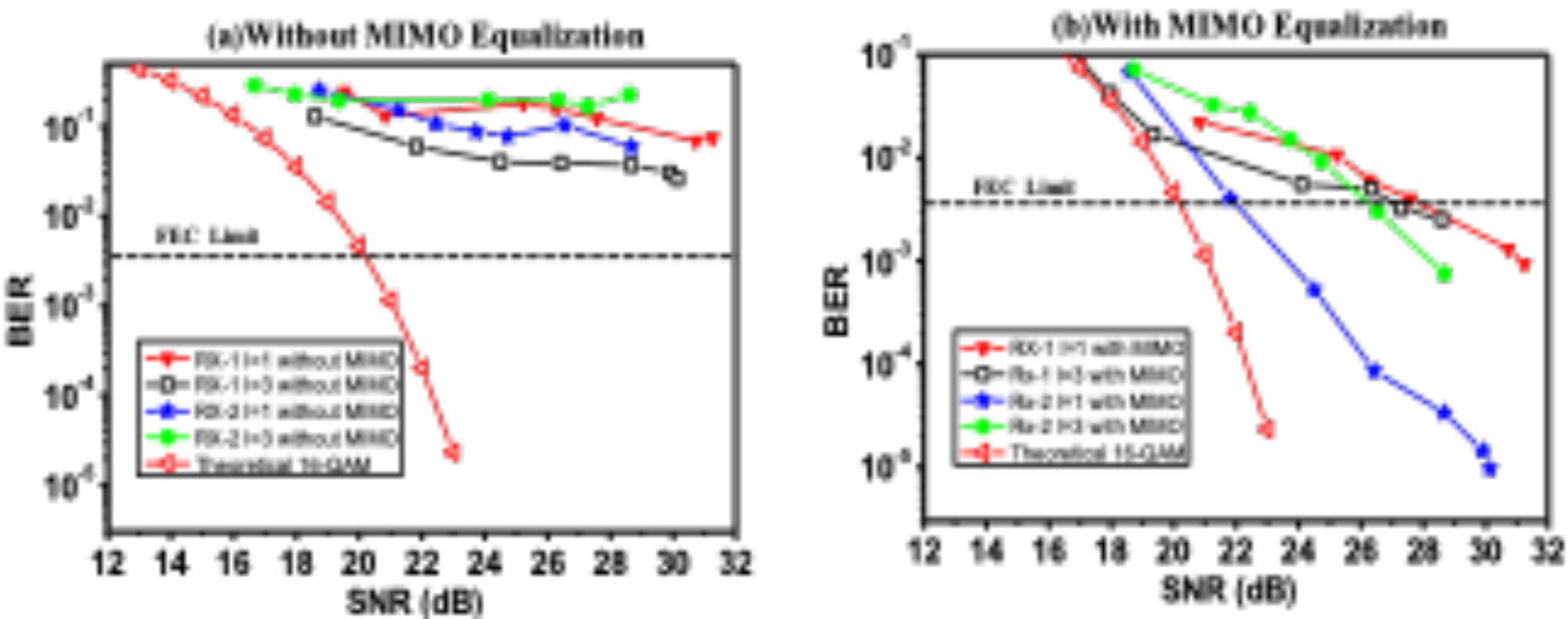
(a)Without MIMO Equalization
BER
SNR (dB)
FEC Limit
Rx-1 h1 without MIMO
Rx-1 h3 without MIMO
Rx-2 h1 without MIMO
Rx-2 h3 without MIMO
Theoretical 16-QAM
(b)With MIMO Equalization
BER
SNR (dB)
FEC Limit
Rx-1 h1 with MIMO
Rx-1 h3 with MIMO
Rx-2 h1 with MIMO
Rx-2 h3 with MIMO
Theoretical 16-QAM

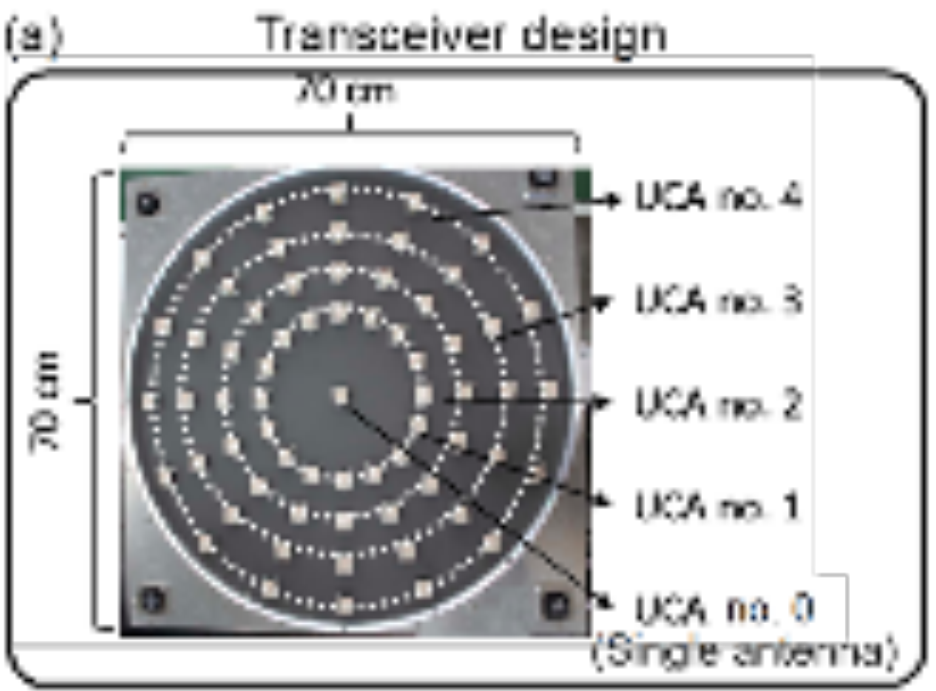
(a)
Transceiver design
70 cm
70 cm
UCA no. 4
UCA no. 3
UCA no. 2
UCA no. 1
UCA no. 0
(Single antenna)

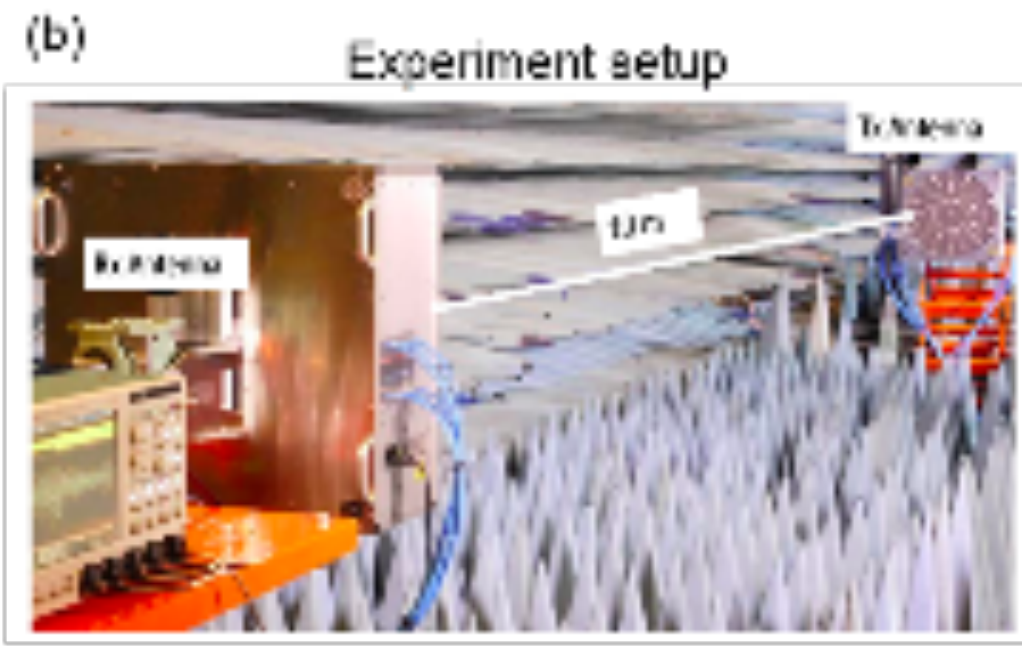
(b)
Experiment setup

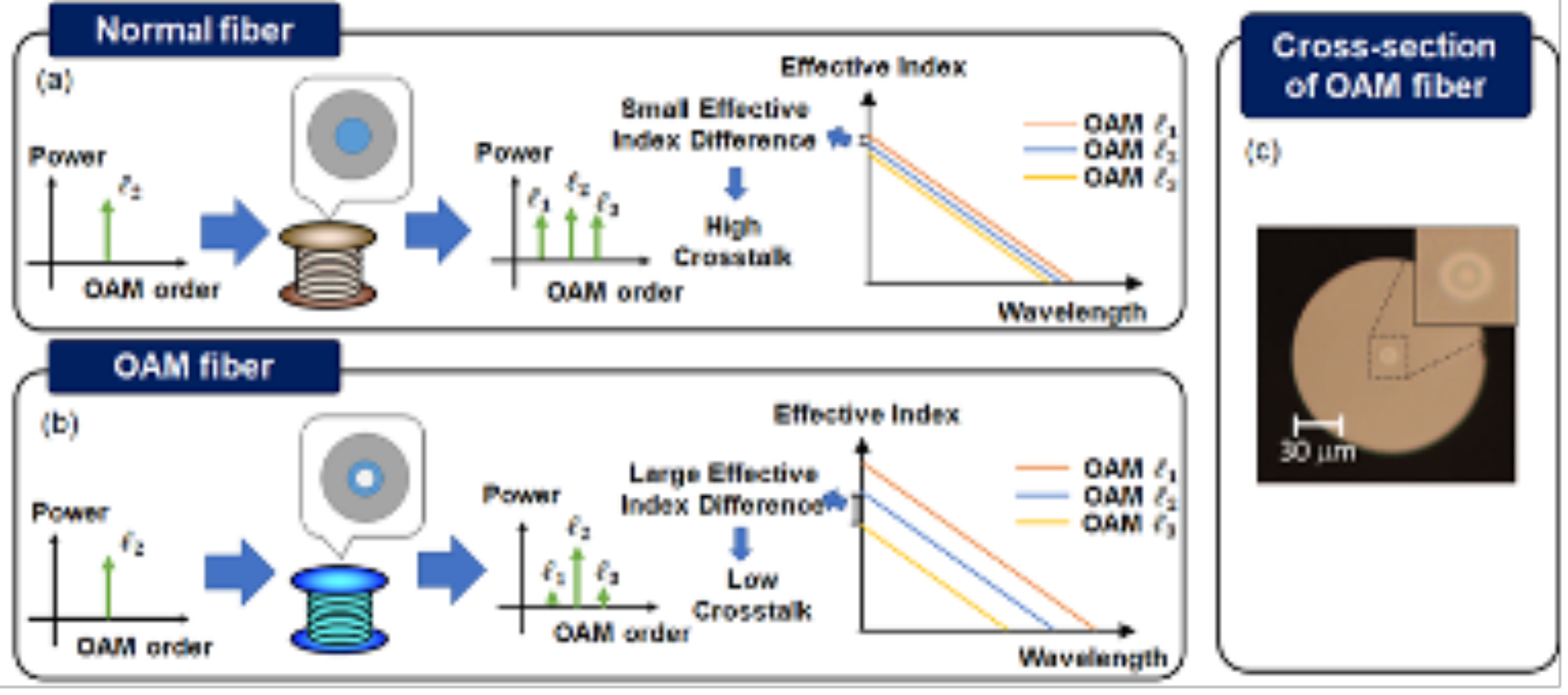
Normal fiber
(a)
Power
OAM order
Power
OAM order
Small Effective
Index Difference
High
Crosstalk
Effective Index
Wavelength
OAM fiber
(b)
Power
OAM order
Power
OAM order
Large Effective
Index Difference
Low
Crosstalk
Effective Index
Wavelength
Cross-section
of OAM fiber
(c)
30 μm

OAM EDFA

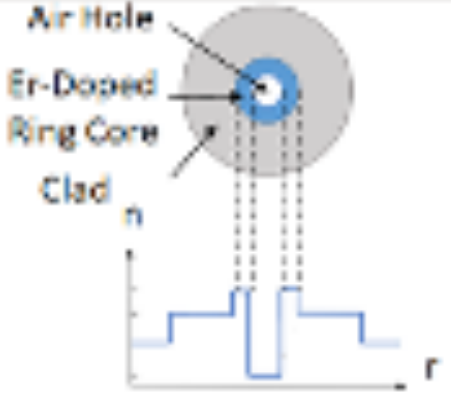

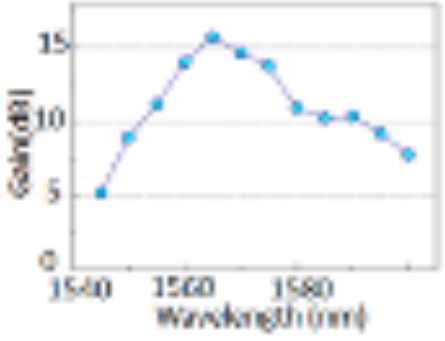

OAM Raman Amplifier